NATIONAL AERONAUTICS AND SPACE ADMINISTRATION

The Deep Space Network
Progress Report 42-21

March and April 1974

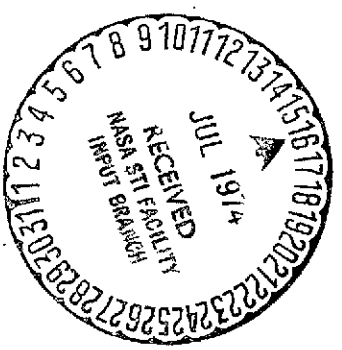

JET PROPULSION LABORATORY
CALIFORNIA INSTITUTE OF TECHNOLOGY
PASADENA, CALIFORNIA

June 15, 1974

NATIONAL AERONAUTICS AND SPACE ADMINISTRATION

The Deep Space Network
Progress Report 42-21

March and April 1974

JET PROPULSION LABORATORY
CALIFORNIA INSTITUTE OF TECHNOLOGY
PASADENA, CALIFORNIA
June 15, 1974

Prepared Under Contract No. NAS 7-100
National Aeronautics and Space Administration

Preface

Beginning with Volume XX, the Deep Space Network Progress Report will change from the Technical Report 32- series to the Progress Report 42- series. The volume number will continue the sequence of the preceding issues. Thus, Progress Report 42-20 is the twentieth volume of the Deep Space Network series, and is an uninterrupted follow-on to Technical Report 32-1526, Volume XIX.

This report presents DSN progress in flight project support, TDA research and technology, network engineering, hardware and software implementation, and operations. Each issue presents material in some, but not all, of the following categories in the order indicated:

Description of the DSN

Mission Support
- Interplanetary Flight Projects
- Planetary Flight Projects
- Manned Space Flight Projects
- Advanced Flight Projects

Radio Science

Supporting Research and Technology
- Tracking and Ground-Based Navigation
- Communications, Spacecraft/Ground
- Station Control and Operations Technology
- Network Control and Data Processing

Network Engineering and Implementation
- Network Control System
- Ground Communications
- Deep Space Stations

Operations and Facilities
- Network Operations
- Network Control System Operations
- Ground Communications
- Deep Space Stations
- Facility Engineering

In each issue, the part entitled "Description of the DSN" describes the functions and facilities of the DSN and may report the current configuration of one of the five DSN systems (Tracking, Telemetry, Command, Monitor and Control, and Test and Training).

The work described in this report series is either performed or managed by the Tracking and Data Acquisition organization of JPL for NASA.

Contents

Contents (contd)

Station Control and Operations Technology

Network Control and Data Processing

NETWORK ENGINEERING AND IMPLEMENTATION

Network Control System

Deep Space Stations

Network Operations

Contents (contd)

PLANNING AND FACILITIES

TDA Planning

Facility Engineering

DSN Functions and Facilities

N. A. Renzetti
Mission Support Office

The objectives, functions, and organization of the Deep Space Network are summarized. The Deep Space Instrumentation Facility, the Ground Communications Facility, and the Network Control System are described.

The Deep Space Network (DSN), established by the National Aeronautics and Space Administration (NASA) Office of Tracking and Data Acquisition under the system management and technical direction of the Jet Propulsion Laboratory (JPL), is designed for two-way communications with unmanned spacecraft traveling approximately 16,000 km (10,000 mi) from Earth to planetary distances. It supports or has supported, the following NASA deep space exploration projects: Ranger, Surveyor, Mariner Venus 1962, Mariner Mars 1964, Mariner Venus 67, Mariner Mars 1969, Mariner Mars 1971, Mariner Venus–Mercury 1973 (JPL); Lunar Orbiter and Viking (Langley Research Center); Pioneer (Ames Research Center); Helios (West Germany); and Apollo (Manned Spacecraft Center), to supplement the Spaceflight Tracking and Data Network (STDN).

The Deep Space Network is one of two NASA networks. The other, STDN, is under the system management and technical direction of the Goddard Space Flight Center. Its function is to support manned and unmanned Earth-orbiting and lunar scientific and communications satellites. Although the DSN was concerned with unmanned lunar spacecraft in its early years, its primary objective now and into the future is to continue its support of planetary and interplanetary flight projects.

A development objective has been to keep the network capability at the state of the art of telecommunications and data handling and to support as many flight projects as possible with a minimum of mission-dependent hardware and software. The DSN provides direct support of each flight project through that project's tracking and

data system. This management element is responsible for the design and operation of the hardware and software in the DSN which are required for the conduct of flight operations.

Beginning in FY 1973 a modified DSN interface has been established with the flight projects. In lieu of the SFOF, a multimission Mission Control and Computing Center (MCCC) has been activated as a separate functional and management element within JPL. This function, as negotiated with each flight project, will provide all computing and mission operations support for missions controlled from JPL. DSN computing support will be provided separately by the DSN. Radio metric, telemetry, and command data interfaces with the DSN are a joint DSN, MCCC, and flight project responsibility. The organization and procedures necessary to carry out these new activities will be reported in this document in the near future.

The DSN function, in supporting a flight project by tracking the spacecraft, is characterized by five network systems:

(1) DSN Tracking System. Generates radio metric data; i.e., angles, one- and two-way doppler and range, and transmits raw data to mission control.

(2) DSN Telemetry System. Receives, decodes, records, and retransmits engineering and scientific data generated in the spacecraft to Mission Control.

(3) DSN Command System. Accepts coded signals from mission control via the GCF and transmits them to the spacecraft in order to initiate spacecraft functions in flight.

(4) DSN Monitor and Control System. Instruments, transmits, records, and displays those parameters of the DSN necessary to verify configuration and validate the network. Provides operational direction and configuration control of the network and primary interface with flight project Mission Control personnel.

(5) DSN Test and Training System. Generates and controls simulated data to support development, test, training and fault isolation within the DSN. Participates in mission simulation with flight projects.

The facilities needed to carry out these functions have evolved in three technical areas: (1) the Deep Space Stations (DSSs) and the telecommunications interface through the RF link with the spacecraft is known as the Deep Space Instrumentation Facility (DSIF); (2) the Earth-based point-to-point voice and data communications from the stations to Mission Control is known as the Ground Communications Facility (GCF); (3) the network monitor and control function is known as the Network Control System (NCS).

I. Deep Space Instrumentation Facility

A. Tracking and Data Acquisition Facilities

A world-wide set of Deep Space Stations with large antennas, low-noise phase-lock receiving systems, and high-power transmitters provide radio communications with spacecraft. The DSSs and the deep space communications complexes (DSCCs) they comprise are given in Table 1.

Radio contact with a spacecraft usually begins when the spacecraft is on the launch vehicle at Cape Kennedy, and it is maintained throughout the mission. The early part of the trajectory is covered by selected network stations of the Air Force Eastern Test Range (AFETR) and the STDN of the Goddard Space Flight Center.[1] Normally, two-way communications are established between the spacecraft and the DSN within 30 min after the spacecraft has been injected into lunar, planetary, or interplanetary flight. A compatibility test station at Cape Kennedy (discussed later) tests and monitors the spacecraft continuously during the launch checkout phase. The deep space phase begins with acquisition by 26-m DSSs. These and the remaining DSSs listed in Table 1 provide radio communications until the end of the mission.

To enable continuous radio contact with spacecraft, the DSSs are located approximately 120 deg apart in longitude; thus a spacecraft in deep space flight is always within the field-of-view of at least one DSS, and for several hours each day may be seen by two DSSs. Furthermore, since most spacecraft on deep space missions travel within 30 deg of the equatorial plane, the DSSs are located within latitudes of 45 deg north and south of the equator. All DSSs operate at S-band frequencies: 2110-2120 MHz for Earth-to-spacecraft transmission and 2290-2300 MHz for spacecraft-to-Earth transmission. An X-band capability is being readied for future missions beginning in 1973.

[1]The 9-m (30-ft) diam antenna station established by the DSN on Ascension Island during 1965 to act in conjunction with the STDN orbital support 9-m (30-ft) diam antenna station was transferred to the STDN in July 1968.

To provide sufficient tracking capability to enable returns of useful data from around the planets and from the edge of the solar system, a 64-m (210-ft) diam antenna subnet will be required. Two additional 64-m (210-ft) diam antenna DSSs are under construction at Madrid and Canberra and will operate in conjunction with DSS 14 to provide this capability. These stations are scheduled to be operational by the middle of 1973.

B. Compatibility Test Facilities

In 1959, a mobile L-band compatibility test station was established at Cape Kennedy to verify flight-spacecraft/DSN compatibility prior to the launch of the Ranger and Mariner Venus 1962 spacecraft. Experience revealed the need for a permanent facility at Cape Kennedy for this function. An S-band compatibility test station with a 1.2-m (4-ft) diameter antenna became operational in 1965. In addition to supporting the preflight compatibility tests, this station monitors the spacecraft continuously during the launch phase until it passes over the local horizon.

Spacecraft telecommunications compatibility in the design and prototype development phases was formerly verified by tests at the Goldstone DSCC. To provide a more economical means for conducting such work and because of the increasing use of multiple-mission telemetry and command equipment by the DSN, a Compatibility Test Area (CTA) was established at JPL in 1968. In all essential characteristics, the configuration of this facility is identical to that of the 26-m (85-ft) and 64-m (210-ft) diameter antenna stations.

The JPL CTA is used during spacecraft system tests to establish the compatibility with the DSN of the proof test model and development models of spacecraft, and the Cape Kennedy compatibility test station is used for final flight spacecraft compatibility validation testing prior to launch.

II. Ground Communications Facility

The GCF provides voice, high-speed data, wideband data, and teletype communications between the Mission Operations Center and the DSSs. In providing these capabilities, the GCF uses the facilities of the worldwide NASA Communications Network (NASCOM)[2] for all long distance circuits, except those between the Mission Operations Center and the Goldstone DSCC. Communications between the Goldstone DSCC and the Mission Operations Center are provided by a microwave link directly leased by the DSN from a common carrier.

Early missions were supported by voice and teletype circuits only, but increased data rates necessitated the use of high-speed and wideband circuits for DSSs. Data are transmitted to flight projects via the GCF using standard GCF/NASCOM formats. The DSN also supports remote mission operations centers using the GCF/NASCOM interface.

III. Network Control System

The DSN Network Control System is comprised of hardware, software, and operations personnel to provide centralized, real-time control of the DSN and to monitor and validate the network performance. These functions are provided during all phases of DSN support to flight projects. The Network Operations Control Area is located in JPL Building 230, adjacent to the local Mission Operations Center. The NCS, in accomplishing the monitor and control function does not alter, delay, or serially process any inbound or outbound data between the flight project and tracking stations. Hence NCS outages do not have a direct impact on flight project support. Voice communications are maintained for operations control and coordination between the DSN and flight projects, and for minimization of the response time in locating and correcting system failures.

The NCS function will ultimately be performed in data processing equipment separate from flight project data processing and specifically dedicated to the NCS function. During FY 1973, however, DSN operations control and monitor data will be processed in the JPL 360/75 and in the 1108. In FY 1974 the NCS data processing function will be partly phased over to an interim NCS processor, and finally, in FY 1975, the dedicated NCS data processing capability will be operational. The final Network Data Processing Area will be located remote from the Network Operations Control Area so as to provide a contingency operating location to minimize single point of failure effects on the network control function.

[2]Managed and directed by the Goddard Space Flight Center.

Table 1. Tracking and data acquisition stations of the DSN

DSCC	Location	DSS	DSS serial designation	Antenna		Year of initial operation
				Diameter, m (ft)	Type of mounting	
Goldstone	California	Pioneer	11	26(85)	Polar	1958
		Echo	12	26(85)	Polar	1962
		(Venus)[a]	13	26(85)	Az-El	1962
		Mars	14	64(210)	Az-El	1966
Tidbinbilla	Australia	Weemala (formerly Tidbinbilla)	42	26(85)	Polar	1965
		Ballima (formerly Booroomba)	43	64(210)	Az-El	1973
–	Australia	Honeysuckle Creek	44	26(85)	X-Y	1973
–	South Africa	Hartebeesthoek	51	26(85)	Polar	1961
Madrid	Spain	Robledo	61	26(85)	Polar	1965
		Cebreros	62	26(85)	Polar	1967
		Robledo	63	64(210)	Az-El	1973

[a]A maintenance facility. Besides the 26-m (85-ft) diam Az-El mounted antenna, DSS 13 has a 9-m (30-ft) diam Az-El mounted antenna that is used for interstation time correlation using lunar reflection techniques, for testing the design of new equipment, and for support of ground-based radio science.

DSN Monitor and Control System

J. E. Maclay
DSN Systems Engineering

The last major upgrade to the DSN Monitor and Control System was during preparation for support of the Mariner Mars 1971 (MM'71) mission. Since then, several improvements have been made, specifically: incremental improvements in the DSS Monitor and Control Subsystem, implementation by the Block I Network Control System (NCS) Project of the network operations control functions, and implementation by the Block II NCS Project of the design of the Network Control Monitor and Control Subsystem. These changes are described in this article.

I. Introduction

Changes to the DSN Monitor and Control System since the last major upgrade (in preparation for MM'71) fall into three areas: (1) new monitor functions in the Station Monitor and Control Subsystem (SMC), (2) monitor functions implemented by the Block I Network Control System (NCS) Project, and the Network Control (NC) Monitor and Control Subsystem (MCS) implemented by the Block II NCS Project.

II. Station Monitor and Control Subsystem

Although changes to the SMC software were extensive, the monitor functional capability was not significantly changed. However, several monitor operational improvements were made. Some non-SMC functions were added (e.g., formatting of radio metric data for output via high-speed data lines), but they are beyond the scope of the Monitor and Control Subsystem.

In the past, there has been a different SMC computer program for each station type; the new program is used at all stations, eliminating multiple programs. A second cathode-ray tube (CRT) display device has been added to each SMC, and the software provides two independent display outputs at the station manager's console. In the 64-m Deep Space Stations (DSSs), a third CRT was added as a slave to one of the SMC displays; it is called "SMC Junior" and is located in the data processing area. Monitoring of the Block IV receiver/exciter has been added.

A significant operational improvement is to give the station manager a wide range of display formats. A specific format is stored on punched paper tape, and changes to it are effected by keyboard. Thus, the station manager selects from an assortment of predefined formats.

III. Network Operations Control Function Implemented By the Block I NCS Project

Inbound high-speed data (HSD), not wideband data (WBD), are examined by a Sigma-5 located in the Network Data Processing Area (NDPA), and some data indicative of data flow conditions are displayed on CRTs, and some on the logging typewriter. The display devices are located both in the NDPA and in the Network Operations Control Area (NOCA).

For each DSS, or equivalent ground communications (GC) circuit, each user-dependent type (UDT) and data-dependent type (DDT) combination is treated as one stream. The streams are displayed on the CRT such that all streams for a given DSS are grouped. The display will accommodate 10 command streams per DSS plus 10 non-command streams. A normal activity overfills one CRT display, so the display is paged. Either a keyboard entry or a function button on the keyboard changes pages (see Fig. 1).

The status available for each stream is:

(1) DSS number.

(2) Percent good data to 1.0% resolution (based on GC error flags of the data blocks; filler blocks are excluded).

(3) User-dependent type.

(4) Data-dependent type.

(5) Block serial number of last block received before display update.

(6) Activity indicator (reads "NEW" for first minute a new stream exists).

(7) Cumulative count of block serial number (BSN) anomalies (i.e., occurrences of a block received not having BSN exactly one greater than the last block received).

The display updates every 5 seconds. If the error rate goes down to 98% or below, an entry is also made on the alarm logging typewriter in the NDPA and NOCA (see Fig. 2).

This capability was used operationally during Mariner Venus/Mercury 1973 (MVM'73) encounters.

IV. NC Monitor and Control Subsystem Functions Being Implemented by the Block II NCS Project

The NC MCS will contain a real-time monitor (RTM) computer dedicated to displaying DSS monitor data (see Fig. 3). The CRT/keyboards and slave CRTs in NOCA are the display devices.

The two CRT display devices are completely independent and will usually have different formats. Two formats have been designed for output. One is a single-DSS detailed format. The other is a two-DSS summary format. The strategy will be to display the two-DSS format on each CRT, thus displaying monitoring of four DSSs. (It would have been highly desirable to have multi-DSS display, not just two-DSS display, but CRT limitations on field size precluded this.) For troubleshooting, one CRT would have the single-DSS format called up instead. Format/DSS selection is from the CRT keyboard.

The RTM software contains logic to process in a suppressed data mode. First, a canned-in station mask is used in the data processing. The mask tells the processor what equipments do not exist at each DSS, so that monitor parameters pertaining to equipment not at a given DSS are not processed. For example, the mask would exclude the data fields pertaining to a second transmitter from being processed for a 26-m DSS. Also, the mask instructs the processor to renumber some equipment. For example, it would cause subcarrier demodulator assembly 1 at a conjoint 26-m DSS to be displayed as SDA 7. Secondly, an initialization message, which is part of the monitor data stream, further instructs the processor on which of the station equipments are in use at a given time. Thus, status data on standby equipment are not displayed in NOCA. This has the effect of limiting the displayed data to only the most meaningful, thereby simplifying operator interpretation.

Computer hardware installation is complete, except for NOCA CRTs, and software is in test phase at this time. During the third quarter of 1974 there will be extensive network-level tests to validate NC MCS display against DSS SMC values. The NC MCS will be operational for Viking operational verification tests.

FORMAT 1, PAGE 1 GMT: 116:05:11:39
HIGH SPEED DATA STATUS NUMBER = 4

DSS	ERR	SC	UDT/DDT		SEQ	BSN	GDD	ACT
12	100	95	107	75	0	155	0	C
12	100	95	70	75	0	100	0	C
12	100	95	107	167	0	152	0	C
12	100	95	70	167	0	95	0	C

Fig. 1. Sample CRT display: real-time accountability

```
** ACC DATA STREAM INACTIVE 014/076/026/104
** ACC DATA STREAM INACTIVE 014/076/026/104
** CMD ALM 18:27:25 DSS ALM BIT 11  14A 076
** ACC DATA STREAM INACTIVE 014/076/026/104
** ACC DATA STREAM INACTIVE 014/076/026/104
** ACC DATA STREAM INACTIVE 014/076/026/104
```

Fig. 2. Sample alarm printer display: real-time accountability alarms

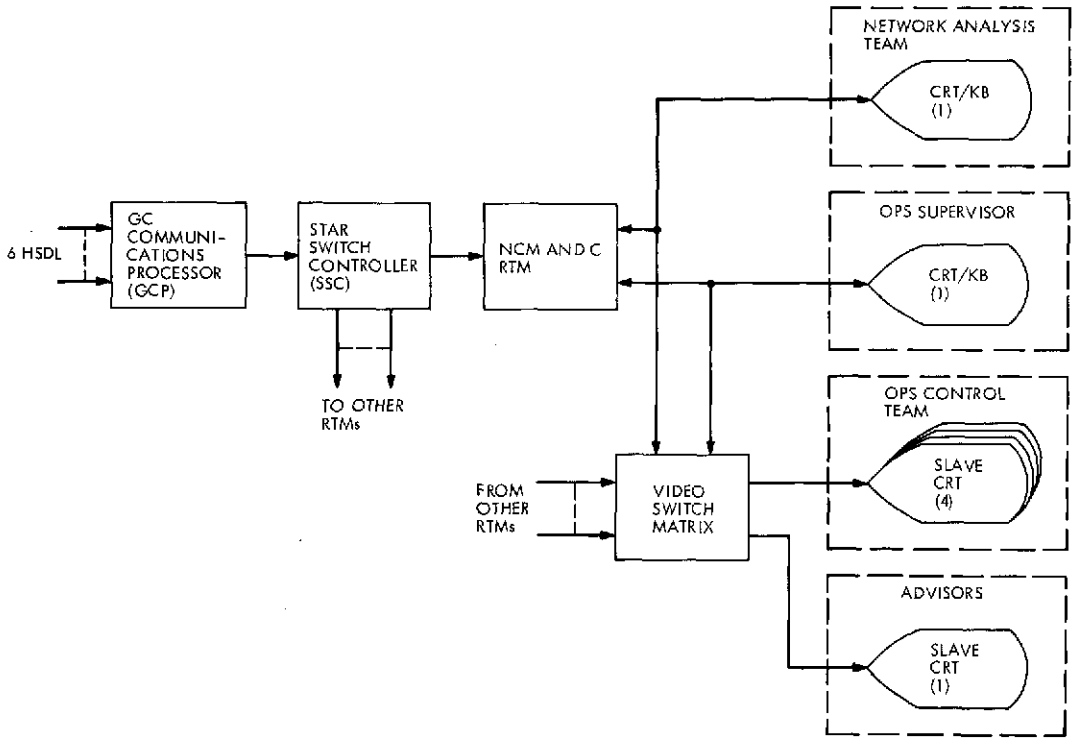

Fig. 3. The NC Monitor and Control Subsystem configuration (Block II NCS implementation)

Mariner Venus-Mercury 1973 Mission Support

E. K. Davis
DSN Systems Engineering Office

During January and February 1974, DSN preparations for the Mariner Venus/Mercury 1973 Venus encounter were completed, and the encounter was supported in a near flawless manner. In addition, this period saw the continuation of spacecraft problems which required the Deep Space Network to respond with additional implementation and new operational techniques to facilitate achievement of mission objectives.

I. Planning Activities

During January 1974, DSN operations planning gave priority to preparations for the second trajectory correction maneuver (TCM) and for Venus encounter. However, in addition, a significant level of effort was required of the DSN Support Team to generate real-time operations plans in response to spacecraft problems. These problems and responses are discussed in *Section IV*, "Operations Summary."

Preparations for TCM No. 2 were well underway in early January 1974 for a mid-January burn. However, the occurrence of a spacecraft emergency on Jan. 8, 1974, involving spacecraft switch to the backup power chain, interrupted and delayed completion of the maneuver sequence. The TCM was rescheduled for Jan. 19, 1974 and then again slipped to Jan. 21, 1974 as additional spacecraft power constraints were factored in. These changes required the DSN to make corresponding adjustments to DSN schedules, sequences, and staffing. During one particular week, sixty-eight real-time schedule changes were required to realign network support for MVM'73, Pioneer 10 and 11, and radio science.

In parallel with TCM activities, the DSN planned a series of comprehensive Venus encounter readiness tests. These test procedures included Class I countdown exercises, appropriate portions of DSS system performance tests, critical requirements of the Venus encounter sequence of events, and use of the spacecraft as a data source. DSSs 14, 43, and 63 were scheduled for participation during the period of Jan. 17-30, 1974.

Following completion of TCM No. 2 activities, primary attention was again given to finalizing the sequence of events and configuration strategies for Venus encounter. However, this effort was complicated by the spacecraft

roll gyro oscillation-attitude gas consumption problem which occurred during the roll calibration maneuver on Jan. 28, 1974. In addition, a high level of effort went into the S/X-band radio science occultation portion of the sequence to assure feasibility of the demanding, rapid radio-frequency (RF) signal acquisition at exit occultation. Consequently, tweaking of the detailed DSN sequence continued until Venus encounter minus one day.

II. Program Control

Weekly status meetings with the Project continued throughout this reporting period. Open implementation items and problem areas were tracked until appropriate closures were accomplished. Weekly teletype status reports to NASA Headquarters and monthly inputs to the Project Management Report continued.

In late January 1974, the DSN conducted a Venus encounter readiness review to evaluate the final status of preparations and potential problem areas. The review and results of encounter readiness tests demonstrated that the DSN was in a high state of readiness for the critical operations.

III. Implementation Activities

A. Deep Space Stations

The previous Progress Report listed post-launch, open implementation tasks, and problem areas. Successful closure of most of these items was accomplished in January 1974 as described in this section. In addition, the DSN accomplished certain emergency implementation to accommodate changes in the spacecraft RF link characteristics.

1. *Antenna microwave subsystem.* The listen-only, low-noise ultracone was installed at DSS 43 without difficulty on the planned mid-January schedule. Excellent performance was demonstrated in follow-up tests. Tests will continue through March 1974 to demonstrate adequate performance for reception of 117-kbits/s video data under expected marginal RF link conditions at Mercury encounter on Mar. 29, 1974.

By mid-February 1974, the spacecraft high gain antenna problem had produced an RF downlink which was 6 dB less than normal, and an antenna pattern which was nearly completely linear rather than circular. About 3 dB of this loss was attributed to cross polarization between circular polarization of the DSS antenna and the now linear polarization of the spacecraft. In response to Project request and to meet Mercury TV experiment objectives, the DSN took emergency action in February to provide, ship, and install linear polarization equipment at each of the three 64-m DSSs. This work is expected to be completed shortly before Mercury encounter.

2. *Telemetry and command data subsystem.* Accomplishment of capabilities in January 1974 for post-track recall of digitally recorded radio metric data marked the end of all required implementation in this subsystem. An existing Telemetry and Command Data Subsystem (TCD) software program was modified and integrated into the DSN to perform this function.

However, continuing engineering support was required to help analyze a problem observed in DSS 43's and 63's Original Data Records (ODRs) containing 117-kbits/s video data from Venus encounter. Essentially all of the video data were recorded on the ODR, but the data were not in the correct time ordered sequence. "Old" and "new" data were interleaved in a repetitive pattern requiring special processing by the Mission Control and Computing Center (MCCC) to recover video frames. Special tests are being planned and will be conducted at DSS 14 and CTA 21 to resolve this problem prior to Mercury encounter. However, the problem is observed only at the 117-kb/s rate which will not be used at Mercury encounter if the spacecraft antenna performance remains 6 dB below normal.

3. *Tracking data handling subsystem (TDH).* Implementation of planetary ranging capabilities was completed at DSSs 43 and 63 in mid-January 1974 approximately two weeks later than planned. Although declared operational on the basis of successful system performance tests, DSS 63 ranging data have exhibited a timing bias which makes it difficult to use for navigation purposes. These capabilities came none too soon. Near simultaneous ranging data were required from DSSs 12, 14, 43, and 63 for critical orbit determination exercises to rapidly redetermine the orbit following perturbations from the gyro-attitude gas usage problem.

4. *Digital instrumentation subsystem.* Update of the Digital Instrumentation Subsystem (DIS) software program was completed and integrated into the DSS in January 1974 as planned. This update provided the required Venus encounter capability for real-time handling of 10 samples/s doppler data via high-speed data lines.

5. *Pre/post detection recording subsystem.* Work continued on DSS 14's dedicated open-loop analog recording assemblies until two days prior to Venus encounter to achieve configuration and performance desired by radio science experimenters. Late modifications were required to adequately integrate both S- and X-band signals from the R&D Block IV receiver assemblies.

Also, quality checks of analog recording produced on the DSS standard analog recorder indicated improvements were needed to facilitate proper recording and recovery of telemetry data from this backup ODR. Tests at CTA 21 demonstrated that significant changes were required in channel assignments to achieve desired results. To avoid unacceptable risks of late configuration changes, this modification was only partially implemented prior to Venus encounter and then was completed thereafter.

6. *S/X-band equipment.* X-band doppler cycle slips and offsets described in the previous article continued to be periodically observed throughout this reporting period. Interface cable replacements and assembly adjustments in January 1974 did, temporarily, eliminate these problems during the Venus encounter period. By mid-February 1974, the problems were back again. Therefore, the DSN initiated a special coordinated team effort between DSN engineering, operations, and Project radio science experimenters to troubleshoot and achieve required performance prior to Mercury encounter. Noise interference appears to be the major cause, but its source is unknown at this time.

In early January 1974, the Command Modulator Assembly Switch required to provide Block IV exciter uplink capabilities was installed at DSS 14 but failed to operate properly due to a wiring logic error. The switch was removed for rework. Since stability of the Block III exciter was sufficient to meet S/X-band requirements at Venus encounter, it was decided that the switch would be reinstalled during the week of Feb. 24, 1974 in preparation for Mercury encounter support. This installation was accomplished as planned. Post-installation tests and operational use demonstrated proper performance with the Block III configuration. However, due to interface signal errors, switch performance in the Block IV configuration was not acceptable. Work on this problem continues.

B. DSN Ground Communications

Appropriate modifications and adjustments to the DSS 14/DSS 12 microwave link were initiated as a means of providing access to DSS 12's telemetry strings for backup to DSS 14's two-string configuration. The planned use of this microwave link is for transmission of 2450 bits/s telemetry data to DSS 12 in the event DSS 14 loses one string while supporting dual subcarrier operations.

The microwave link between DSS 63 and DSS 62 was reactivated and adjusted to support real-time transmission of low rate telemetry data from DSS 63 to DSS 62. This capability permitted continuation of the DSS 63 communications terminal relocation/reconfiguration without interrupting data flow to project users. This work was satisfactorily completed on Feb. 28, 1974.

IV. Operations Summary

Following is a brief summary of DSN operations activities for January and February 1974. Primary attention is given to certain spacecraft problems which placed an unplanned, heavy load on the DSN in terms of revised plans, sequences, tests, schedules, and new implementation.

During this period, Mariner 10 coverage continued to be provided by a combination of 26- and 64-m subnet DSSs. January 1974 saw a rather equal sharing of the 64-m subnet between Pioneer and Mariner. DSN readiness tests for Venus encounter were satisfactorily completed between January 17 and 30, 1974. Beginning Feb. 1, 1974, DSS 14, 43, and 63 configurations were frozen for Venus encounter operations. DSN support continued to be very satisfactory, with exceptional performance demonstrated during the critical Venus sequence and during a number of spacecraft problems.

The spacecraft high-gain antenna went through a number of fail-heal-fail cycles during this period. Degradation finally stabilized at a downlink loss of 6 dB and a linear polarization rather than circular. This problem made performance of the link marginal for 26-m subnet reception of 2450 bits/s telemetry at a bit error rate of 1 in 10^4 or less. Furthermore, even 22 kbits/s video data would have been marginal via 64-m DSS at Mercury encounter. In response, the DSN performed frequent precision signal level measurements, conducted ellipticity measurements, and implemented linear polarization tracking capability in the 64-meter subnet.

Spacecraft roll gyro oscillations caused periodic high usage of attitude control gas. This perturbed the well-

defined trajectory requiring rapid generation of additional amounts of accurate radio metric data in the DSN. In response, the DSN negotiated with the Pioneer Project for additional 64-m coverage for Mariner 10 and scheduled a series of near-simultaneous ranging acquisitions.

Spacecraft power problems were varied but were primarily observed by the DSN in the form of power-on resets (PORs). PORs were frequent during roll calibrations and gyro turn ons. These cause the spacecraft to automatically switch, without warning, to a different data mode and to the interplex configuration. To minimize response time and data loss when PORs occurred, the DSN developed special procedures for subcarrier demodulator configurations, phasing, notch filter installation, and for analog record handling.

Flight and ground tests showed that the spacecraft auxiliary oscillator had a frequent one-half cycle offset when in the one-way mode. This instability would have masked Venus atmospheric effects on the RF signal severely degrading radio science occultation results. Proper auxiliary oscillator performance was obtained in the two-way mode but required use of the DSS 14 100-kW transmitter to gain adequate link performance. The two-way, 100-kW sequence had to be planned between Feb. 1, 1974 and Venus encounter on Feb. 5, 1974.

These problems caused delays of certain critical mission events such as trajectory correction maneuvers, calibrations and spacecraft computer updates. DSN operations was hard pressed to accommodate these changes in plans, schedules, and ground command activities.

Pioneer 10 and 11 Mission Support

R. B. Miller
DSN Systems Engineering Office

The functional requirements, detailed design, and implementation of the Direct Interface between the Deep Space Network and the Pioneer Project are described.

I. Introduction

The existing Ground Data System used to support the Pioneer 10 and 11 missions was described in a previous Progress Report article (Ref. 1). The block diagram contained in the referenced article is repeated here as Fig. 1. An additional unique aspect of the Pioneer 10 and 11 missions is that they are the first unmanned missions supported by the Jet Propulsion Laboratory which have involved a Remote Control Center. The Ground Data System as it exists involves three major elements which are separated geographically. The first element is the Deep Space Stations which are located around the world, the second is the Mission Control and Computing Center and Network Operations located at the Jet Propulsion Laboratory, and the final element is the Pioneer Mission Operations Control Center located at the Ames Research Center (ARC). As was described in more detail in the referenced article, the data flow from the Pioneer Mission Operations Control Center (PMOCC) passes from the Ames Research Center via high-speed data line to the Computer System located at the Jet Propulsion Laboratory where extensive processing takes place, and then the data flows on to the Deep Space Stations (DSSs). Recognizing the complexity of the Ground Data System as it currently exists, ARC initiated an activity to implement a Direct Interface between the Pioneer Mission Operations Control Center and the Deep Space Stations. Over the past several months, representatives of the Deep Space Network and the Pioneer Project Office have jointly formulated a detailed technical plan for the implementation of such a Direct Interface. The technical plan has been completed and has undergone a formal review and acceptance by DSN Management and Pioneer Project Office Management.

The basic objective in implementing the Direct Interface is to simplify the Ground Data System for Pioneer Operations by eliminating Pioneer telemetry and command processing in the 360/75 computers of the Mission Control and Computing Center located at the Jet Propulsion Laboratory and interfacing the Pioneer Mission Operations Control Center at ARC directly with the DSS. This simplification of the Ground Data System should reduce the complexity of operational interfaces and should improve reliability since a major element, with its independent mean time between failure and

mean time to recover, is no longer in series with the data flow. The direct mode will also reduce the interaction between Pioneer Project and other in-flight missions since only the radio metric data processing for Pioneer will remain in the multimission co-resident 360/75 environment.

II. Design Guidelines

The following general requirements were used in formulating the detailed design of the Direct Interface.

In the direct mode and during the implementation period, Pioneer 10 and 11 operations should not be degraded. Because of the time scale of the planned implementation, it was decided that the Pioneer 11 Jupiter encounter should not be supported in the direct interface mode, but rather in the same fashion that the Pioneer 10 Jupiter encounter was supported.

Simplicity of the resulting interface was a primary concern. For this reason, the development of additional interactive computer-to-computer interfaces between ARC and the Deep Space Stations was avoided. In particular, the automatic telemetry recall system will not be implemented in the Direct Interface. It was also a design objective that both the Pioneer Project and the DSN should be able to self-test that they have met the agreed-upon interface prior to calling upon each other to test across that interface.

In order for the implementation of the Direct Interface to be cost-effective, it was deemed necessary to develop an implementation schedule which matched the implementation schedule of the Network Control System. This was so that when the Pioneer processing was no longer necessary in the 360/75 for Pioneer Project purposes, it would also no longer be necessary for DSN Network Operations Control purposes.

The DSN is ordinarily responsible for the quality of the data at the point they are delivered to a Mission Operations Control Center. However, in the case of the Pioneer Mission Operations Control Center located at ARC, there is no DSN equipment nor personnel at the ARC end of the high-speed data system to monitor the quality of the incoming data. For this reason, it was agreed that the Pioneer Project would be responsible for assessing the quality in realtime of the data flowing into the PMOCC.

III. Detailed Design

The functional block diagram for the telemetry and command portion of the Direct Interface Ground Data System is shown in Fig. 2. The Telemetry System involves the implementation in the realtime Sigma 5 system at ARC of additional realtime analysis functions and a logging function for the purpose of producing data records.

The interface for producing the Master Data Record for the Telemetry System will eventually be the Intermediate Data Record (IDR), which will be produced in the Network Control Data Processing Center from the GCF log tape. The IDR will be shipped from JPL to ARC and undergo processing in an off-line Sigma 5 computer in order to produce the Master Data Records and the resulting Experimenter Data Records. The GCF log and IDR will not be a Network Control System capability until December of 1975. In the time frame prior to when the IDR is available, the Telemetry Master Data Record will be produced by the PMOCC using a limited selected recall directly from the Deep Space Stations. This recall will ordinarily be performed during the one-hour post-pass. In order to determine the required recall, there will be realtime accountability software implemented in the Sigma 5 which will produce a summary of missing data upon request. From that summary of missing telemetry data, an operator at ARC will be able to select by computer input a subset of data gaps that should be recalled. A message will then automatically be produced by the Sigma 5 and transmitted over the high-speed data line to a line printer at the Deep Space Stations to list for the station operator the outages that should be recalled from the Digital Original Data Records. No implementation was required by the Deep Space Network for this system of doing telemetry data recalls since the message produced by the Sigma 5 will be compatible with the DSS capability of receiving text messages from the Network Control System.

The Command System is being implemented in a PDP-11 computer at ARC. The Direct Interface will utilize the Mark III-74 Telemetry and Command Processor software known as the Command Redesign. The command message construction, verification, and high-speed block formatting functions will be performed by the PDP-11 computer system. Response message blocks returning from the Deep Space Station will be routed to the PDP-11 for verification, and to the Sigma 5 system for post-transmission processing. Mode change and recall request messages will be generated by the PDP-11 computer. Initialization of the Command System will take place from the Network Control System, although backup

initialization can be accomplished at the DSS in the event of an NCS failure. In order for the NCS to have access to the Command System at the DSS over the same single high-speed data line which interfaces with the PMOCC, a special piece of hardware was developed at JPL. This equipment, known as a Filler Multiplexer, detects filler blocks in the data flowing from the PMOCC and replaces the detected filler blocks with high-speed data blocks from the Network Control System.

There will be three Filler Multiplexers implemented for the Direct Interface, two of them on line and the third functioning as a spare. When station handovers require a third high-speed data line into the PMOCC, the spare Filler Multiplexer will be utilized if available. Special procedures will be required in the event that a third Filler Multiplexer is not available when a handover between stations occurs on one Pioneer spacecraft while another Pioneer spacecraft is being tracked.

The Command MDR will be produced in the Pioneer Mission Operations Control Center, utilizing the same log tape function which will be used for Telemetry Data Records. Ordinarily any missing command messages will be provided by Network Operations Control via voice or written message provided to the Pioneer Mission Operations Control Center.

It was decided that at least in the initial implementation there would be no requirement at ARC to process the monitor data which are present on the in-bound high-speed data line. In the existing Ground Data System, the sequence of events generated at JPL is reformatted in the 360/75 into a high-speed data message which is compatible with existing ARC software. For the Direct Interface, it was necessary to implement in the Sigma 5 realtime system a capability to receive Xerox Data System 6-bit binary coded data, which is the same system used for transmitting text data from the Network Control System to the DSS.

The flow of radio metric data for navigation purposes is unchanged in the Direct Interface and is pictured in Fig. 3. The only difference between the Tracking System end-to-end in the Direct Interface and in the existing Ground Data System is the addition of the off-line Network Control System for the purposes of DSN operations control and the deletion of DSN operations control functions from the 360/75 realtime system. The Pioneer Project Office will look to their existing contract with Division 39 for monitoring any changes to the Tracking System functions in the 360/75.

It was mentioned above that the Direct Interface will utilize the Mark III-74 Telemetry and Command Processor software. The advantages of using this new software in the Direct Interface are that Pioneer Mission Operations will then be utilizing the same new generation of multimission software which will be used for all other missions without the Mission Control and Computing Center having to implement this capability for Pioneer in the 360/75. The disadvantage of using the new software is that, when the direct mode is utilized between the Ames Research Center and the DSS, the Command and Telemetry formats will not be compatible with the existing 360/75 realtime system. This meant that it was not possible to phase the implementation by a gradual buildup of capability, such as implementing the Command System first, then the Telemetry Realtime System, and then the Telemetry MDR. Instead, the Direct Interface must go into operation with the full required capability at one time. Because of this, it was decided to phase the implementation by spacecraft, placing Pioneer 10 operation in the direct mode first prior to Pioneer 11 Jupiter encounter and adding Pioneer 11 to the Direct Interface immediately after Jupiter encounter.

IV. Implementation Status

The implementation of the Direct Interface involves principally software development at ARC but is dependent on the implementation of the Network Control System by the DSN. ARC software development is at the current time on or ahead of schedule. Extensive testing has been in progress on the command portion of the Direct Interface. End-to-end testing of the command portion of the Direct Interface has utilized special configurations at the Deep Space Stations during actual Pioneer 10 and 11 tracking passes. This testing has involved using one Telemetry and Command Processor at the DSS to support the existing Ground Data System configuration with MCCC, and a second Telemetry and Command Processor with the Mark III-74 software configured so as to prevent commands from the second Telemetry and Command Processor from being radiated to the spacecraft. In this way, the testing has been accomplished without requiring additional Deep Space Network resources and without interrupting the ongoing realtime operations on the Pioneer 10 and 11 missions. Essentially all of the test and training for the Direct Interface will be accomplished in this same fashion.

The current plans are leading to having the Direct Interface operational for Pioneer 10 on September 1, 1974 and on Pioneer 11 on January 15, 1975. The opera-

tional date for Pioneer 10 is a compromise between avoiding the Pioneer 11 Jupiter encounter time frame and waiting for the Network Control System to be fully operational. As a result, Pioneer 10 in the direct mode will be utilizing the Block I NCS for two months until the Block II NCS becomes operational on November 1, 1974. Final acceptance testing of the direct mode will take place during the month of August concurrent with extensive activity in preparation for the Helios launch and the Pioneer 11 Jupiter encounter. This scheduling was deemed necessary because postponing the implementation of the Direct Interface to after the Pioneer 11 Jupiter encounter would have placed it on top of the Helios first perihelion, which is in January and February of 1975. Pushing it beyond the Helios first perihelion would have placed it on top of the heavy Viking preparation activity which gets into full swing at that time.

All testing accomplished to date has been highly successful, and no serious difficulty with the implementation has been uncovered. It is anticipated that the most difficult part of the interface to develop will be that portion associated with Telemetry Data Records. Previous experience with developing Telemetry Data Record interfaces on both Pioneer and other missions has shown that a fair amount of operational resources are consumed before the data record production becomes routine. A principal design aspect in the Direct Interface, which it is hoped will alleviate some of these previous problems with data record production, is that the accountability which will take place in the Sigma 5 will be by high-speed data block number rather than by data time. This is the same concept that will be utilized in the design of the NCS GCF log capability. One of the main time-consuming problems in data record production in the past has been the determination of what data should be recalled and what data are available for recall. Using high-speed data block serial number instead of data time should be a better indication that the data are actually available on the Digital Original Data Record at the DSS.

V. Summary

The design of the Direct Interface between the DSN and the Pioneer Project has been completed, and the implementation is well underway. No significant problems have yet been uncovered in the interface implementation and the Direct Interface should eventually provide a simplified and more reliable Ground Data System and operational interfaces for the Pioneer missions.

Reference

1. Miller, R. B., "Pioneer 10 and 11 Mission Support," in *The Deep Space Network Progress Report*, Technical Report 32-1526, Vol. XVIII, pp. 16–19, Jet Propulsion Laboratory, Pasadena, Calif., Dec. 15, 1973.

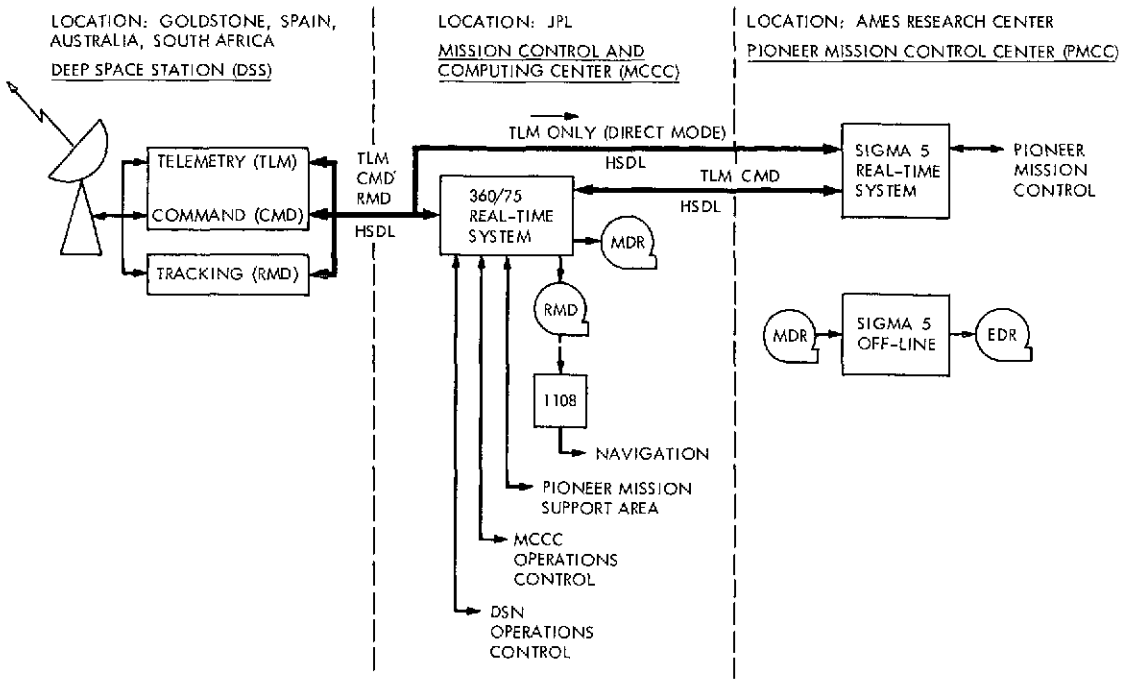

Fig. 1. Existing Pioneer 10 and 11 Ground Data System configuration

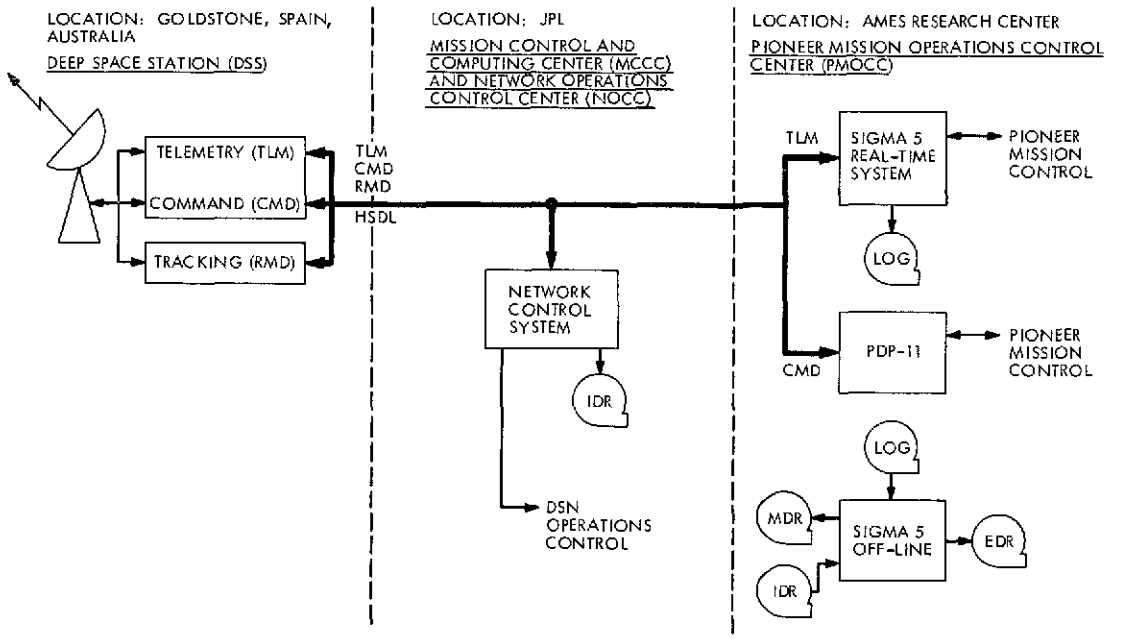

Fig. 2. Pioneer 10 and 11 Direct Interface Ground Data System configuration for Telemetry and Command

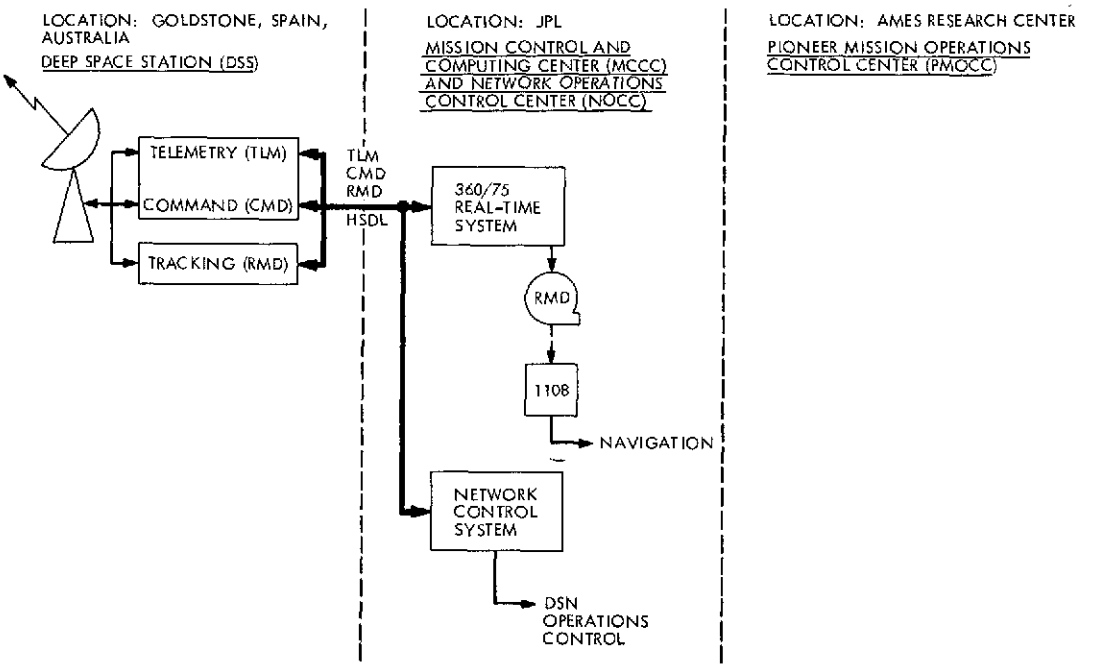

Fig. 3. Pioneer 10 and 11 Direct Interface Ground Data System configuration for radio metric data

A Reformulation of the Relativistic Transformation Between Coordinate Time and Atomic Time

J. B. Thomas
Tracking and Orbit Determination Section

In this report, the relativistic time transformation is reformulated to allow simpler time calculations relating analysis in a solar system frame (using coordinate time) with Earth-fixed observations (using atomic time). After an interpretation of terms, this simplified formulation is used to explain the conventions required in the synchronization of a world-wide clock network. In addition, two synchronization techniques—portable clocks and radio interferometry—are discussed in terms of the relativistic time transformation.

I. Introduction

In the relativistic analysis of the very long baseline interferometry (VLBI) and spacecraft radio metric data, primary calculations are often most conveniently made in a frame at rest with the solar system barycenter. However, observations in these applications are often made relative to an Earth-fixed frame. Consequently, such analyses usually involve a relativistic time transformation (Refs. 1, 2) between the solar system frame (using coordinate time) and Earth-fixed observers (using atomic time). In this report, the time transformation, including both speed and potential terms, is reformulated in order to facilitate both interpretation and analysis in these applications. After an interpretation of the terms in the reformulation, the transformation is used to consider the synchronization conventions associated with a world-wide clock network. Since clock stabilities are beginning to routinely enter a relativisticly significant range (10^{-12} to 10^{-13}), a discussion of such conventions is presently more than an academic exercise. Finally, two synchronization techniques, portable clocks and VLBI, are analyzed in terms of the simplified time transformation.

II. Time Transformation Reformulation

In many VLBI and spacecraft applications, relativistic effects are most conveniently handled by performing primary calculations in a frame at rest with respect to the solar system barycenter and then making a relativistic transformation to Earth-fixed antenna observers. Consequently, these calculations usually involve a relativistic time transformation from the solar system frame

to Earth-fixed observers. In this section, the time transformation is manipulated in a simple manner to cast it in a form that is more convenient for most applications.

In this analysis of the time transformation, approximations will be guided by the following considerations. State-of-the-art oscillator technology (H-maser standards) can, at best, provide clocks with a long-term stability of the order of $\Delta f/f = 10^{-14}$. Because of this instrumental limitation on time measurement, theoretical rate corrections ($d\tau/dt$) of the order of 10^{-15} or less are presently not experimentally significant. Consequently, terms that lead to clock rate corrections of the order of 10^{-15} or less will not be retained in the following analysis.

Suppose that observers in the solar system frame note that a given event occurs at coordinate time t at a given point j on the Earth's surface. Earth-fixed observers at this point will note that the same event occurs at proper time τ_j according to their (atomic) clock. Figure 1 defines the location of point j as measured in the solar system frame. Note that the position vector of point j ($\mathbf{Y}_j$) is represented as the sum of a vector to the Earth center of mass ($\mathbf{X}_e$) and a vector ($\mathbf{X}_j$) from the Earth's center of mass to the given point. This separation of orbit and spin geometry leads naturally to a simplified version of the transformation from coordinate time t to proper time τ_j, as the following manipulations will show.

If one retains only the most significant terms in the metric tensor (i.e., the terms that lead to rate corrections greater than 10^{-15}), then the relativistic transformation (Ref. 1) relating times in the two frames is given by

$$\frac{d\tau_j}{dt} = \left[1 - \frac{(\dot{\mathbf{Y}}_j)^2}{c^2} + \frac{2\phi(\mathbf{Y}_j)}{c^2}\right]^{1/2} \tag{1}$$

where

$$\dot{\mathbf{Y}}_j = \mathbf{V}_e + \mathbf{V}_j$$

and $\phi(\mathbf{Y}_j)$ is the Newtonian potential at point $\mathbf{Y}_j$ in the solar system frame. The order of magnitude of the various terms in Eq. (1) is as follows:

$\frac{V_e}{c} \approx 10^{-4}$ for Earth orbital speed

$\frac{V_j}{c} \approx 10^{-6}$ for Earth observer rotational speed with respect to Earth's center of mass

$\frac{\phi}{c^2} \approx 10^{-8}$ for gravitational potential at Earth's orbit

Therefore, to order 10^{-15} in the rate expression, we have

$$\frac{d\tau_j}{dt} = 1 - \frac{V_e^2 + V_j^2 + 2\mathbf{V}_e \cdot \mathbf{V}_j}{2c^2} + \frac{\phi}{c^2} \tag{2}$$

The last equation must be integrated to give proper time as a function of coordinate time, which yields

$$\tau_j(t) = \tau_c + \tau_j^f + t - t_c - \int_{t_c}^{t} \left[\frac{V_e^2 + V_j^2 + 2\mathbf{V}_e \cdot \mathbf{V}_j - 2\phi}{2c^2}\right] dt \tag{3}$$

where the initial value for $\tau_j(t)$ has been separated into two parts, τ_c and τ_j^f. The term τ_c is common to all clocks while the term τ_j^f allows for possible adopted differences in initial clock readings at $t = t_c$. These terms will be discussed in Section III.

Two terms, $\mathbf{V}_e \cdot \mathbf{V}_j$ and ϕ, will now be manipulated into more useful forms. As shown below, these manipulations lead to a time transformation for Earth-fixed clocks that does not involve an integral over $\mathbf{X}_j$, the clock's motion relative to the Earth's center of mass.

The potential term ϕ can be separated into a sum of two potential terms:

$$\phi(\mathbf{Y}_j) = \phi_e(\mathbf{X}_j) + \phi_R(\mathbf{X}_e + \mathbf{X}_j) \tag{4}$$

where $\phi_e \approx 10^{-9}\ c^2$ is the Earth potential, and ϕ_R is due to all other bodies. The Earth potential is very nearly constant for a given Earth-fixed point, while the potential ϕ_R varies as the clock moves about due to both Earth spin and Earth orbital motion. In order to separate the Earth spin and Earth orbital motion, expand ϕ_R as follows:

$$\phi_R(\mathbf{X}_e + \mathbf{X}_j) \approx \phi_R(\mathbf{X}_e) + \nabla\phi_R(\mathbf{X}_e) \cdot \mathbf{X}_j \tag{5}$$

It is readily shown that quadratic terms in this expansion are of the order of 10^{-17}. If one neglects relativistic terms of the order 10^{-15}, the gradient $\nabla\phi_R$ is the acceleration of Earth's center of mass so that

$$\phi_R(\mathbf{X}_e + \mathbf{X}_j) = \phi_R(\mathbf{X}_e) - \mathbf{a}_e \cdot \mathbf{X}_j \tag{6}$$

The time transformation can be further modified by integrating the $\mathbf{V}_e \cdot \mathbf{V}_j$ term by parts to obtain

$$\int_{t_c}^{t} \mathbf{V}_e \cdot \mathbf{V}_j \, dt = \mathbf{V}_e(t) \cdot \mathbf{X}_j(t) - \mathbf{V}_e(t_c) \cdot \mathbf{X}_j(t_c) - \int_{t_c}^{t} \mathbf{a}_e \cdot \mathbf{X}_j \, dt \tag{7}$$

Substituting Eqs. (4), (6) and (7) in Eq. (3), we obtain the expression

$$\tau_j(t) = t - t_c - \int_{t_c}^{t} \left[\frac{V_e^2 - 2\phi_K(\mathbf{X}_e) + V_j^2 - 2\phi_e(\mathbf{X}_j)}{2c^2} \right] dt - \frac{\mathbf{V}_e(t) \cdot \mathbf{X}_j(t)}{c^2} + \frac{\mathbf{V}_e(t_c) \cdot \mathbf{X}_j(t_c)}{c^2} + \tau_j^I + \tau_c \tag{8}$$

Note that the two acceleration integral terms produced by the velocity and potential terms have canceled. Furthermore, except for the $\mathbf{V}_e \cdot \mathbf{X}_j$ terms, the orbital and spin motions have been separated.

For a clock fixed with respect to Earth, the speed V_j and potential $\phi_e(\mathbf{X}_j)$ are constant to about one part in 10^9. Therefore, to excellent approximation, we obtain for an Earth-fixed clock

$$\tau_j(t) = t - t_c - \int_{t_c}^{t} \left[\frac{V_e^2 - 2\phi_K(\mathbf{X}_e)}{2c^2} \right] dt - \frac{\mathbf{V}_e(t) \cdot \mathbf{X}_j(t)}{c^2} + \frac{\mathbf{V}_e(t_c) \cdot \mathbf{X}_j(t_c)}{c^2} - \left[\frac{V_j^2 - 2\phi_e(\mathbf{X}_j)}{2c^2} \right] (t - t_c) + \tau_j^I + \tau_c \tag{9}$$

These expressions for proper time simplify the analysis of clock synchronization which follows.

III. Clock Synchronization Conventions

World-wide timekeeping is now accomplished by a network of atomic clocks placed at various locations over the Earth. In this network, member clocks are periodically synchronized with a master clock, which is carefully maintained at a fixed location. ("Master clock" in practice is the average time reading of a set of reference atomic clocks. Specific techniques for synchronization will be discussed in Section V on the basis of the relativistic transformation.) Present synchronization work, based on the principles of classical physics, assumes that clocks, once synchronized in time and rate, will continue to indicate the same times, within instrumental accuracy, wherever they are moved on Earth's surface. However, relativistic analysis, such as Eq. (8), indicates that classical assumptions may not be adequate if clock accuracies surpass the μs level in time and the 10^{-12} level in rate. That is, sufficiently accurate clocks can lose synchronization due to relativistic effects if they are separated on the Earth's surface. Consequently, an accurate clock network based on relativity theory must take these effects into account.

An understanding of the synchronization problem is facilitated by the relativistic formulation in Eq. (9) which connects coordinate time with the proper time of a given Earth-fixed clock. Even though this equation is not a direct comparison of Earth-fixed clocks, it contains all the information needed to study the synchronization problem, provided the various terms are properly interpreted. The following discussion attempts such an interpretation with emphasis on the establishment of synchronization conventions. Even though some aspects of this discussion are relatively well-known, they have been included, sometimes without reference, for the sake of completeness.

First, we will divide the terms of the time transformation Eq. (9) into two categories, terms that are the same for all clocks and terms that are different:

$$\tau_j(t) = t - t_c + \Delta t_s + \Delta t_j + \tau_c \tag{10}$$

where the common terms are given by

$$\Delta t_s \equiv -\int_{t_c}^{t} \frac{V_e^2 - 2\phi_K(\mathbf{X}_e)}{2c^2} \, dt \tag{11}$$

and the clock-specific terms by

$$\Delta t_j \equiv -\left[\frac{V_j^2 - 2\phi_e(\mathbf{X}_j)}{2c^2} \right] (t - t_c) - \frac{\mathbf{V}_e(t) \cdot \mathbf{X}_j(t)}{c^2} + \frac{\mathbf{V}_e(t_c) \cdot \mathbf{X}_j(t_c)}{c^2} + \tau_j^I \tag{12}$$

The common term Δt_s contains the factors that cause the same rate offset for all clocks: the speed of the Earth center-of-mass and the "clock-invariant part" of the potential which is located at the Earth center-of-mass. Since this term is common to all clocks in the network, it will not cause a loss of synchronization. That is, this term is not significant in "Earth-bound" comparisons of clocks but is significant in transformations from Earth-fixed

clocks to coordinate time. In practice, the common term must be modified to account for any conventions affecting overall clock rates. For example, in principle, the present system defines the second so that all clocks run at the same average rate as coordinate time (Ref. 1). This rate definition is represented formally in Δt_s by subtracting the time-average rate from the total rate in Eq. (11) as follows.

$$\tilde{\Delta t}_s \equiv \Delta t_s - \overline{\Delta t}_s = -\int_{t_c}^{t} \frac{\Delta V_e^2 - 2\Delta\phi_R(\mathbf{X}_e)}{2c^2}\, dt \qquad (13)$$

where

$$\Delta V_e^2 = V_e^2 - \overline{V_e^2}$$

$$\Delta\phi_R = \phi_R - \overline{\phi_R}$$

This rate adjustment, which is of the order of 10^{-8}, leaves only the periodic effects in Δt_s. Even though these periodic effects do not cause loss of synchronization, they must still be included in transformations between proper time and coordinate time. For example, the predominant effect, orbital eccentricity, has an integrated amplitude of approximately 2 ms and an annual period.

The clock-specific term Δt_j can lead to synchronization loss between Earth-fixed clocks. This term can be subdivided into three categories of time dependence: constant, linear, and periodic. The constant terms are defined by the synchronization convention established below.

In the second category, the linear term, $[v_j^2/2 - \phi_e]$ $(t - t_c)$, is a rate correction based on clock geopotential and speed relative to Earth's center of mass. Note that this term is essentially the effective potential at point $\mathbf{X}_j$ as seen in an Earth-fixed frame. That is, the gradient of $V_j^2/2 - \phi_e$ gives the sum of the "centrifugal force" and gravitational force at that point. Since mean sea level represents, to good approximation, a surface of constant effective potential, clocks at sea level should run at essentially the same rate without relativistic corrections. However, for two arbitrary Earth-fixed clocks, the differential rate correction is easily calculated on the basis of differential altitude by the approximate formula $g\Delta h$, which predicts that the rate correction changes by approximately 1.1×10^{-13} per kilometer of altitude above mean sea level. For airborne clocks, it is readily shown that differential rate corrections of the order of 10^{-12} are possible. (In the airborne case, of course, $V_j^2 - 2\phi_e$ is not necessarily a constant at a given altitude since the clock is no longer an Earth-fixed object).

Finally, in the third category, the periodic term $\mathbf{V}_e(t) \cdot \mathbf{X}_j(t)$ is never greater than 2 μs and is essentially diurnal since $\mathbf{V}_e$ changes very little over one day. This term is a relativistic consequence of the time transformation between frames and corresponds to the special relativity clock synchronization correction. That is, it accounts for the relativistic principle that simultaneous events in one frame are not necessarily simultaneous in a frame passing by with speed V_e. Consequently, it is of significance in transformations from Earth-fixed time to coordinate time but is not present in "Earth-bound" comparisons between Earth-bound clocks. This fact is supported analytically by noting that the periodic term "changes" to match another clock if the two clocks are brought together on Earth.

The following conventions regarding synchronization are designed to accommodate these clock-specific terms. Since the linear terms can lead to gross disagreements between clocks over long time periods, they will be removed, either explicitly or implicitly, by making appropriate location-dependent definitions of clock rate. In principle, these corrections could be applied by means of explicit on-site rate adjustments based on a fundamental physical process. For example, at each location a second could be established in terms of a particular altitude-dependent number of cycles (Ref. 3) on a cesium beam frequency standard where the cycle-count differential between altitudes would be based on the calculated differential in effective potential. Since these rate adjustments are of the order of 10^{-13}, the oscillators would necessarily have to be capable of independent (absolute) calibration at a few parts in 10^{-14}. Unfortunately, routine calibrations at this level are not feasible at present. In practice, this rate adjustment will be implicitly applied in a differential sense whenever a worldwide clock network is kept in time synchronization. For example, as in the present system, a "master clock" would be utilized, at a given location, to define the second and maintain a reference time. Other clocks over the world would then be forced into synchronization by means of "Earth-bound" synchronization techniques (see Section V). Since the synchronization process prevents clock divergence, the appropriate differential rate correction will automatically be implicitly applied without recourse to relativistic calculations.

Since the periodic term $\mathbf{V}_e(t) \cdot \mathbf{X}_j(t)$ does not affect the synchronization of Earth-bound clocks, it is not of consequence in the establishment of a synchronization convention.

In order to complete the synchronization convention, the constant term τ_j' must be defined. This term will be defined by requiring that the clocks exhibit zero disagreement *on the average* according to solar system observers. This goal is accomplished by letting

$$\tau_j' = -\mathbf{V}_e(t_c)\cdot\mathbf{X}_j(t_c)/c^2 \tag{14}$$

As we shall see in Section V, this definition is appropriate for synchronizing clocks according to Earth-bound observers.

By applying the definitions and conventions described above, one obtains a standardized time transformation for clock j:

$$\tilde{\tau}_j(t) = t - t_c - \int_{t_c}^{t} \frac{\Delta V_c^2 - 2\Delta\phi_R(\mathbf{X}_c)}{2c^2}\,dt - \frac{\mathbf{V}_e(t)\cdot\mathbf{X}_j(t)}{c^2} + \tau_c \tag{15}$$

Note that the time transformation no longer involves an integral over clock coordinates but only over coordinates for the Earth's center-of-mass. Therefore, relative to the original transformation, time calculations are much simpler.

In summary, with the conventions outlined above, the network clocks would be given selected initial times (at coordinate time t_c) and the same average rate (i.e., $d\tau/dt = 1$) according to solar system observers. With these conventions, the clock network could be kept in synchronization according to Earth-bound observers by means of two synchronization methods now in use. These two techniques, portable clocks and VLBI, will be discussed in Section V in terms of these synchronization conventions.

IV. VLBI Time Delay

The VLBI time delay is readily calculated using Eq. (15) as follows. Suppose that radio waves emitted by a distant source are observed by two Earth-fixed antennas. Let a given wavefront reach antenna 1 at time t and antenna 2 at t' when observed in the solar system frame. According to the two antenna teams, the wavefront arrives at time $\tilde{\tau}_1(t)$ at antenna 1 and time $\tilde{\tau}_2(t')$ at antenna 2. When the two antenna teams compare arrival times, they will calculate the "geometric" delay:

$$\tau_g(t) \equiv \tilde{\tau}_2(t') - \tilde{\tau}_1(t) \tag{16}$$

We have assumed that the antenna clocks have been synchronized according to the conventions described in Section III.

Since $|t' - t|$ is less than 30 ms for Earth-fixed baselines, the terms containing t' can be expanded about t to yield

$$\tau_g(t) = \tilde{\tau}_2(t) - \tilde{\tau}_1(t) + \dot{\tilde{\tau}}_2(t)\,(t' - t) \tag{17}$$

$$= \left[1 - \frac{\Delta V_c^2 - 2\Delta\phi_R(\mathbf{X}_c)}{2c^2} - \frac{\mathbf{V}_e\cdot\mathbf{V}_2}{c^2}\right](t' - t) - \frac{\mathbf{V}_e(t)\cdot\mathbf{B}(t)}{c^2} \tag{18}$$

where the baseline $\mathbf{B}$ equals $\mathbf{X}_2 - \mathbf{X}_1$. In this expression, we have neglected a $\mathbf{a}_e\cdot\mathbf{x}$ term and terms of order higher than the first in $t' - t$ with negligible loss of accuracy. Note that the geometric delay is equal to the "coordinate time delay", $t' - t$, plus transformation corrections of two types. The first type is a "time dilation" correction, consisting of three terms proportional to $t' - t$. It is easily demonstrated that these terms are less than 0.5 cm in magnitude. Consequently, these corrections are of marginal importance for even the most ambitious VLBI applications.

The second correction category, which corresponds to the clock synchronization correction (or aberration correction) found in a special relativity treatment, can be estimated as follows:

$$\frac{\mathbf{V}_e\cdot\mathbf{B}}{c} \lesssim 10^{-4} \times 6000\ \text{km} = 600\ \text{m} \tag{19}$$

Since $\mathbf{V}_e$ changes very little over a day, this term exhibits essentially diurnal time variations. In time delay calculations, this large correction must be treated very precisely.

Up to this point, the coordinate time delay $t' - t$ has been treated in a general fashion and could denote any two events recorded by relevant solar system observers. In VLBI applications, the times, t and t', denote the arrival times of a given wavefront at two antennas as seen by solar system observers. The description of this wavefront in VLBI applications can be divided into two formulations: a plane-wave description for sources at "infinite" distances (e.g., extragalactic sources) and a spherical wave description for "close" sources (e.g., a

spacecraft in the solar system). Since this article is primarily concerned with the relativistic time transformation of a given coordinate time delay from solar system observers to antenna observers, a general discussion of delay calculations, including all factors, will not be attempted. However as an example, the time delay for an extragalactic source will be analyzed.

The time delay for an extragalactic source can be derived by first calculating the delay observed in the solar system frame and then transforming to antenna observers according to Eq. (18). We will give the signal a plane-wave representation that ignores transmission media and general relativity effects. According to solar system observers, the delay for a plane wave is easily shown to be given by

$$t' - t = -\frac{\mathbf{S}\cdot\mathbf{B}}{c\,[1 + \mathbf{S}\cdot(\mathbf{V}_e + \mathbf{V}_2)/c]} \tag{20}$$

where S is a unit vector in the direction of the radio source relative to the solar system barycenter. The observed time delay is obtained by inserting this expression into the time transformation, Eq. (18), to obtain

$$\tau_g(t) = -\left[1 - \frac{\Delta V_c^2 - 2\Delta\phi_R}{2c^2} - \frac{\mathbf{V}_e\cdot\mathbf{V}_2}{c^2}\right] \cdot \frac{\mathbf{S}\cdot\mathbf{B}}{c\,[1 + \mathbf{S}\cdot(\mathbf{V}_e + \mathbf{V}_2)/c]} - \frac{\mathbf{V}_e(t)\cdot\mathbf{B}(t)}{c^2} \tag{21}$$

All quantities in this expression are evaluated at time t, the time the wave front reaches antenna 1.

As an alternate approach, the geometric delay can easily be derived to order v/c on the basis of a geocentric approximation (Ref. 4). In that derivation, the $\mathbf{V}_e\cdot\mathbf{B}$ term enters the delay as a result of the aberration correction to the source direction. As indicated by the two derivations, this large term can be viewed in two ways. For Earth-bound observers, it is a *geometric* correction applied to the position of the source. For solar system observers, it is viewed as a *time* correction representing a loss of synchronization between Earth-fixed clocks.

The preceding analysis of the geometric delay will facilitate the discussion of VLBI clock synchronization that follows in the next section.

V. Clock Synchronization Techniques

This section will show how two synchronization techniques, portable clocks and VLBI, can be used to synchronize a world-wide clock network according to the synchronization conventions defined in Section III. The portable clock technique will be discussed first.

In the present world-wide timekeeping network, a set of atomic clocks ("the master clock") at one location is used to define a reference time. Clocks at other locations around the world are periodically resynchronized by comparing them with a portable clock that is carried to each member clock. Before traveling overseas each time, the portable clock is synchronized on-site with the master-clock. In this manner, a world-wide network of clocks is kept in synchronization at the level allowed by the instrumental and transportation stability of the clocks involved.

Let a portable clock be synchronized with the master clock at coordinate time, $t = t_0$. Then let the portable clock follow some path[1] $\mathbf{X}_p(t)$ over Earth to some member of the clock network. (Note that $\mathbf{X}_p(t)$ and $\mathbf{V}_p(t)$ consist of Earth-spin effects as well as clock transportation). After the portable clock has reached the member clock j at time t', the clock-specific correction for the portable clock will be

$$\Delta t_p = -\int_{t_0}^{t'} \frac{V_p^2(t) - V_m^2 - 2\,[\phi_e(\mathbf{X}_p) - \phi_e(\mathbf{X}_m)]}{2c^2}\,dt - \frac{\mathbf{V}_e(t')\cdot\mathbf{X}_j(t')}{c^2} \tag{22}$$

where V_p and V_m are the geocentric speeds of the portable and master clock. (We have not included the other terms in Eq. (10) in this discussion since they are common to all clocks and do not affect synchronization). The integral term in this expression accounts for the fact that the master clock rate adjustment (passed on to the portable clock during synchronization) will not suppress the $V_p^2 - 2\phi_e$ integral for the portable clock once it starts its journey and changes its geocentric position and speed.

According to the synchronization convention established in Section III, the portable clock-member clock comparison must be handled as follows. The desired value for the member clock is given by

$$\Delta t_j = -\frac{\mathbf{V}_e(t')\cdot\mathbf{X}_j(t')}{c^2} \tag{23}$$

[1]Relative to Earth center-of-mass.

Thus, comparing Eq. (22) and Eq. (23), we see that the portable clock must be corrected to account for the speed-potential integral that has accumulated in transit:

$$\Delta\tau_p = \Delta t_p - \Delta t_j = -\int_{t_0}^{t'} \frac{V_p^2(t) - V_m^2 - 2\left[\phi_e(\mathbf{X}_p) - \phi_e(\mathbf{X}_m)\right]}{2c^2}\, dt \quad (24)$$

For one day transit times, this correction can be of the order of $10^{-12} \times 10^5$ s = 100 ns. Furthermore, the portable clock rate will differ from the conventional rate for site j by

$$\frac{V_j^2 - V_m^2 - \phi_e(\mathbf{X}_j) - \phi_e(\mathbf{X}_m)}{2c^2}$$

so that clock rate comparisons must include this correction factor. Thus, we see that, during transit, the periodic term $\mathbf{V}_e \cdot \mathbf{X}_p$ changes into the appropriate value while the linear term loses its adjustment and must be corrected.

It is interesting to note that the integral contained in Eq. (24) is essentially the theoretical time gain predicted by Hafele and Keating for their Earth-circumnavigation experiment (Ref. 5). In that paper, theoretical calculations only considered geocentric speed and geopotential effects. With a more general approach, the present formulation indicates that this integral is the total time gain, provided one can neglect rate terms less than 10^{-15}. Thus, the warning in Ref. 5 that effects of the sun and moon may not be entirely negligible appears to be unwarranted for present clock stabilities.

Clock synchronization by means of VLBI is conceptually, if not operationally, straightforward. For a given natural source, the time delay is measured between two antennas and appropriately corrected for transmission media and instrumental delays. The resulting delay should be equal to the geometric delay calculated according to Eq. (21). (We assume here that geophysical and astronomical parameters are known with sufficient accuracy.) Any difference between the measured delay and the calculated delay represents the synchronization loss between antenna clocks. In this manner, a world-wide system of clocks could be synchronized at interferometer accuracies.

VI. Experimental Tests

In a treatment of this nature, some discussion should be devoted to the tests of relativity that are suggested by the reformulation. As indicated in Section III, only the "effective potential" term will be evident in "Earth-bound" comparisons of Earth-bound clocks. Contingent on instrumental feasibility, several Earth-bound experiments might be suggested to test the presence of this effect. One experiment, involving airborne clocks (Ref. 5), has already been carried out. As an alternate approach, an experiment could be designed to take advantage of the clock synchronization precision of the VLBI technique. Time synchronization at the 10 ns level is now feasible with current VLBI instrumentation (Ref. 4). With this precision, a typical Earth-fixed rate differential of 10^{-13} (1 km altitude differential) would be visible in about three days. However, a test of this type requires "station-clock" rate stability and calibration at a few parts in 10^{-14}. Except perhaps at standards labs, this clock requirement would presently be the most difficult aspect of the VLBI approach.

VII. Summary

In the preceding sections, a reformulation of the relativistic time transformation has simplified interpretation of the various effects entering the transformation between coordinate time and Earth-bound proper time (atomic time). Based on this analysis, the conventions required for the synchronization of a world-wide clock network have been investigated. In addition, the new formulation has simplified a relativistic analysis of the "geometric" delay measured in VLBI applications. Finally, a brief discussion has been devoted to possible "Earth-bound" experimental tests of predictions of the theory.

References

1. Moyer, T. D., *Mathematical Formulation of the Double-Precision Orbit Determination Program,* Technical Report 32-1527, Jet Propulsion Laboratory, Pasadena, May 1971.

2. Ash, M. E., "Determination of Earth Satellite Orbits," Technical Note 1972-5, Lincoln Laboratory, Lexington, Mass., April, 1972.

3. Moyer, T. D., "Expressions for ET-A1 and UTC-ST in the ODP," TM 391-396, December 1972 (JPL internal document).

4. Thomas, J. B., "An Analysis of Long Baseline Radio Interferometry," in *The Deep Space Network Progress Report,* Technical Report 32-15, Vol. VII, Feb. 15, 1972.

5. Hafele, J. C., and Keating, R. E., "Around-the-World Atomic Clocks: Predicted Relativistic Time Gains," *Science,* Vol. 177, p. 166, July 1972.

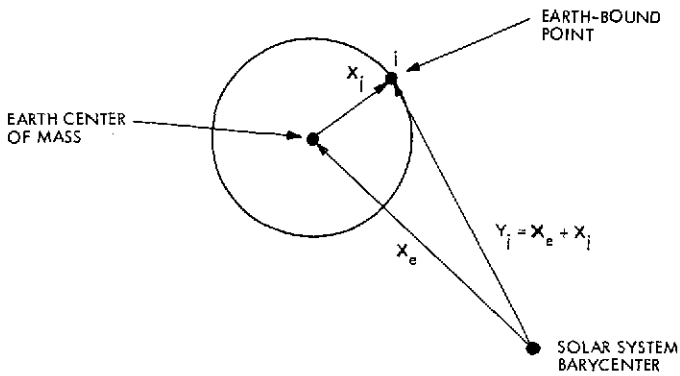

Fig. 1. The position vector of Earth-bound point *j* as measured by solar system observers

Results of the Tau/Mu Alternate Ranging Demonstration

B. D. L. Mulhall[1]
DSN Systems Engineering

F. Borncamp[2]
Network Operations

D. E. Johnson
Tracking and Orbit Determination Section

On August 14, 1971, an experiment to determine the relative accuracies of the Tau ranging machine and the Mu ranging machine was performed at the Goldstone Deep Space Communications Complex. The results of this demonstration are described. The two ranging measurements agreed to 7.925 ns over the pass.

I. Introduction

On August 14, 1971, an experiment involving the Tau ranging machine at DSS 14, the Mu ranging machine at DSS 12, and the Mariner 9 spacecraft was performed to determine the relative accuracies of the two ranging machines. The result of this demonstration is summarized in Table 1.

II. Experiment Procedures

The experiment was performed by ranging the Mariner 9 spacecraft from DSS 12 for approximately 30 minutes. The spacecraft was then handed over to DSS 14 where ranging data were taken for the next 30 minutes. The spacecraft was then returned to DSS 12 for the next range point. This procedure was repeated until six independent Mu range points were recorded by DSS 12. Groups of Tau range points clustered in five groups were recorded between the Mu data points.

The delay through both stations was measured before and after the test. Faraday rotation measurement of the ionosphere and radiosonde balloon measurements of the troposphere were obtained for the same period.

The ranging data obtained were processed by the DSN Tracking System. The data were fitted by the Tracking Data Editor (TRKED) Program (Ref. 1). Figure 1 shows the range residuals produced by TRKED after two iterations. The data were corrected as described below. The Mu points were averaged (nominally 20 minutes) and related to time of initial acquisition by

[1]This work was performed when Mr. Mulhall was in the Mission Analysis Division.

[2]This work was performed when Mr. Borncamp was in the Telecommunications Division.

linear extrapolation. The Tau data for the last acquisition by DSS 14 were not usable for some unknown reason.

The equations for a differenced range observable are given in Ref. 2 along with a discussion of the errors for an intercontinental baseline. The error for this type of observable is given as

$$\begin{aligned}\epsilon_{\rho_{\mathrm{DSS}\,12}-\rho_{\mathrm{DSS}\,14}}(t) = {} & [z_b \cos\delta_{s/c} - r_b \sin\delta_{s/c} \\ & \times \cos(\alpha_{s/c} - \alpha_b)]\,\epsilon_{\delta_{s/c}} \\ & - r_b \cos\delta_{s/c} \sin(\alpha - \alpha_B) \\ & \times [\epsilon_{\alpha_{s/c}} - \epsilon_{\alpha_b}] + \sin\delta\,\epsilon_{z_b} \\ & + \cos\delta\cos(\alpha_{s/c} - \alpha_b)\,\epsilon_{r_b} \\ & + \epsilon_{\text{measurement system}}\end{aligned}$$

where

z_b, r_b, α_b = baseline z-height, equatorial projection length and right ascension at time t. (These quantities are functions of polar motion and UT1)

$\delta_{s/c}, \alpha_{s/c}$ = declination and right ascension of the spacecraft at time, t

$\epsilon_{()}$ = error of subscripted term

$\epsilon_{\text{measurement system}}$ = includes uncertainties in calibrations applied for transmission media, ground link delays, clock synchronization and rate differences and spacecraft transponder delay. (For the work reported in this paper, signal-to-noise ratio (S/N) dependent errors are assumed negligible because of the relatively long averaging times)

For the short baseline case (as opposed to the intercontinental baseline case discussed in Ref. 2) the difference in transmission effects will also be negligible.

The other contributors to the error in range differences are discussed below and their effects are illustrated in Fig. 2.

The errors which can bias the data are:

(1) Differences in station height above the equatorial plane

(2) Spacecraft declination error

(3) Station clock offset

(4) Station frequency differences

(5) Station zero delay calibration difference

III. Difference in Station Height Above Equatorial Plane

DSSs 12 and 14 have been linked by ground surveys (Ref. 3) and very-long-baseline interferometry (VLBI). The largest uncertainty is in the difference in height for DSSs 12 and 14 which is inferred to better than 50 cm by comparing these survey measurements. The relative station equatorial height uncertainty of 50 cm would cause an error in range measurement between the two stations of 1.5 ns. This error is not negligible for the short baseline experiment, and will have to be measured by VLBI for long baseline alternate range experiments. Errors in polar motion and UT1 have a negligible effect due to the relatively short baseline between DSSs 12 and 14.

IV. Spacecraft Declination Error

An error in spacecraft declination can cause a bias in measurement in range from two stations. If the spacecraft declination were in error by 0.1 arcsec, this would cause an error of 30 ps (3×10^{-2} ns) in round-trip time measurements for the two stations.

Consequently, since the spacecraft declination is known to much better than 0.1 arcsec, this is a negligible error.

V. Station Clock Offset

The error in station clocks—that is the offset between the two clocks—can produce an error in their relative measurement of range. This error is multiplied by the spacecraft velocity. The Mariner 9 has a geocentric velocity of 7 km/s on August 14, based on the Double Precision Trajectory Program, (DPTRAJ) calculations (Ref. 4). The clock offset between DSSs 12 and 14 amounted to Station 14 lagging Station 12 by 18.2 μs. This causes a measurement of range from Station 14 to be greater than the range measured at Station 12 by 0.9 ns. This error is not negligible and the Tau data were adjusted. For long baseline alternate range experiments, clock offsets should be measured to remove this bias. Uncertainties of less than 1 μs in the determination of the clock offset are negligible.

VI. Station Frequency Difference

The clock (Varian R20 Rubidium standard) at DSS 14 was running faster than the clock at DSS 12, which caused an error of 1.1 ns (DSS 14 range measurement was greater than DSS 12) and the Tau data were adjusted. The accuracy of this calibration leaves an uncertainty $\sigma_{\Delta f/f}$ of 2 to 6×10^{-12}. For the signal round-trip time of 173 s this causes an 0.1 to 0.3 m uncertainty in the differenced range.

VII. Station Ranging Calibration

The delay through the station as measured with the zero delay device for DSS 12 was 2140 ns. For DSS 14, the delay was 911 ns. The difference, 1229 ns, was removed from the data prior to the fitting by TRKED. Clearly, this quantity will always have to be measured for any future work. The calibration certainty σ_{delay} of 3 to 7 ns for each station results in a 1.3 to 3 m uncertainty in the differenced range.

VIII. Variations in Transponder Ranging Delays

There are two possible sources of different ranging delays through the spacecraft transponder. Namely, those due to the fact that the Mu and Tau systems have different side characteristics and those due to the difference in uplink S/N between DSS 12 and DSS 14. The total effect due to these two sources is assumed to be between 0.1 and 0.5 m.

IX. Conclusions and Recommendations

The remarkable consistency of the Tau and Mu ranging machines indicates that long baseline experiments, for example, California/Australia, are feasible and should be conducted. The relative accuracy of the two range measurements of one meter for the Mariner 9, which was 3×10^{10} meters from the Earth on August 14, amounts to better than one part in 10^{10}.

Acknowledgment

The authors wish to thank C. F. Peters for help in using TRKED and W. L. Martin, R. W. Tappan, D. W. Trask, S. K. Wong, and J. W. Zielenbach for their helpful suggestions in analysis of the data.

References

1. Peters, C. F., *User's Guide for the TRKED, Mark I, Mode 5 Program*, IOM 391.13-458, Mar. 1, 1972 (JPL internal document).

2. Rourke, K. H., and Ondrasik, V. J., "Application of Differenced Tracking Data Types to the Zero Declination and Process Noise Problems," in *The Deep Space Network Progress Report*, Technical Report 32-1526, Vol. IV, Jet Propulsion Laboratory, Pasadena, Calif., Aug. 15, 1971.

3. Thomas, J. B., et al., "Radio Interferometry Measurements of a 16-km Baseline With 4-cm Precision," in *The Deep Space Network Progress Report*, Technical Report 32-1526, Vol. XVIII, Jet Propulsion Laboratory, Pasadena, Calif., Dec. 15, 1973.

4. Khatib, A. R., *DPTRAJ Program, Vol. I, Design and Implementation of Models*, Document 900-495, June 30, 1972 (JPL internal document).

Table 1. Mu/Tau alternate range residuals

Mu residuals, ns			Tau residuals, ns		
Mean	Std. Dev.	No. of points	Mean	Std. Dev.	No. of points
22.7	62	26			
−35.6	50	26	8.6	9	4
−16.7	42	26	0.1	11	35
18.6	50	26	0.9	11	79
−9.0	61	26	−2.3	15	24
−16.6	57	26	[a]	[a]	[a]

Summary over pass	Mean	Std. Dev.
Mu data	−6.10	22.5
Tau data	1.825	4.7
Difference	−7.925	

[a]See text, Section II, paragraph 3.

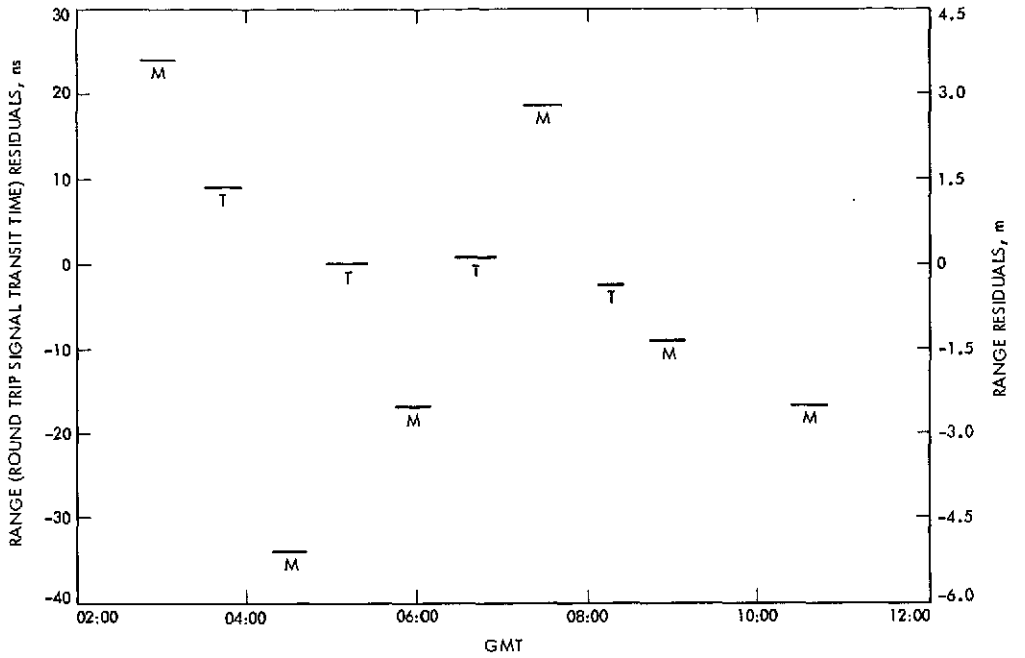

Fig. 1. TRKED range residuals, Mu versus Tau range

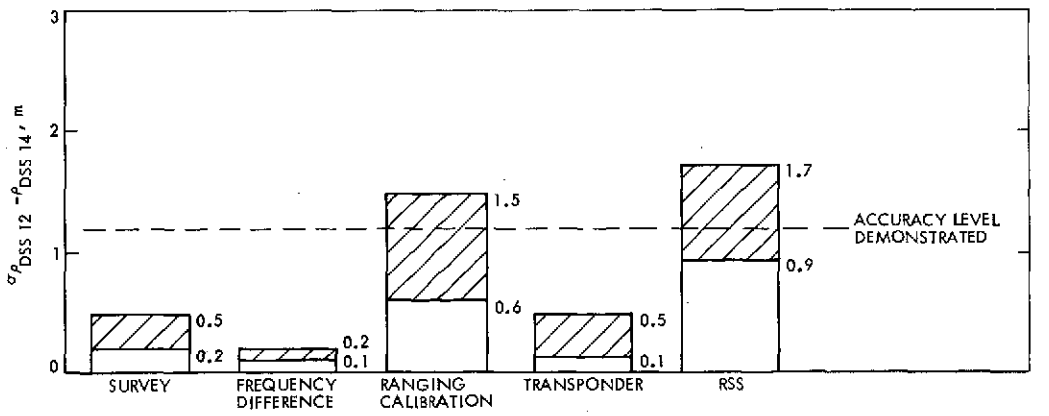

Fig. 2. Limitations to differenced range measurements for Mariner 9 demonstration

Three Topocentric Range Measurements to Pioneer 10 Near Jupiter Encounter and a Preliminary Estimate of an Earth Barycenter to Jupiter Barycenter Distance

A. S. Liu
Tracking and Orbit Determination Section

By using ground digitally controlled oscillator (DCO) apparatus installed at Goldstone (DSS 14) and Ballima, Australia (DSS 43), ramped carrier frequency doppler data were received from Pioneer 10 just prior to and shortly after Jupiter encounter. The analysis of these DCO doppler data resulted in three independent topocentric range measurements. These range measurements were individually accurate to at least ±5 km. The observed accuracy was 500 m but because of suspected systematic errors which were masked by the orbit adjustment procedure the actual accuracy was probably larger than 500 m. From the data residuals based on local orbital adjustments, the DCO data were no different from conventional doppler. The data error was on the order of 2 mHz. A longer solution was also attempted, whereby a Jupiter barycenter to Earth barycenter distance was found. The difference between the estimated barycenter-to-barycenter distance and that from the reference planetary ephemeris DE84 was −107 km. This difference was not significant because DE84 has a one standard deviation error of 250 km.

I. Introduction

Three passes of Pioneer 10 data near Jupiter using the Deep Space Network's digitally controlled oscillator (DCO) devices at Goldstone (DSS 14) and Ballima, Australia (DSS 43) were analyzed. Two of the passes of data were taken about 10 days before encounter and the last pass about a week after encounter. Each of the passes possessed a 100-Hz/s S-band sawtooth carrier frequency pattern, which lasted about 20 min. The data were reduced to three topocentric spacecraft range estimates with an estimated accuracy of 5 km in one-way range. The random noise observed on all of these passes was about 1.5 mHz. A larger data sample comprising of a continuous set beginning on November 23, 1973 and ending on December 13, 1973 was also analyzed. This larger set contained the three aforementioned DCO data; this entire span of data was used to infer an Earth–moon barycentric to Jupiter + moon barycentric distance at Jupiter encounter on December 4, 1973.

This determination was compared with the barycenter-to-barycenter distance as tabulated by JPL Development Ephemeris 84 (DE84), an ephemeris which was based on

previous optical observations. This ephemeris placed an uncertainty of ±250 km in the barycenter-to-barycenter distance on December 4, 1973. Our orbit reduction gave a shift of −107 km from DE84 in the barycenter-to-barycenter distance. This shift is within the acknowledged uncertainty of ±250 km in this coordinate of DE84.

II. Analysis and Measurement Errors

The received observable ϕ is the difference between the accumulated (integrated) cycles at time t of received signal and a locally accumulated reference. Assume that at time t_1, $C(t_1)$ cycles were transmitted to the spacecraft. At a later time t_3, $C(t_1)$ is received again at the ground. The ground reference cycle is $C(t_3)$. Assume further that there were no cycles "lost" between transmission and reception due to troposphere, ionosphere, etc. The observable $\phi(t_3)$ is then:

$$\phi(t_3) = C(t_3) - C(t_1) + \phi_0 \tag{1}$$

where ϕ_0 is an arbitrary number of cycles or phase and

$$C(t) = \int_{t_0}^{t} \omega(\tau)\, d\tau \tag{2}$$

$$C(t) = \int_{t_0}^{t} [\omega_0 + \dot{\omega}(\tau - t_0)]\, d\tau$$

$$= \omega_0 (t - t_0) + \frac{\dot{\omega}}{2}(t - t_0)^2$$

where

ω = phase rate

τ = station time

t_0 = ramp initiation time

ω_0 = some reference frequency

$\dot{\omega}$ = frequency ramp

Thus, at reception time t_3, the observable is

$$\phi(t_3) = \omega_0 (t_3 - t_1) + \frac{\dot{\omega}}{2}[(t_3 - t_0)^2 - (t_1 - t_0)^2] + \phi_0$$

$$= \omega_0 (t_3 - t_1) + \frac{\dot{\omega}}{2}[(t_3 - t_1)^2 + 2(t_3 - t_1)(t_1 - t_0)] + \phi_0 \tag{3}$$

We recognize $(t_3 - t_1)$ to be the round-trip time of the signal.

Let

c = speed of light

$R = c(t_3 - t_1)$ = two-way range

$$\phi(t_3) = \frac{\omega_0 R}{c} + \frac{\dot{\omega}}{2c^2}R^2 + \frac{\dot{\omega}}{c}R(t_1 - t_0) + \phi_0 \tag{4}$$

At a later or subsequent reception time t_3', the observable is

$$\phi(t_3') = \frac{\omega_0 R'}{c} + \frac{\dot{\omega}}{2c^2}R'^2 + \frac{\dot{\omega}}{c}R'(t_1' - t_0) + \phi_0 \tag{5}$$

To eliminate the unknown arbitrary constant ϕ_0, the phase counts at t_3' and t_3 are differenced:

$$\Delta\phi(T) = \phi(t_3') - \phi(t_3)$$

$$= \frac{\omega_0 (R' - R)}{c} + \frac{\dot{\omega}}{c}[R'(t_1' - t_0) - R(t_1 - t_0)] + \frac{\dot{\omega}}{2c^2}(R'^2 - R^2) \tag{6}$$

The differenced cycle or phase count $\Delta\phi$ can be associated with any time between t_3 and t_3'. Customarily, the observable is time tagged half way between t_3' and t_3:

$$T = t_3 + \frac{1}{2}(t_3' - t_3) \tag{7}$$

Notice from Eq. (6) that conventional differential phase ($\dot{\omega} = 0$) will tell us the range change from time t_3 to t_3'. With the DCO data ($\dot{\omega} \neq 0$), we can also determine range. To see this, assume a static case where the transmitter, spacecraft, and receiver are stationary (such as might be the situation for a geostationary satellite). Then

$$R' = R$$

and

$$t_1' - t_1 = t_3' - t_3 = \tau$$

where τ is the doppler averaging time. Differential phase

$$\Delta\phi(T) = \frac{\dot{\omega}}{c}R\tau \tag{8}$$

Whereas conventional data with a zero frequency rate have zero differential phase, the DCO or ramp frequency data (differential phase between two successive data readouts) have values which are proportional to the round-trip distances.

From Eq. (8), we find the expression relating the phase errors ($\delta\phi$) and the resulting range error (ΔR) to be:

$$\Delta R = \frac{c}{T}\frac{\delta\phi}{\dot{\omega}} \tag{9}$$

where

ΔR = two-way range error, km

c = speed of light, 2.99×10^5 km/s

$\dot{\omega}$ = S-band ramp rate, Hz/s

T = ramp averaging time, s

$\delta\phi$ = phase error, cycles

Additionally, an error in the ramp initiation time appears directly in a round-trip range error. The expression is

$$\Delta R = c\Delta t \tag{10}$$

where Δt is the ramp initiation time error in seconds. A discussion of each individual error follows.

A. Phase Error (Short Term) or "Jitter"

From Ref. 1 a test was conducted whereby phase jitter could be measured. The phase noise has a standard deviation scatter of 0.02 cycles. For a ramp rate of 100 Hz/s and an averaging time of 600 s, the two-way range error from this is

$$\Delta R = \frac{3 \times 10^5 \times 0.02}{100 \times 600} = 0.1 \text{ km (100 m)}$$

B. Phase Drift

Reference 2 gives a value of the stability for the rubidium standard as 5 parts/10^{12}, which gives an S-band frequency error of 11.5×10^{-3} Hz, or about 7 cycles in 10 min. The range error for a ramp rate of 100 Hz/s for 10 min is

$$\Delta R = \frac{3 \times 10^5 \times 7}{6 \times 10^4} = 35 \text{ km}$$

Reference 2 also points out that the rubidium standard has been improved by a factor of 10 so that the range error is

$$\Delta R = 3.5 \text{ km}$$

C. Tropospheric Effects

The number of cycles added is a function of elevation angle of the spacecraft. If we assume that the elevation angle is above 20 deg, then the addition or subtraction of 10 refractivity (N) units (refractivity unit = (index of refraction minus 1) $\times 10^6$) will add or subtract about a cycle during one hour. Ten N units correspond to a 3% error in the troposphere. The error due to a 3% change over an hour of the troposphere causes a 1/6-cycle error in 10 min. For a ramp averaging time of 10 min and a rate of 100 Hz/s:

$$\Delta R = \frac{3 \times 10^5}{600 \times 100 \times 6} = 0.83 \text{ km}$$

D. Ramp Initiation Time Error

References 1 and 3 indicate a 5-μs uncertainty in the initiation of the ramp. This uncertainty is the time quantization limit of the equipment. Translated into range, we have:

$$\Delta R = 3 \times 10^5 \times 5 \times 10^{-6} = 1.5 \text{ km}$$

Table 1 summarizes the various errors and the corresponding two-way range measurement error. The limiting or the largest error is caused by the instability or drift of the frequency standard. This error is about 1.5 km (one way), and is larger than errors due to the troposphere or to ramp-on-time errors.

III. Data Equation

The track synthesizer frequency (TSF) is controlled by the digitally controlled oscillator (DCO). The DCO frequency is related to the TSF by:

DCO frequency = 3 TSF − 20 MHz

DCO frequency rate = 3 TSF rate

TSF is typically around 22 MHz. For conventional doppler the TSF is multiplied by 96 so that the transmission to the spacecraft is near 2200 MHz (S-band frequency). The spacecraft multiplies the received frequency by

240/221 and transmits it to Earth. Thus the received frequency, ω (received) at the station, with all relative doppler motion removed is

$$\omega\,(\text{received}) = 96 \times \frac{240}{221} \times \text{TSF}$$

For the new swept DCO carrier frequency, the initial DCO frequency is ω_0 for initiation of ramp-on time t_0. The DCO frequency ω at any later time t is $\omega = \omega_0 + \dot{\omega}\,(t - t_0)$.

A 20-MHz frequency is added to this signal and the result multiplied by 32. This signal is at S-band and is transmitted to the spacecraft. As in conventional doppler, the up-signal is received by the spacecraft and multiplied by 240/221 and transmitted back to Earth. We have this situation:

$$\omega_0 = (3 \times \text{TSF} - 20 \times 10^6)\ \text{Hz} \approx 46\ \text{MHz initially.} \tag{11}$$

At any later time t, the frequency is

$$\omega = \omega_0 + \dot{\omega}\,(t - t_0)$$

The transmitted frequency ω_T is

$$\omega_T = 32 \times (\omega + 20 \times 10^6) \tag{12}$$

The received signal is at a frequency ω (received):

$$\begin{aligned}
\omega\,(\text{received}) &= \frac{240}{221}\,\omega_T \\
&= 32 \times \frac{240}{221}\,(\omega + 20 \times 10^6) \\
&= 32 \times \frac{240}{221}\,[\omega_0 + \dot{\omega}\,(t - t_0) + 20 \times 10^6] \\
&= 32 \times \frac{240}{221}\,[3 \times \text{TSF} - 20 \times 10^6 \\
&\quad + \dot{\omega}\,(t - t_0) + 20 \times 10^6] \\
&= 96 \times \frac{240}{221} \times \text{TSF} + 32 \times \frac{240}{221}\,\dot{\omega}\,(t - t_0)
\end{aligned} \tag{13}$$

The first term is the received S-band frequency for conventional doppler. The second term is the additional frequency introduced by the DCO device.

This analysis forms the basis for our data reduction scheme.

IV. Data Analysis

We analyzed a data span which began on November 23, 1973, 03:34:32 GMT and ended on December 13, 1973, 11:33:32 GMT. This data set encompassed the Jupiter encounter by Pioneer 10 which occurred on December 4, 1973, 02 h GMT. Also included in these data were three sets of DCO carrier ramps. These ramps occurred on November 23 and 26, 1973 and December 11, 1973. Table 2 tabulates the ramp pattern for those dates.

On each of those dates, a sawtooth pattern is impressed upon the S-band carrier by the DCO device. This pattern consists of an upswing of the carrier of 100 Hz/s for 5 min, followed by a downswing of −100 Hz/s for 10 min and another upswing of 100 Hz/s for 5 min. The final carrier frequency at the end of this saw-tooth is at the same frequency as at the beginning of the sawtooth. There is a known ramp initiation time delay of 1.000040 s which our data reduction scheme automatically takes into account. The 5-μs random on-time error discussed in Section II-D is not compensated and appears as a random range measurement error.

The ramp information presented in Table 2 was passed to an orbit determination program POEAS. This program automatically least square adjusted the orbit to the data whose representation was given by Eq. (13) (with the addition of appropriate extra terms for doppler motion). The orbit adjustments were done separately for the three passes containing the DCO data (November 24, 26, and December 11, 1973).

The data for each local orbit solution were comprised of normal unramped doppler for about an hour before the onset of the ramped (DCO) doppler data. The station locations for DSS 14 and DSS 43 are given in Table 3. Since the uncertainties of these locations amount to less than 5 m, we assumed these locations to be fixed and no adjustments to these parameters were made. Each of these orbit determinations resulted in a topocentric range measurement. The individual range measurements are tabulated in Table 4. The indicated uncertainties for these measurements were estimated by POEAS to be ±5 km. This figure is very different from the 100-m error mentioned in Section II-A. The explanation is that the assumed doppler data accuracy figure given to POEAS is about 1 Hz for 1-s doppler averaging time or about 50 times

larger than the ground test noise measurement. The less accurate figure given to the program was used as an attempt to account for systematic effects such as those mentioned in Sections II-A, -B, -C, -D. The orbit determination process removes systematic effects by interpreting these errors as errors in the orbit and adjusts it accordingly. The actual observed data noise after the orbit adjustments was in fact about 0.1 Hz, or 10 times smaller than given to the program. Figure 1 is a plot of doppler residuals for November 26, 1973, from DSS 14. The residuals have a one standard deviation (1-σ) spread of about 2 mHz. The ramped data on the transmission, which was not delivered to us by the project, are shown as missing in the figure. The ramped return signal, which was delayed by 1½-h round-trip time is marked off on Fig. 1. There was no difference between the conventional data and DCO data as seen from Fig. 1.

Figure 2 shows the number of S-band cycles that are gained or lost over the 2-h span of data from DSS 14. On the whole, there is about a cycle or 13-cm error during this entire period.

A longer span of data was also analyzed. This set of data began on November 23, 1973 and extended past encounter for 7 more days, ending on December 11, 1973. The purpose here was to use the 3-ramped DCO data as range data in combination with standard doppler data in order to determine a Earth–moon barycenter to Jupiter–Galilean moon barycenter distance. The standard unramped doppler data would yield an orbit relative to the Jovian center, and the DCO doppler data would determine the topocentric distance to the spacecraft. A combination of the two data types would reveal errors in the JPL planetary ephemeris DE84. The determination of the spacecraft orbit relative to Jupiter was, however, complicated by the perturbative effects caused by the four large moons, and the nonspherical gravity field of Jupiter. In order to separate these important effects from a misplacement of the position of Jupiter, it was necessary not only to adjust the spacecraft orbit, but also to adjust simultaneously the masses of the four moons, mass of Jupiter, and the heliocentric coordinates of Earth and Jupiter. This was attempted and the results of such an adjustment leading to an estimation of the barycenter-to-barycenter distance are summarized in Table 5. There is a slight displacement of Jupiter of about −107 km at encounter from DE84. This displacement is not significant since the DE84 coordinates have a one standard (1-σ) deviation of about 250 km at that time. Further, POEAS was extensively modified to allow for the additional perturbative effects of the four moons and a code error was incurred which prevented a Jovian mass adjustment. Because of this, a good orbit solution to the level of 10 mHz was not possible. Just prior to encounter, the orbit was warped to produce about 0.5-Hz residual in doppler. Throughout the orbit convergence procedure, however, the barycenter-to-barycenter distance estimation never deviated more than 300 km from DE84, indicating a stable solution in this respect.

V. Summary of Results

By using the DCO doppler data, we were able to obtain three range estimates to Pioneer 10. These range measurements were, individually at least, accurate to ±5 km. The observed accuracy was 500 m but, because of suspected systematic errors which were masked by the orbit adjustment procedure, the actual accuracy was probably larger than 500 m. From the data residuals based on local orbital adjustments, the DCO data were no different from conventional doppler. The data error was on the order of 2 mHz. A longer solution was also attempted, whereby a Jupiter barycenter to Earth barycenter distance was found. The difference between the estimated barycenter-to-barycenter distance and that from the reference planetary ephemeris DE84 was −107 km. This difference was not significant because DE84 had a 1-σ error of 250 km.

References

1. Spradlin, G., *DSS 43 Ramp Test of 21 September 1973*, IOM 421-PF-A506, Oct. 2, 1973 (JPL internal document).

2. Cain, D. L., *Hydrogen Masers for Pioneer 10*, IOM 391.4-561, Sept. 12, 1973 (JPL internal document).

3. Berman, A., *Analyses of DCO Ramp Data*, IOM 431-G-73-57, July 11, 1973 (JPL internal document).

Table 1. Two-way range errors due to various sources for ramp rate 100 Hz/s (S-band) and 10-min averaging

Source	Error	Range error (two way), km
Phase noise (jitter)	0.02 cycles	0.1
Phase drift	4.2 cycles/h	3.5
3% Tropospheric error (EL $>$ 20°)	1 cycle/h	0.83
Time initiation	5×10^{-6} s	1.5

Table 2. Ramp frequency pattern near Jupiter encounter

Date	Day of year	DSS	Ramp	DCO ramp rate, Hz/s	Ramp-on time,[a] GMT
11/24/73	328	43	1	3.125	04:00:00
			2	−3.125	04:05:00
			3	3.125	04:15:00
			4	0.0	04:20:00
11/26/73	330	14	1	3.123	00:05:00
			2	−3.123	00:10:00
			3	3.123	00:20:00
			4	0.0	00:25:00
12/11/73	345	43	1	3.125	04:05:00
			2	−3.125	04:10:00
			3	3.125	04:20:00
			4	0.0	04:25:00

[a]Conventional command time. Actual start time will be 1.000040 seconds later.

Table 3. Station locations referred to 1903.0 pole

DSS	Longitude, deg	Distance from rotation axis, km	Distance from equatorial plane, km
14	243.1104806	5203.9952949	3677.052
43	148.981274	5205.2472152	−3674.788

Table 4. Estimated topocentric distance to Pioneer 10[a]

DSS	Date	UTC time, GMT	Two-way light time,[b] UTC second	One-way[c] range, km
43	11/24/73	05:28:26	5316.70302147	796,953,845.29
14	11/26/73	01:43:50	5351.76510073	802,209,520.47
43	12/11/73	05:48:22	5600.36541890	839,473,774.94

[a]Measurement error of ±5 km (one way).
[b]Round-trip light time error is $\pm 0.3 \times 10^{-4}$ s.
[c]Speed of light is defined as 299792.5 km/s.

Table 5. Estimated barycenter-to-barycenter distance on December 4, 1973 0 hour GMT

Reference ephemeris distance (DE84), km	825,852,685.77
Correction to reference ephemeris, km	−107.89[a]
Corrected ephemeris distance, km	825,852,577.87[a]

[a]Measurement error of ±5 km.

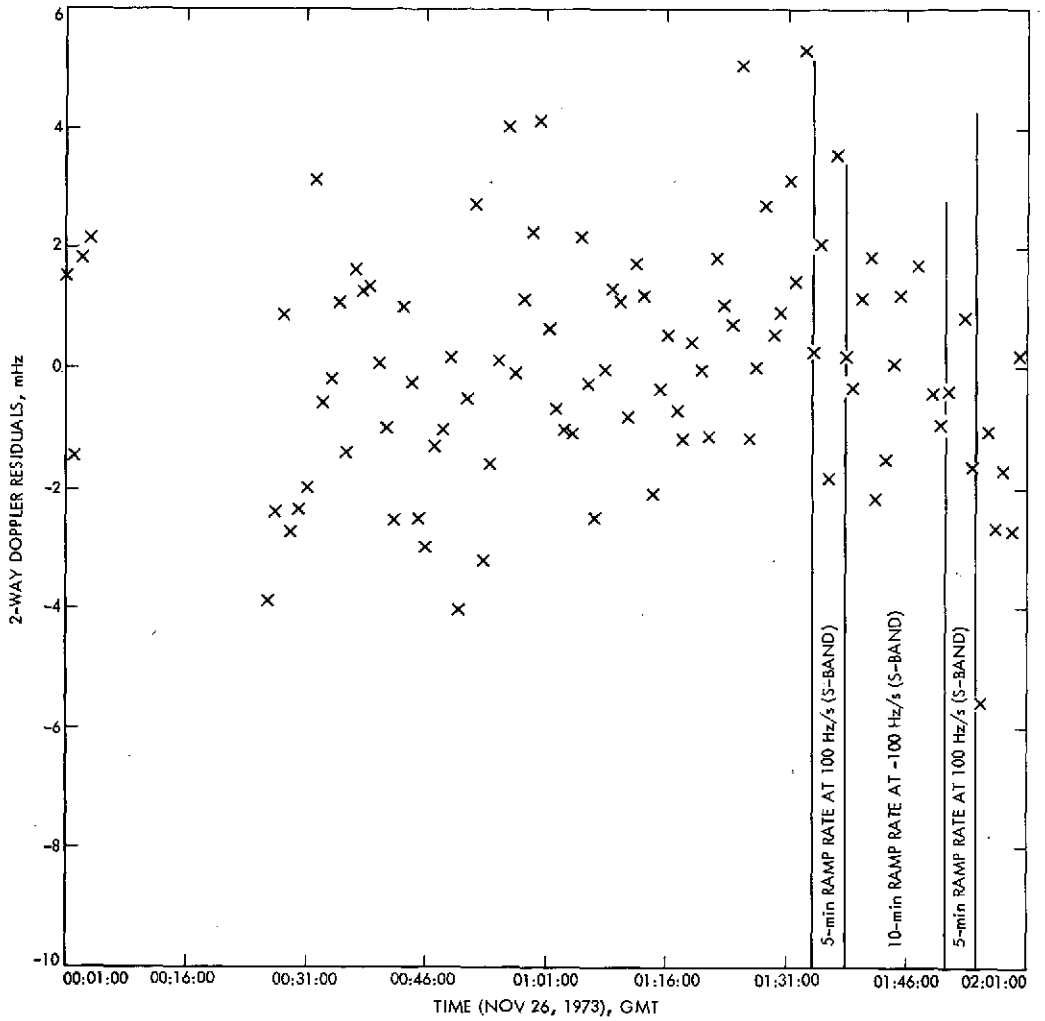

Fig. 1. Pioneer 10 doppler residuals from DSS 14 on November 26, 1973

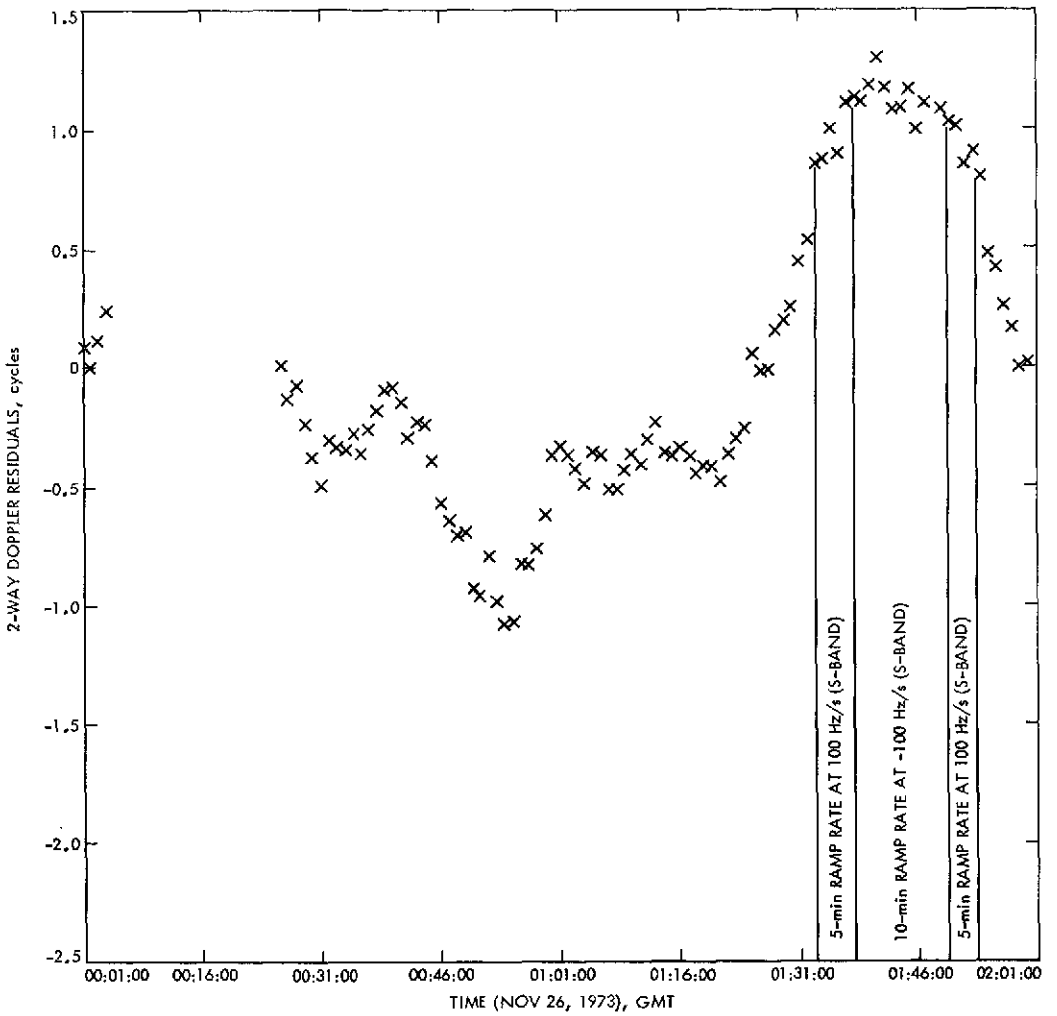

Fig. 2. Pioneer 10 S-band phase residuals from DSS 14 on November 26, 1973

Low-Noise Receivers: Microwave Maser Development

R. C. Clauss
Communications Elements Research Section

A new multijunction, cryogenically coolable, X-band circulator has been developed and tested. Isolation exceeding 20 dB per junction and insertion loss less than 0.2 dB per junction between 8100 and 8800 MHz have been measured at 4.5 K. The new circulator will be used with a maser to provide low noise amplification across a wide instantaneous bandwidth.

I. Introduction

An X-band multijunction, cryogenically coolable circulator has been purchased and tested at 4.5 Kelvins. The circulator will be used with a maser to provide low noise amplification across a wide instantaneous bandwidth. Excellent isolation and low insertion loss have been demonstrated from 8100 to 8800 MHz. Two special refrigerator systems were assembled to enable the development and the testing of the circulator.

II. Application

Isolation required for stable maser amplification can be obtained by using either circulators or resonance isolators. Cavity-type masers built and operated by the Jet Propulsion Laboratory (JPL) from 1960 to 1965 used room temperature circulators; traveling-wave masers used in the Deep Space Network since 1963 had resonance isolators built into the maser structure at 4.5 K (Ref. 1). The requirements of very low noise input temperature (less than 5 K) and wide instantaneous bandwidth (more than 100 MHz) have established the need for improved isolation techniques.

The circulator described here is suitable for use with a very low noise amplifier because it has low insertion loss at 4.5 K. Wide bandwidth operation is possible because high isolation is obtained across a 700 MHz bandwidth.

The use of a traveling wave type of slow-wave structure (without resonance isolators) and line broadened maser material in combination with a circulator results in a reflection-type traveling-wave maser with a bandwidth capability of several hundred MHz. The cryogenically coolable circulator described here has been developed for this purpose.

III. Circulator Development

A special cryogenic system using a Cryogenic Technology, Inc. model 350 refrigerator with four coaxial transmission lines was assembled and supplied to P and H Laboratories (Chatsworth, Calif.) to enable the development of the cryogenically coolable circulator. This refrigerator system is easy to use and is capable of operation at temperatures between 13 and 290 K. The coaxial transmission lines are 0.36 cm. outside diameter with SMA connectors and can be used at any frequency up to 18 GHz.

A second, more complicated 4.5 K cryogenic system was assembled and has been used to test the X-band circulator at JPL.

IV. Circulator Performance Measurements

The circulator, mounted on the 4.5 K station of the refrigerator, is shown in Fig. 1. Mounting brackets for a maser and superconducting magnet are included for future tests. Four coaxial lines are connected so that isolation, loss, and impedance measurements of each circulator port can be made. A schematic diagram of the circulator is shown in Fig. 2. Input, output, and amplifier ports are identified by number (1 through 4). Isolation provided by the first circulator junction (port 2 to port 1) is shown in Fig. 3. Data were recorded at 4.5, 20, 100 and 290 K. Figure 4 shows isolation data for other ports recorded at 4.5 K.

Initial loss measurements show the dissipative loss of the circulator to be less than 0.2 dB per junction. Additional measurements will be made to more accurately determine the match and loss of each individual junction.

V. Conclusion

The new 4-port cryogenically coolable X-band circulator works well at any temperature between 4.5 and 290 K. The internal isolation is adequate to permit stable wideband maser amplification at any frequency between 8100 and 8800 MHz.

Reference

1. Reid, M.S., et al., "Low-Noise Receiving Systems in a Worldwide Network of Large Antennas," *Proceedings of the IEEE*, Vol. 61, No. 9, pp. 1330–1335, September 1973.

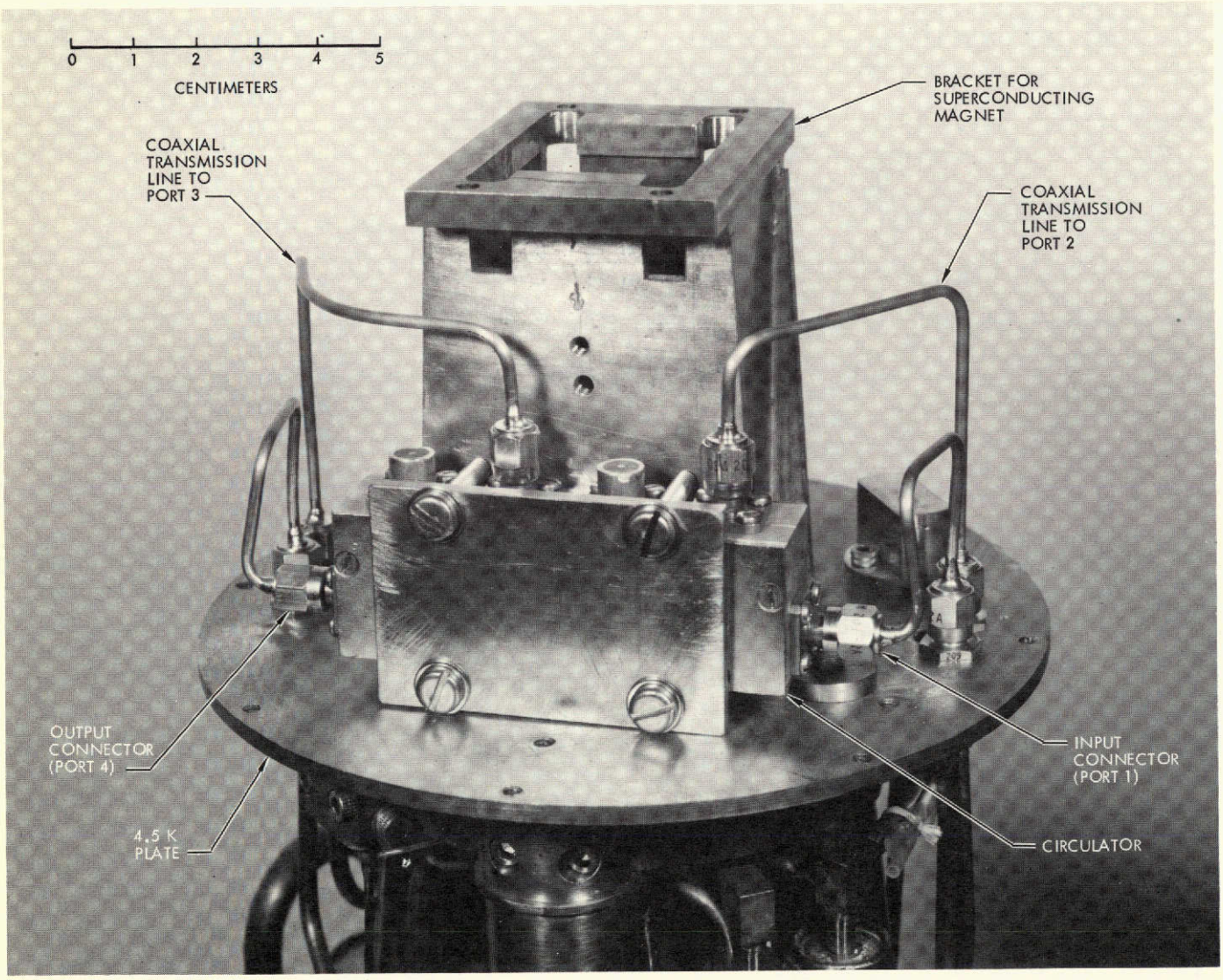

Fig. 1. X-band multijunction cryogenically coolable circulator

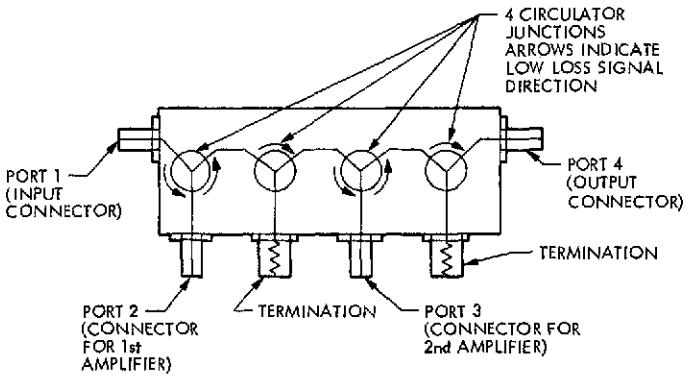

Fig. 2. Schematic diagram of multijunction circulator

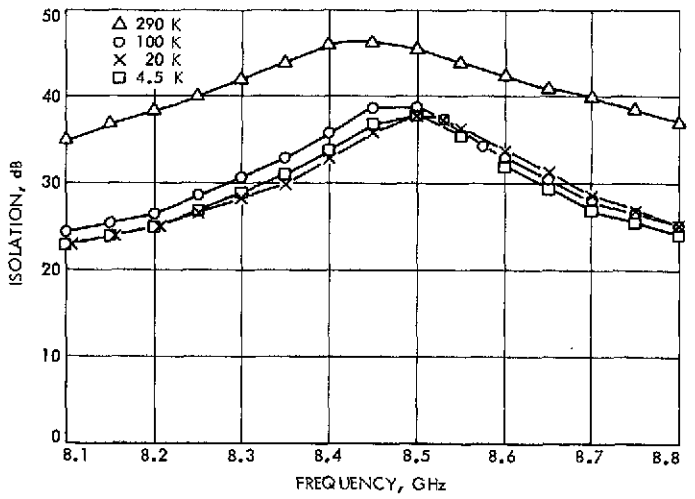

Fig. 3. Isolation of one circulator junction as a function of frequency and temperature (port 2 to port 1)

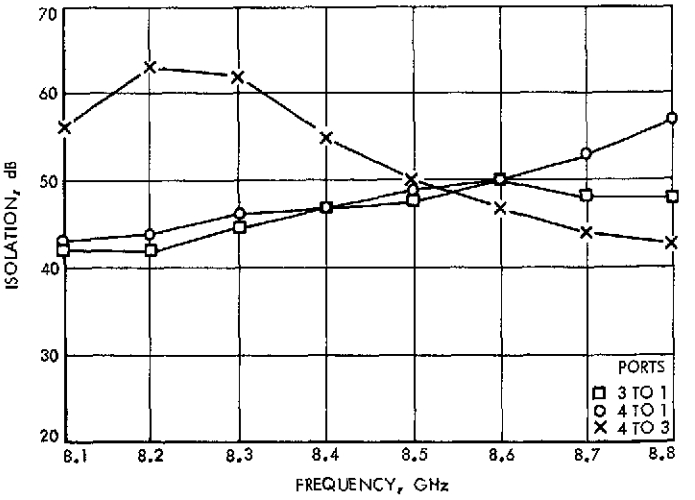

Fig. 4. Isolation of various circulator junction combinations at 4.5 K

Effects of Lognormal Amplitude Fading on Bit Error Probability for Uncoded Binary PSK Signaling

B. K. Levitt and M. Y. Rhee
Communications Systems Research Section

The 1978 Pioneer Venus mission will require direct communication links between the planetary probes and Earth. Data from the Russian spacecraft Venera 4 indicate that these links will be subjected to lognormal fading resulting from atmospheric turbulence. This article analyzes the bit error rate degradation for uncoded binary phase-shift-keyed (PSK) telemetry in the presence of such fading.

I. Introduction

The 1978 Pioneer Venus mission will require direct communication links between the planetary probes and Earth. A review of the Russian Venera data indicates that these links will be subjected to lognormal fading due to the turbulent atmosphere of Venus (Ref. 1). This paper analyzes the degradation of the bit error rate for uncoded binary phase-shift-keyed (PSK) signals received over the additive white Gaussian noise (AWGN) channel in the presence of such fading.

II. Low and High Rate Bounds

Consider an uncoded binary PSK communication link over the AWGN channel. In the absence of fading, the received signal has the form

$$r(t) = \sqrt{2}A\cos[\omega_c t + \theta_m d(t)\, sq(\omega_s t)] + n(t) \qquad (1)$$

where ω_c is the carrier frequency, θ_m is the modulation index ($\theta_m < 90°$), $d(t)$ is the binary data with baud time T_B ($d(t) = \pm 1$), $sq(\omega_s t)$ is the squarewave subcarrier at frequency ω_s ($2\pi/T_B << \omega_s << \omega_c$), and $n(t)$ is a wideband Gaussian noise process. If the channel has atmospheric fading of the form anticipated for Pioneer Venus, the received signal will be (Refs. 2 and 3)

$$r(t) = \sqrt{2}A\, e^{\chi(t)}\cos[\omega_c t + \theta_m d(t)\, sq(\omega_s t) + \phi(t)] + n(t) \qquad (2)$$

where $\chi(t)$ and $\phi(t)$ are stationary, jointly Gaussian random processes, and $e^{\chi(t)}$ is a lognormal random process.

From Venera 4 data, Woo (Ref. 1) has concluded that $\chi(t)$ and $\phi(t)$ are narrowband processes, with one-sided power spectral bandwidths

$$W_\chi, W_\phi \sim 1\ \text{Hz} \qquad (3)$$

It is assumed that the phase fading process is sufficiently narrowband relative to the carrier phase-locked loop bandwidth in the receiver that it can be tracked without difficulty. Consequently, the analysis below neglects $\phi(t)$ and assumes that all of the degradation in link performance due to the fading is caused by the amplitude fading process $e^{\chi(t)}$. The bit error rate, conditioned on the fading, has the form (Ref. 4)

$$p(\epsilon \mid \alpha) = Q(\alpha\sqrt{2\rho}) \tag{4}$$

where

$$\alpha \equiv \frac{1}{T_B}\int_0^{T_B} dt\, e^{\chi(t)} \tag{5}$$

$$\rho \equiv \frac{A^2 \sin^2 \theta_m T_B}{N_0} \tag{6}$$

$$Q(\zeta) \equiv \frac{1}{\sqrt{2\pi}}\int_\zeta^\infty dx \exp\left(-\frac{\chi^2}{2}\right) \tag{7}$$

Suppose the data rate R_B is high:

$$R_B \equiv \frac{1}{T_B} >> W_\chi \tag{8}$$

Then $\chi(t)$ is essentially constant over the baud time T_B, and α reduces to a lognormal random variable

$$\alpha = e^\chi \tag{9}$$

where $\chi \equiv \chi(t_0)$ for some $t_0 \epsilon (0, T_B)$, and its mean m_χ is the negative of its variance σ_χ^2 (Ref. 3). Then the expected bit error rate is given by

$$P(\epsilon) = \overline{Q(e^\chi\sqrt{2\rho})}^{\chi} \tag{10}$$

Now consider the extremely low data rate case, defined by

$$R_B << W_\chi \tag{11}$$

Then α is a long time average of $e^{\chi(t)}$, and assuming $\chi(t)$ is ergodic,

$$\alpha = \overline{e^\chi} = \exp\left(-\frac{\sigma_\chi^2}{2}\right) \tag{12}$$

Then

$$P(\epsilon) = Q\left[\sqrt{2\rho \exp\left[-\sigma_\chi^2\right]}\right] \tag{13}$$

Woo has computed a variance $\sigma_\chi^2 = 0.014$ for the Venusian atmosphere (Ref. 1). For this variance, Eqs. (10) and (13) are compared in Fig. 1 with the nonfading case ($\chi = 0$); the parameter β in Fig. 1 is defined by

$$\beta \equiv 2\pi W_\chi / R_B \tag{14}$$

The $\beta = 0$ curve corresponds to Eq. (10); it had to be computed numerically using a 20th-order Hermite integration formula (Ref. 5). This curve indicates a signal-to-noise ratio degradation of 0.4 dB at a bit error rate of 10^{-2}, and 0.9 dB at 10^{-4} due to the fading. By comparison, the infinite β curve of Eq. (13) has a degradation of

$$-10 \log_{10}(\exp[-\sigma_\chi^2]) = 0.06 \text{ dB};\ \sigma_\chi^2 = 0.014 \tag{15}$$

independent of the bit error rate.

For intermediate data rates ($0 < \beta < \infty$), it can be shown that the bit error rate curve is bounded by the $\beta = 0$ and infinite β curves. Applying Eq. (A.4) derived in Appendix A, we have

$$Q\left(\sqrt{2\rho e^{-\sigma_\chi^2}}\right) \le P(\epsilon) \le \overline{Q(e^\chi\sqrt{2\rho})}^{\chi} \tag{16}$$

In particular, the $\beta = 0$ curve of Eq. (10) represents a worst-case fading degradation of the bit error rate over all data rates.

III. Intermediate Rate Model

The following analysis is adapted from the work of Tausworthe (Ref. 6) and Layland (Ref. 7) on noisy reference detection.

Suppose the covariance function of $\chi(t)$ can be approximated by the expression

$$\begin{aligned} R_\chi(\tau) &\equiv \overline{[\chi(t+\tau) - \overline{\chi(t+\tau)}]\,[\chi(t) - \overline{\chi(t)}]} \\ &\cong \sigma_\chi^2 \exp(-2\pi W_\chi |\tau|) \end{aligned} \tag{17}$$

Equation (17) satisfies the requirement that $R_\chi(0) = \sigma_\chi^2$. It also yields a power spectral density of the form

$$S_\chi(f) \equiv \int_{-\infty}^{\infty} d\tau\, R_\chi(\tau)\, e^{-j2\pi f\tau} = \frac{\sigma_\chi^2}{\pi W_\chi} \Big/ \left[1 + \left(\frac{f}{W_\chi}\right)^2\right] \tag{18}$$

Equation (18) shows that $\chi(t)$ has the required one-sided bandwidth W_x. Furthermore,

$$S_x(f)/S_x(0) \cong \left(\frac{f}{W_x}\right)^{-2}; \qquad |f| >> W_x \tag{19}$$

This high-performance asymptotic behavior conforms fairly well with Woo's theoretical analysis (Ref. 1), which shows that in fact

$$S_x(f)/S_x(0) \cong \left(\frac{f}{W_x}\right)^{-8/3}; \qquad |f| >> W_x \tag{20}$$

Using Eq. (17), and applying the results of Appendices B and C to the random variable α in Eq. (5), it follows that

$$\begin{aligned} \bar{\alpha} &= \exp\left(-\frac{\sigma_x^2}{2}\right) \\ \overline{\alpha^2} &\cong \exp(-\sigma_x^2)\left[1 + \frac{2\sigma_x^2}{\beta^2}(e^{-\beta} - 1 + \beta)\right]; \quad \sigma_x^2 << 1 \end{aligned} \tag{21}$$

where β is defined in Eq. (14).

Note that for $\beta << 1$ (or $R_B >> 1$), α becomes a lognormal random variable as in Eq. (9). At the other extreme, when $\beta >> 1$, the integral expression for α in Eq. (5) can be approximated by a sum:

$$\alpha \approx \frac{1}{N}\sum_{i=1}^{N} e^{x_i} \tag{22}$$

where the x_i's are identically distributed, statistically independent Gaussian random variables, and N is the number of degrees of freedom of $\chi(t)$ over a baud time T_B:

$$N = \frac{T_B}{\left(\frac{1}{W_x}\right)} = \frac{\beta}{2\pi} \tag{23}$$

One might consider applying the Central Limit Theorem to Eq. (22) to conclude that α becomes Gaussian for large N (or β). But the probability density functions of the lognormal random variables e^{x_i} are characterized by long tails, which makes the Gaussian approximation inaccurate, except near $\bar{\alpha}$. A better approximation for the probability density function of α, which is accurate farther into its tail, is the lognormal density. Mitchell (Ref. 8) has demonstrated that the sum of N statistically independent, identically distributed lognormal random variables may be accurately approximated by a lognormal random variable for large N.

Since α looks lognormal in the limits as $\beta \to 0$ and $\beta \to \infty$, it will be assumed that α is approximately lognormal over the entire range of β:

$$\alpha \cong e^{\gamma} \tag{24}$$

where γ is a Gaussian random variable with mean m_γ and variance σ_γ^2. Then

$$\begin{aligned} \bar{\alpha} &= \exp\left(m_\gamma + \frac{\sigma_\gamma^2}{2}\right) \\ \overline{\alpha^2} &= \exp(2m_\gamma + 2\sigma_\gamma^2) \end{aligned} \tag{25}$$

Comparing Eqs. (21) and (25), it follows that

$$\begin{aligned} \sigma_\gamma^2 &= \ln\left[1 + \frac{2\sigma_x^2}{\beta^2}(e^{-\beta} - 1 + \beta)\right] \\ m_\gamma &= -\frac{1}{2}(\sigma_x^2 + \sigma_\gamma^2) \end{aligned} \tag{26}$$

In Fig. 2, m_γ/m_x ($m_x = -\sigma_x^2$) and $\sigma_\gamma^2/\sigma_x^2$ are plotted vs β, for $\sigma_x^2 = 0.014$. These curves show that for small β, the probability density function for γ is a broad Gaussian curve, with standard deviation σ_x, centered at $-\sigma_x^2$; as β increases, there is a smooth trend wherein the mean of γ shifts towards $-\sigma_x^2/2$ while the standard deviation drops to zero. For very large β, the probability density function of γ is essentially a Dirac-delta function centered at $-\sigma_x^2/2$.

Using this model, the expected bit error rate is given by the formula

$$P(\epsilon) = \frac{1}{\sqrt{2\pi\sigma_\gamma^2}}\int_{-\infty}^{\infty} d\gamma \exp -\left[\frac{(\gamma - m_\gamma)^2}{2\sigma_\gamma^2}\right] Q(e^{\gamma}\sqrt{2\rho}) \tag{27}$$

Applying numerical integration techniques to Eqs. (14), (26), and (27), we computed $P(\epsilon)$ as a function of ρ for $\sigma_x^2 = 0.014$, $W_x = 1$ Hz, and various values of R_B. The resulting bit error rate curves for $R_B = 16$ and 256 bps (the lowest and highest data rates currently being considered for Pioneer Venus 1978) are compared with the nonfading case in Fig. 3. (The bit error rate curves

for $R_B = 64$ and 128 bps, the other two rates under consideration for the mission, lie too close to the $R_B = 256$ bps curve to be distinguished from it.) Comparing Figs. 1 and 3, it is evident that the bit error rate curves for the Pioneer Venus data rates, predicted by the intermediate rate model, lie close to the upper bound ($\beta = 0$) derived in the previous section. The deviation in ρ between the fading and non-fading curves in Fig. 3, at a given bit error probability $P(\epsilon)$, is the fading loss entry that would appear in the data channel section of a corresponding uncoded telemetry link design control table. In particular, for $\sigma_x^2 = 0.014$, $W_x = 1$ Hz, and $R_B = 256$ bps, the intermediate rate model predicts a fading loss of 0.6 dB at a bit error rate of 10^{-3}, and 1.0 dB at 10^{-5}.

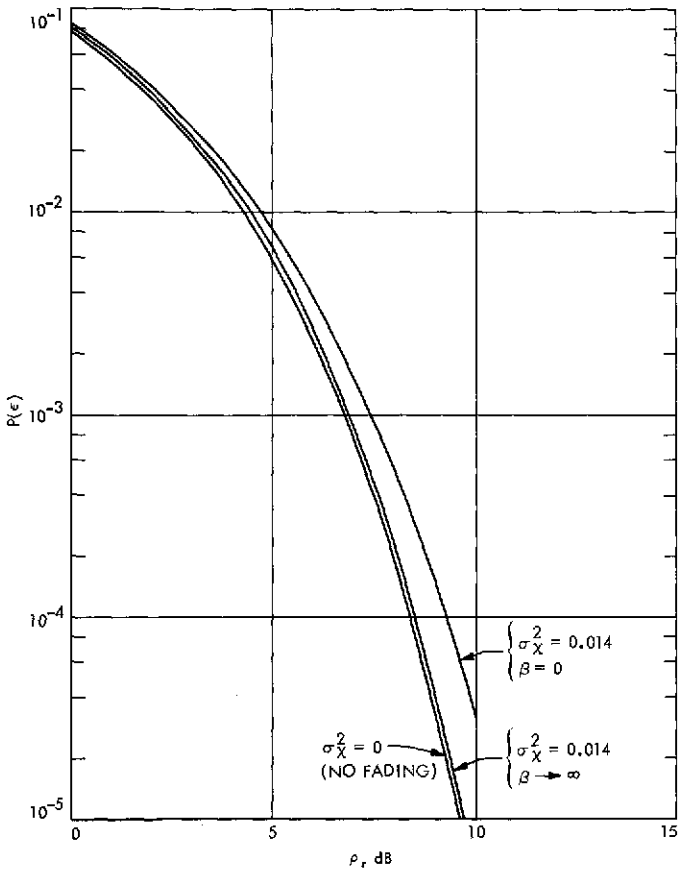

Fig. 1. Upper and lower bounds on the bit error rate for uncoded data received over a lognormal fading channel

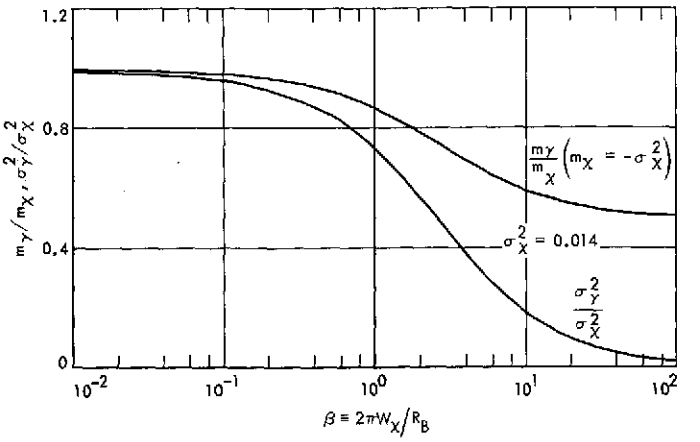

Fig. 2. Variation of intermediate rate model fading parameters with data rate $R_\beta = 2\pi W_x/\beta$

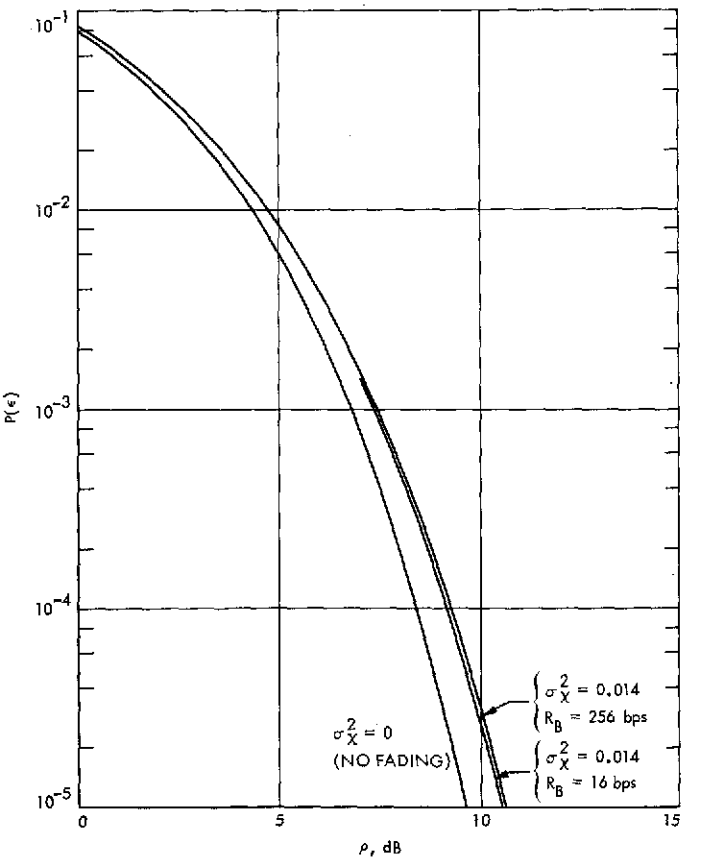

Fig. 3. Bit error rate performance of Pioneer Venus uncoded telemetry links, predicted by intermediate rate model

Appendix A

Lemma: Bounds on the Bit Error Rate for Uncoded Binary Data Received Over a Fading Gaussian Channel

In this section we will prove a general lemma developed by Dr. E. R. Rodemich of the Communications Systems Research Section.

LEMMA

Consider the random variable

$$\alpha = \frac{1}{T}\int_0^T dt\, x(t) \tag{A.1}$$

which is a T-second time average of the positive, stationary random process x(t). Define the parameter

$$\epsilon = \overline{Q(k\alpha)} \tag{A.2}$$

where k is positive and fixed, $Q(\cdot)$ is the normalized Gaussian error function defined by

$$Q(\gamma) \equiv \frac{1}{\sqrt{2\pi}}\int_\gamma^\infty d\beta\, e^{-\beta^2/2} \tag{A.3}$$

and the overbar in Eq. (A.2) indicates the expectation of $Q(k\alpha)$. Then ϵ is bounded by

$$Q(k\bar{x}) \le \epsilon \le \overline{Q(kx)} \tag{A.4}$$

where the random variable $x \equiv x(t_0)$ for any fixed t_0.

Proof

For arbitrary integer n, define

$$\alpha_j \equiv \frac{n}{T}\int_{(j-1)(T/n)}^{j(T/n)} dt\, x(t); \qquad j = 1, 2, \cdots, n \tag{A.5}$$

so that

$$\alpha = \frac{1}{n}\sum_{j=1}^n \alpha_j \tag{A.6}$$

The α_j's are positive, identically distributed, (correlated) random variables. For positive γ, $Q(\gamma)$ is concave, since Eq. (A.3) implies that

$$\frac{d^2Q}{d\gamma^2} = \frac{1}{\sqrt{2\pi}}\gamma e^{-\gamma^2/2} \tag{A.7}$$

Therefore, applying Jensen's inequality for concave functions,

$$Q(k\alpha) \le \frac{1}{n}\sum_{j=1}^n Q(k\alpha_j) \tag{A.8}$$

$$\epsilon = \overline{Q(k\alpha)} \le \frac{1}{n}\sum_{j=1}^n \overline{Q(k\alpha_j)} = \overline{Q(k\alpha_j)}, \quad \text{for any } n, j \tag{A.9}$$

In particular,

$$\epsilon \le \overline{Q(k\alpha^*)} \tag{A.10}$$

where

$$\alpha^* \equiv \lim_{n\to\infty} \alpha_j; \qquad \text{for any } j \tag{A.11}$$

But α^* has the same probability distribution as x, so that

$$\epsilon \le \overline{Q(kx)} \tag{A.12}$$

Now define a new set of α_j's according to

$$\alpha_j \equiv \frac{1}{T}\int_{(j-1)T}^{jT} dt\, x(t); \qquad j = 1,2, \cdots, n \tag{A.13}$$

so that $\alpha_1 = \alpha$. These α_j's are also positive, identically distributed random variables. Define

$$\alpha' \equiv \frac{1}{nT}\int_0^{nT} dt\, x(t) = \frac{1}{n}\sum_{j=1}^n \alpha_j \tag{A.14}$$

Again, using Jensen's inequality, it follows that

$$\overline{Q(k\alpha')} \le \frac{1}{n}\sum_{j=1}^n \overline{Q(k\alpha_j)} = \overline{Q(k\alpha_1)} = \epsilon, \qquad \text{for any } n \tag{A.15}$$

In particular,

$$\epsilon \geq \overline{Q(k\alpha^*)} \tag{A.16}$$

where we have redefined the random variable

$$\alpha^* \equiv \lim_{n\to\infty} \alpha' \tag{A.17}$$

But if $x(t)$ is an ergodic random process,

$$\alpha^* = \lim_{n\to\infty}\left[\frac{1}{nT}\int_0^{nT} dt\, x(t)\right] = \overline{x} \tag{A.18}$$

so that

$$\epsilon \geq Q(k\overline{x}) \qquad \text{(Q.E.D.)} \tag{A.19}$$

Appendix B

Crosscorrelation of Two Lognormal Random Variables

Suppose x_1 and x_2 are identically distributed, jointly Gaussian random variables, each with mean m and variance σ^2. The joint characteristic function of x_1 and x_2 is given by (Ref. 4, p. 163)

$$M_{x_1,x_2}(\nu_1,\nu_2) \equiv \overline{\exp\left(j(\nu_1 x_1 + \nu_2 x_2)\right)} = \exp\left[jm(\nu_1 + \nu_2) - \rho\nu_1\nu_2 - \frac{\sigma^2}{2}(\nu_1^2 + \nu_2^2)\right] \tag{B.1}$$

where ρ is the covariance of x_1 and x_2 defined by

$$\rho \equiv \overline{(x_1 - \overline{x_1})(x_2 - \overline{x_2})} \tag{B.2}$$

In particular, if $m = -\sigma^2$ and $\nu_1 = \nu_2 = -j$, Eq. (B.1) yields the result

$$\overline{e^{x_1} e^{x_2}} = \exp(\rho - \sigma^2) \tag{B.3}$$

Appendix C

Computation of First Two Moments of Lognormal Amplitude Fading Parameter α

Suppose $x(t)$ is a stationary, Gaussian random process with mean m equal to the negative of its variance σ^2. Suppose further that its covariance function is specified by

$$R_x(\tau) = \overline{[x(t+\tau) - \overline{x(t+\tau)}][x(t) - \overline{x(t)}]} = \sigma^2 e^{-2\pi W|\tau|} \tag{C.1}$$

where W is the approximate one-sided spectral bandwidth of $x(t)$. We would like to compute the first two moments of the random variable

$$\alpha = \frac{1}{T}\int_0^T dt\, e^{x(t)} \tag{C.2}$$

Clearly,

$$\overline{\alpha} = \overline{e^{x(t)}} = e^{-\frac{\sigma^2}{2}} \tag{C.3}$$

Also,

$$\overline{\alpha^2} = \frac{1}{T^2}\int_0^T dt \int_0^T d\mu\, \overline{\exp[x(t)]\exp[x(\mu)]}$$

$$= \frac{e^{-\sigma^2}}{T^2}\int_0^T dt \int_0^T d\mu\, e^{\sigma^2} e^{-2\pi W|t-\mu|} \tag{C.4}$$

where we have applied Eqs. (B.3) and (C.1). Defining the parameter

$$\beta \equiv 2\pi WT \tag{C.5}$$

and making the variable change

$$\eta = \frac{t}{T}$$

$$\zeta = \frac{t-\mu}{T} \tag{C.6}$$

the double integral of Eq. (C.4) becomes

$$\overline{\alpha^2} = e^{-\sigma^2}\int_0^1 d\eta \int_{\eta-1}^{\eta} d\zeta \exp[\sigma^2 \exp(-\beta|\zeta|)] \tag{C.7}$$

Equation (C.7) cannot in general be solved explicitly; however, for small σ^2 we can write

$$\overline{\alpha^2} \cong e^{-\sigma^2}\int_0^1 d\eta \int_{\eta-1}^{\eta} d\zeta\,(1 + \sigma^2 e^{-\beta|\zeta|}); \qquad \sigma^2 << 1 \tag{C.8}$$

$$\Downarrow$$

$$\overline{\alpha^2} \cong e^{-\sigma^2}\left[1 + \frac{2\sigma^2}{\beta^2}(e^{-\beta} - 1 + \beta)\right]; \qquad \sigma^2 << 1 \tag{C.9}$$

As a check on Eq. (C.9), note that

$$\overline{\alpha^2} \underset{\beta \to 0}{\longrightarrow} \exp(-\sigma^2)(1+\sigma^2) \cong 1; \qquad \sigma^2 << 1$$

$$\overline{\alpha^2} \underset{\beta \to \infty}{\longrightarrow} \exp(-\sigma^2) \tag{C.10}$$

But from the definition of α in Eq. (C.2), we can write

$$\alpha \underset{T \to 0}{\longrightarrow} e^{x(t)}$$

$$\alpha \underset{T \to \infty}{\longrightarrow} \overline{e^{x(t)}} = \exp\left(-\frac{\sigma^2}{2}\right) \tag{C.11}$$

$$\Downarrow$$

$$\overline{\alpha^2} \underset{T \to 0}{\longrightarrow} \overline{e^{2x(t)}} = 1$$

$$\overline{\alpha^2} \underset{T \to \infty}{\longrightarrow} \exp(-\sigma^2) \tag{C.12}$$

which confirms Eq. (C.10).

References

1. Woo, R., Kendall, W., Ishimari, A., and Berwin, R., *Effects of Turbulence in the Atmosphere of Venus on Pioneer Venus Radio—Phase 1*, Technical Memorandum 33-644, Jet Propulsion Laboratory, Pasadena, Calif., June 30, 1973.
2. Tatarski, V. I., *Wave Propagation in a Turbulent Medium*, McGraw-Hill, New York, 1961.
3. Brookner, E., "Atmospheric Propagation and Communication Channel Model for Laser Wavelengths," *IEEE Trans. Comm. Tech.*, Vol. COM-18, No. 4, August 1970.
4. Wozencraft, J. M., and Jacobs, I. M., *Principles of Communication Engineering*, John Wiley, New York, 1965.
5. *Handbook of Mathematical Functions*, U.S. Govt. Printing Office, M. Abromowitz and I. A. Stegun, ed., Washington, D.C., 1964.
6. Tausworthe, R. C., "Efficiency of Noisy Reference Detection," in *Space Programs Summary 37-54*, Vol. III, Jet Propulsion Laboratory, Pasadena, Calif., pp. 195–201, Dec. 31, 1968.
7. Layland, J. W., *A Note on Noisy Reference Detection*, Technical Report 32-1526, Vol. XVII, pp. 83–88, Jet Propulsion Laboratory, Pasadena, Calif., Oct. 15, 1973.
8. Mitchell, R. L., "Permanence of the Log-Normal Distribution," *J. Opt. Soc. Am.*, Vol. 58, pp. 1267–1272, Sept. 1968.

A Preliminary Deep Space Station Operational Availability Model

I. Eisenberger and F. Maiocco
Communications Systems Research Section

G. Lorden[1]
California Institute of Technology

A method is given for determining deep space station operational availability as a function of the reliability of replaceable subassemblies and the time required to replace them when they fail. It is shown that a reduction in replacement time can have a significant effect on station operational availability.

I. Introduction

In this paper DSS operational availability is analytically defined in terms of subassembly failure rates and replacement rates. In Ref. 1 we assumed that down time occurred only when a spare was not available to replace a failed piece of equipment. Replacement time was assumed to be negligible. However, since replacement time is very often not negligible, its effect on system down time is analyzed. Thus, down time for a piece of equipment is defined to occur only from time delays due to fault detection, fault isolation, disassembly, removal and replacement of the faulty unit, reassembly, checkout, and alignment if required. It is shown that a reduction in these time delays may significantly increase DSS operational availability.

II. General Assumptions

We assume that a signal data path for any DSS function (system) can be characterized by s unique subassemblies which are functionally required for station operations. Failure of the system occurs when any one of the required subassemblies fails. Any subassembly may be configured as a single module or as a standby or parallel configuration having several identical modules. All failed modules can be removed and replaced by operational off-line spares, and then repaired. We further assume that the optimal

[1]Consultant.

number of offline operational spares has been determined in accordance with Ref. 2, and the frequency of running out of spares is negligible.

III. Determination of DSS Operational Availability

The up-time ratio (UTR) for a system or subassembly is defined as the fraction of the time that the system or subassembly is operational, i.e. "up." This ratio turns out (Ref. 3) to be given by

$$UTR = \frac{1}{1 + \frac{MDT}{MTBF}}$$

where MTBF is the mean time between failures and MDT is the mean down time before operation is restored. Applying this formula to the DSS as a whole, we can see that system reliability is only one factor in assuring high operational availability. Short downtimes are equally important. Figure 1 shows how station operational availability (UTR) increases as the MDT is decreased.

Actual computation of MDTs and MTBFs for an entire station is not feasible. Instead, station UTR can be calculated by analyzing directly the failure rates and replacement rates of subassemblies. For operation along a signal data path, assume that s subassembly functions must be performed, indexed by $i = 1, \cdots, s$. Then the UTR for that data path is given by

$$\text{UTR} = \prod_{i=1}^{s} \text{UTR}_i$$

where UTR_i is the up-time ratio for the ith subassembly. This formula is based on the assumed independence of failures of distinct subassemblies.

To calculate the UTR_i's, we assume that for a given subassembly function there are $n + N$ identical modules which perform the given function. Of these, only n are operating at any time (and even fewer may be required to perform the required function). The other N are on-line spares ($N = 0$ is allowed). While operating, each of the n modules is subject to a constant failure rate, λ. Once failed, it takes a time T, which is assumed exponentially distributed, to restore the module to an operating condition. T includes the time required to detect and isolate the fault, disassemble and verify, remove and replace with an off-line spare component, etc., until the subassembly is finally checked out and restored to operation or to the on-line spare status. The switching time to an on-line spare is assumed to be negligible. The restoration rate, μ, is defined as the reciprocal of the mean value of T.

These assumptions lead to the model of a Birth and Death process. The state variable, j, is the number of modules down among the total $n + N$. The possible values of j are 0, 1, 2, $\cdots$ up to the point (if any) where shutdown is prescribed. In any case, $j \leq N$ means that all n operating modules are operable, while $j = N + 1, \cdots$ means that fewer than n modules are operable. Over a long period of time, the fraction of the time spent in states $j = 0, 1, 2, \cdots$ is given by the so-called stationary probabilities, $P_0, P_1, \cdots$. These can be calculated by the following scheme.

Define

$$\lambda_j = \begin{cases} n\lambda \text{ for } j \leq N \\ (N+n-j)\lambda \text{ for } j > N \end{cases}, \qquad j \geq 0$$

$$\mu_j = \mu \cdot \text{minimum } (j, r), \qquad j \geq 1$$

where

r = number of module replacements that can be worked on simultaneously

$$q_0 = 1$$

$$q_1 = \lambda_0$$

$$q_{j+1} = \mu_{j+1}^{-1}[q_j(\lambda_j + \mu_j) - q_{j-1}\lambda_{j-1}], \qquad j \geq 1 \quad .$$

Then

$$P_j = \frac{q_j}{\sum_i q_i} \quad , \quad j \geq 0.$$

Now, suppose m of the operating modules are required to perform the intended function ($1 \leq m \leq n$). Then

$$UTR_i = \sum_{j=0}^{n+N-m} P_j$$

After determining the values of UTR_i separately for each subassembly $i = 1, \cdots, s$, we multiply these values together to obtain the UTR for the entire signal data path. Where there are redundant data paths in the DSS, their UTRs are easily used to compute an overall UTR for the station.

As an example of these considerations, consider the signal data path with five subassembly functions as diagrammed in Fig. 2. The first three functions are performed by individual modules with no redundancy. The fourth function is performed by a module with N on-line spares. The fifth function is performed by an (m, n) parallel configuration of modules. Here there are $N = 0$ on-line spares, but only m of the n modules are required to operate.

Letting $P_j^{(k)}$ denote the probabilities of states, j, for subassemblies $k = 1, 2, 3, 4, 5$, we have

$$UTR_1 = P_0^{(1)}, \quad UTR_2 = P_0^{(2)}, \quad UTR_3 = P_0^{(3)}$$

since the first three subassemblies are up only when $j = 0$. For the fourth subassembly we have

$$UTR_4 = \sum_{j=0}^{N} P_j^{(4)}$$

since only the N on-line spares could be down without causing the subassembly function to fail. For the fifth subassembly, which is in the (m, n) configuration, we have

$$UTR_5 = \sum_{j=0}^{n-m} P_j^{(5)}$$

Thus, overall

$$UTR = P_0^{(1)} \cdot P_0^{(2)} \cdot P_0^{(3)} \cdot \sum_{j=0}^{N} P_j^{(4)} \cdot \sum_{j=0}^{n-m} P_j^{(5)}$$

IV. Conclusions

The present model expresses DSS operational availability as a computable function of the failure rates and restoration rates of subassemblies. In so doing, it permits a quantitative analysis of the effect upon station availability of many factors. Among these factors are component reliability, subassembly redundancy design, DSS operating configuration, fault detection and diagnosis, the type of spares provided, and crew size and skill levels. These and other factors affect the parameters of the Birth and Death process model from which the uptime ratios are computed.

In particular, the model provides a suitable framework for analyzing the DSS availability resulting from the various automation schemes currently under study. It is anticipated that this analysis can be used to equate system availability levels for different schemes, thereby permitting a meaningful comparison of extended life-cycle costs.

References

1. Eisenberger, I., et al., "A Preliminary Study of Spares Provisioning for the Deep Space Network," in *The Deep Space Network*, Technical Report 32-1526, Vol. XVIII, pp. 102–110, Jet Propulsion Laboratory, Pasadena, Calif., Dec. 15, 1973.
2. Eisenberger, I., et al., "Cost Effective Spares Provisioning for the Deep Space Network," in *The Deep Space Network*, Progress Report 42-20, pp. 128–135, Jet Propulsion Laboratory, Pasadena, Calif., April 15, 1974.
3. Rau, J. G., *Optimization and Probability in Systems Engineering*, Van Nostrand Reinhold Company, New York, 1970.

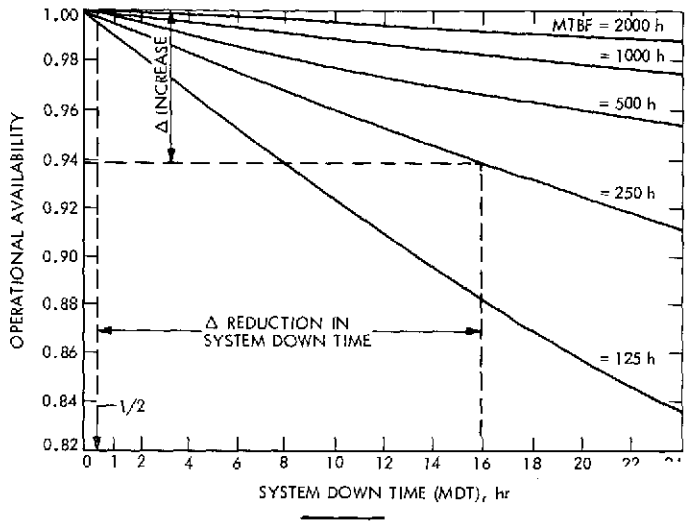

Fig. 1. DSS operational availability versus system mean down time

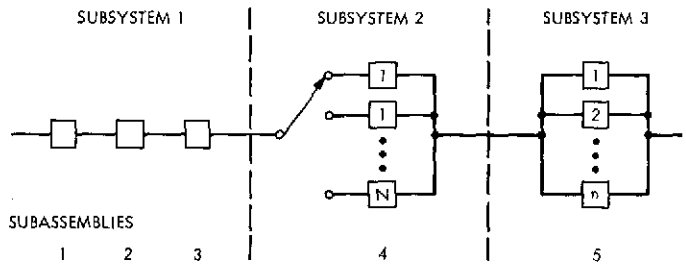

Fig. 2. Signal data path at a DSS

Automation of Microwave Configuration Control

J. G. Leflang
R. F. Systems Development Section

Hardware is being developed for the purpose of permitting computer control of a portion of the DSS 14 configuration control group. The configuration control group is part of the antenna microwave subsystem.

I. Introduction

Within the antenna microwave subsystem, there are numerous waveguide and coaxial radio-frequency switches which are used to establish various configurations by selecting the appropriate feed cone, low-noise amplifier, transmitter, etc. Manually operated, illuminated pushbuttons provide the only means of controlling and monitoring switch position at this time.

The goal of the present effort is to provide the hardware necessary to interface with a DSN standard minicomputer in order to permit the computer to control and monitor the position of switches within the antenna microwave subsystem.

II. Design Requirements

There are many design requirements placed upon equipment which is to be used at a deep space station. Three requirements are described here because they affect the design noticeably.

(1) The hardware must be installed and tested in an operating deep space station. The station must continue to perform its duty of communicating with spacecraft in spite of problems encountered in the development hardware. Therefore, the digital interface equipment must work in parallel with the existing manual control panel.

(2) Low cost is another important restriction. Where it is practical and performance requirements can be met, existing equipment must be utilized.

(3) Because ease of maintenance is important, the new equipment must be designed so that its digital interface is electrically and functionally compatible with the DSN standard, 14-line interface.

III. Design Detail

Figure 1 is a block diagram which shows where the digital equipment ties into one bay of the existing five-bay configuration control group. With the exception of the 14-line interface test fixture, all of the logic shown

by the function blocks is packaged in a single card file. The 14-line interface is fully compatible with the DSN standard both electrically and functionally. It double strobes the control lines and includes the capability of handling command and status byte interrupts. The 14-line interface logic is designed to be independent of this particular application so that it may be easily used as the digital interface for other assemblies of the microwave subsystem.

Figure 2 is a photograph of the card file. Figure 3 is a photograph of the 14-line interface test fixture. The test fixture contains a full capability 14-line interface which is controlled by toggle switches and is monitored by light-emitting diodes.

Figure 4 is a photograph of a relay assembly which is used for testing. It simulates the function of the relay assemblies existing at the deep space stations.

Figure 5 provides the detail of the electrical connection of the computer-controlled equipment to the existing configuration control equipment. The control connection is a wire "or" which permits operation using the manual control panel whether the interface adapter is operating or not.

The optical isolators provide a convenient means of reducing the 24-volt indicator level to the 5-volt logic level. However, they are expensive and, because of the quantity involved, account for a significant portion of the cost of the control logic. Ground loop problems do not exist because the control and indicator lines are isolated from ground to the antenna end of the line. While isolators were provided for the first tests, it is anticipated that they will not be required for noise rejection. If this proves to be the case, the level shift will be accomplished with low-cost zener diodes (80% savings).

Position control is accomplished with an 8-bit word which is decoded and used to actuate the relays. The 8 bits are received in parallel as one command byte in a 14-line interface transfer. Actually, only 5 bits are used at this time.

Position monitoring is accomplished with an 8-bit word which is returned to the computer as a status byte through the 14-line interface. Whenever data are requested by the computer, the multiplexer clocks through all 32 addresses. The clocking is accomplished by the asynchronous interlock signals which occur within the 14-line interface.

With the exception of the 14-line interface and the relay drivers, the logic is constructed using complementary symmetry metal-oxide semiconductor (CMOS) digital integrated circuits. If these devices prove to be durable enough to withstand the field environment, they will provide a significant reduction in power consumption when compared to standard transistor-transistor logic (TTL) devices.

IV. Progress and Plans

Both test fixtures (Figs. 2 and 3) and most of the logic cards for the cage have been fabricated and tested in the lab. The 14-line interface card is being revised to incorporate recent changes in the standard interface protocol. Some of the other cards are also being revised in order to simplify the logic. The plan is to complete all of the changes and lab testing by the end of June 1974. The control logic assembly will then be taken to Goldstone for testing using the 14-line interface test fixture. After tests at Goldstone are completed, the logic assembly will be returned to JPL for integration into the hardware and software package which is being developed for the FY 76 automation demonstration.

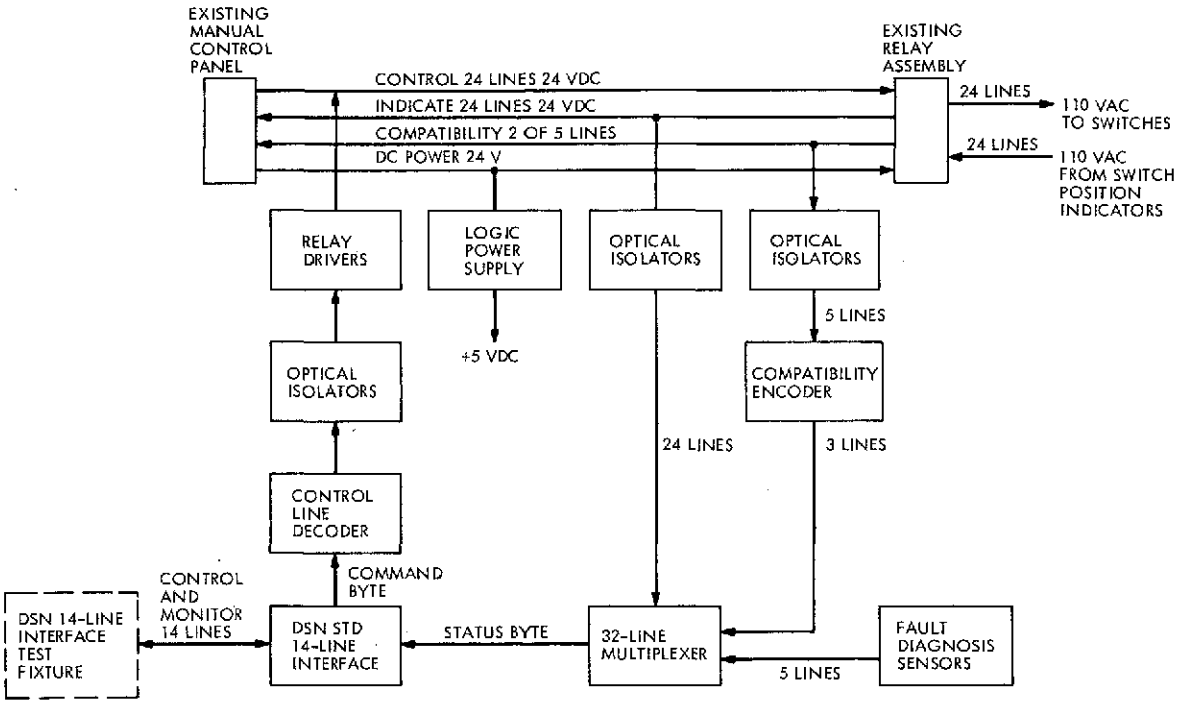

Fig. 1. Automation block diagram of configuration control group, single bay

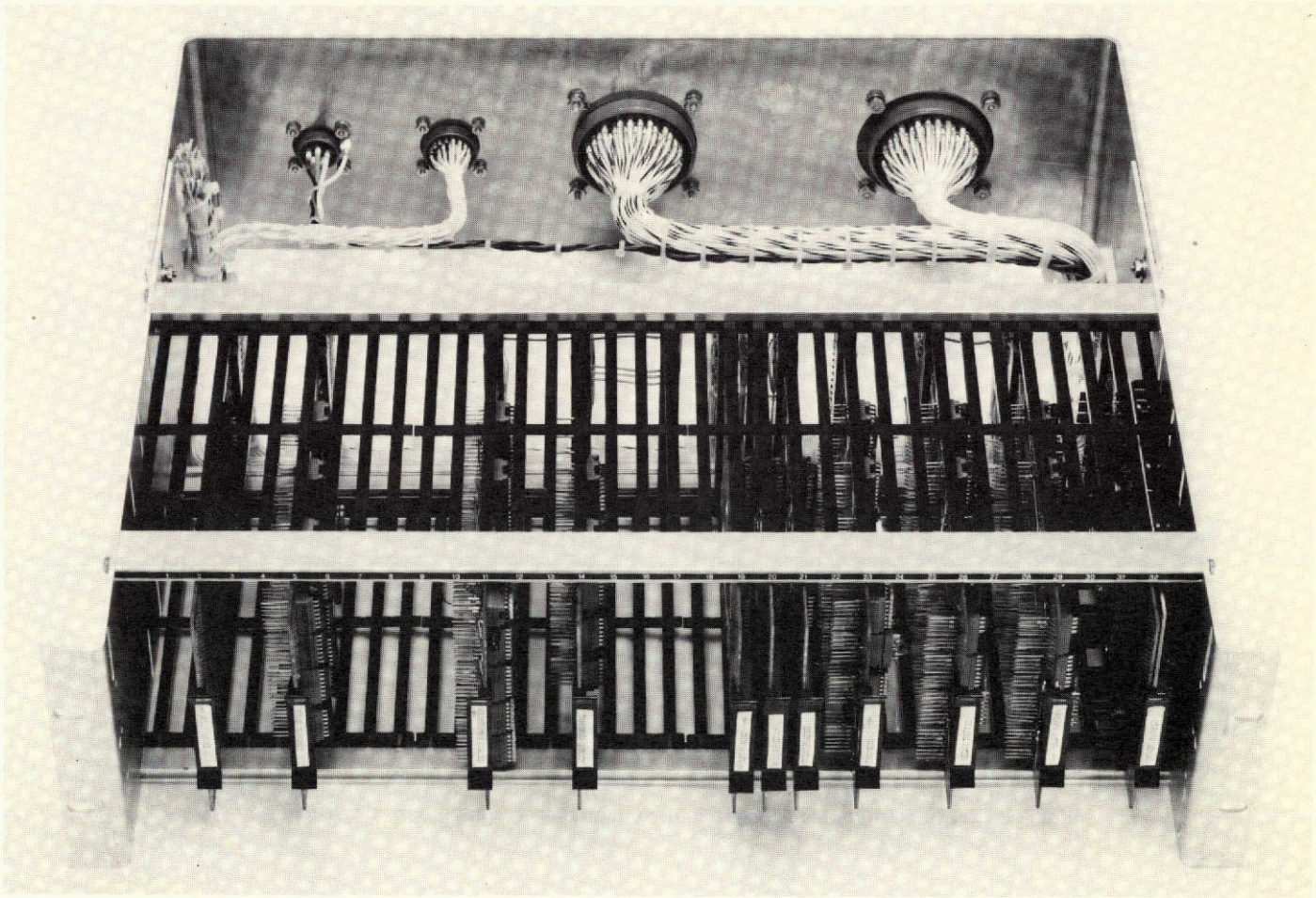

Fig. 2. Logic card cage

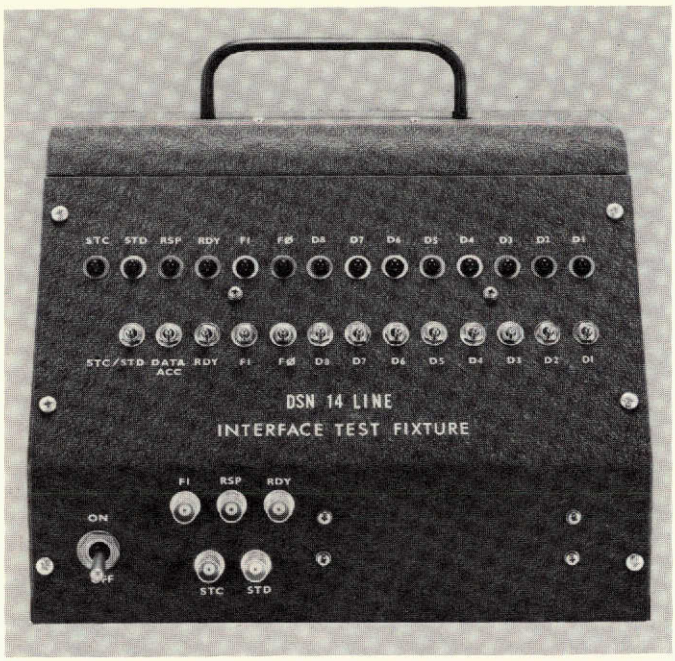

Fig. 3. 14-line interface test fixture

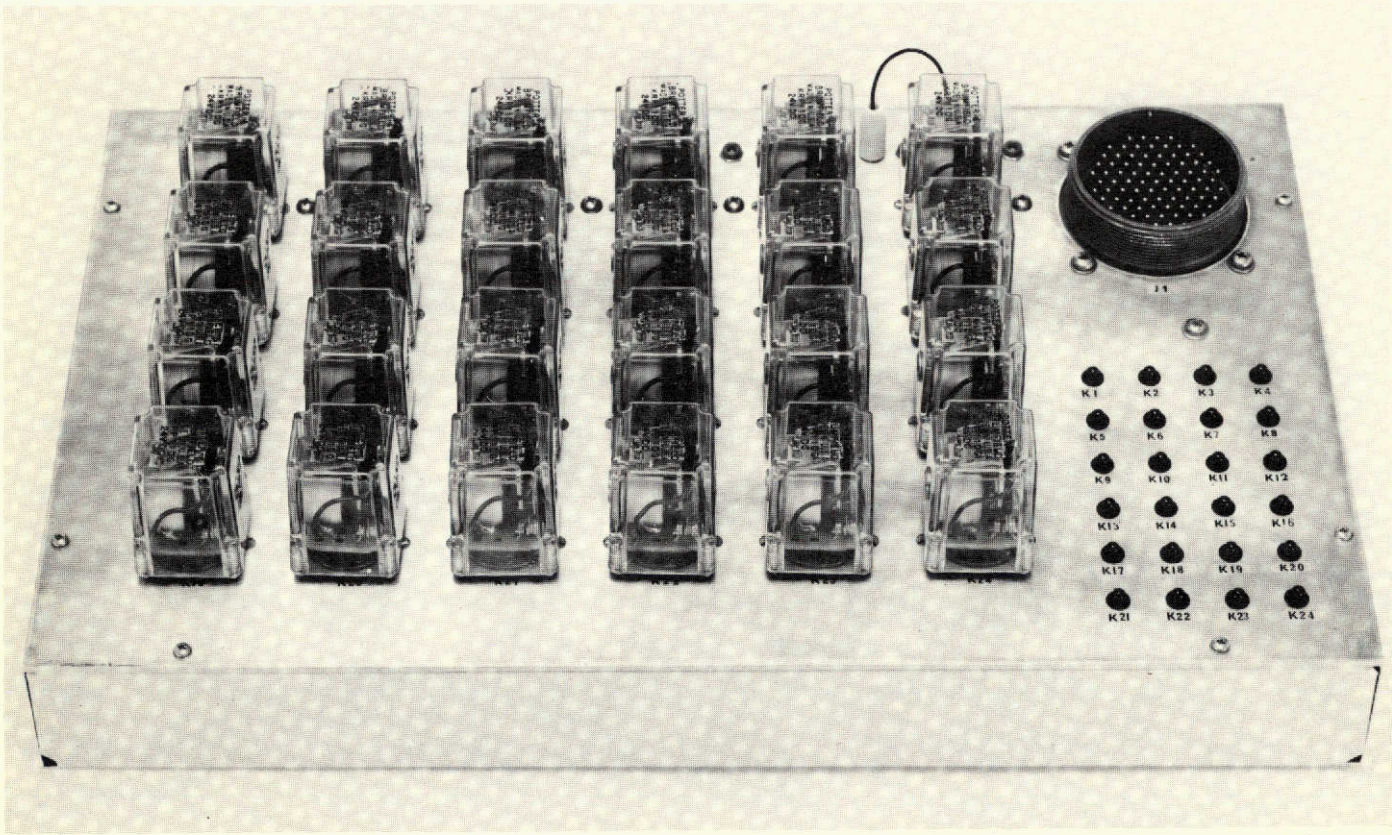

Fig. 4. Configuration control relay simulator

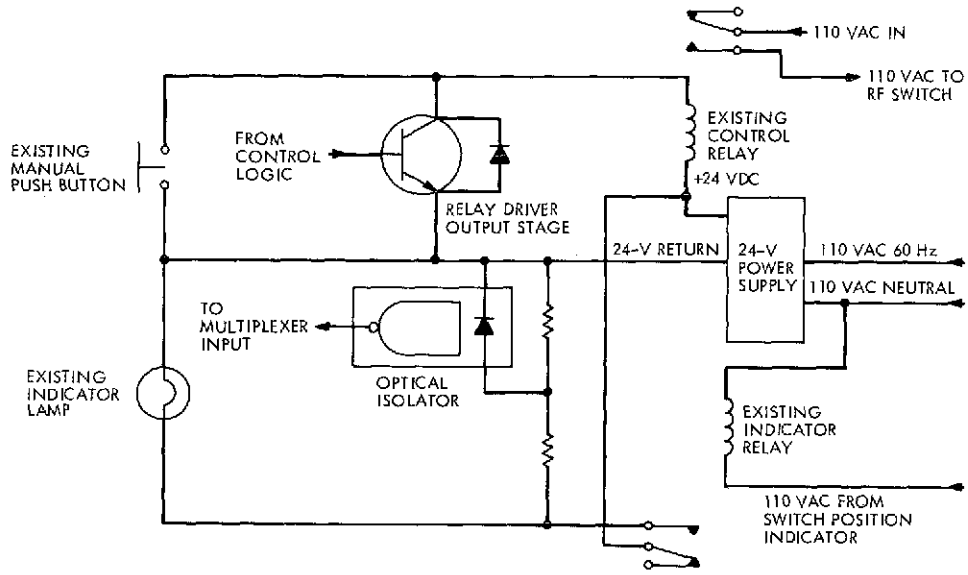

Fig. 5. Electrical connection of computer interface hardware to existing configuration control hardware

DSN Research and Technology Support

E. B. Jackson
R. F. Systems Development Section

The activities of the Development Support Group in operating and maintaining the Venus station (DSS 13) and the Microwave Test Facility are discussed and progress noted. Activities include interferometric planetary radar measurements of the surface of Venus, support of station automation (pulsar) testing and observing, weak radio source observation for 64-m antenna gain calibration, completion of the sidelobe measurements on the 26-m antenna (with resultant changes in gain and system temperature), and extensive sky survey measurements. Additionally, major support was given to spacecraft projects with Faraday rotation data collection, support of the Block IV receiver/exciter at DSS 14, X-band (400-kW) radar testing and DSS 63 100-kW transmitter testing.

During the two-month period ending April 15, 1974, the Development Support Group, in its operation of the Venus station (DSS 13) and the Microwave Test Facility, made progress on various projects as discussed below.

I. In Support of Section 331

A. Planetary Radar

In support of the Mariner Venus/Mercury 1973 (MVM'73) mission, ground-based planetary radar mapping of the Venusian surface continued. The planet was illuminated with the 400-kW transmitter and 64-m antenna at DSS 14, and the reflected signals were simultaneously received by DSS 13 with its 26-m antenna and DSS 14. A total of 17 hours, during which 57 separate data runs were collected, was devoted to this project.

B. Station Automation (Pulsars)

As part of the overall DSN Station Automation Project (Station Monitor and Control (RTOP-68)), a demonstration is planned using the Venus station to perform a pulsar track under remote control from JPL in Pasadena. The dedicated 26-m antenna pointing computer has been interfaced with the "master" computer at DSS 13, and a computer-to-computer link has been successfully established between the SDS-930 computer at DSS 13 and the SDS-930 computer in building 238 at JPL. Testing of the automation hardware and software has consumed 70

hours during these 2 months, while during the 103 hours devoted to observing, the 22 pulsars tabulated in Table 1 were monitored.

II. In Support of Section 333

A. Weak Source Observation

During the 81½ hours devoted to observing weak radio sources (Ref. 1), the sources tabulated in Table 2 were observed.

B. Radio Star Calibration

With the receiver tuned to 2278.5 MHz, and right circular polarization selected on the 26-m antenna, flux measurements were made on radio sources 3C123, 3C218, and Cygnus A during the 41½ hours of observation performed during these 2 months.

C. 26-m Antenna Sidelobe Measurements

Using the Sun as a source of signal, measurements were made for 30 hours with the quadripod on the 26-m antenna covered with flat perforated aluminum sheet. Other radio source measurements indicate that the antenna gain has decreased approximately 0.1 dB, and system temperature at zenith has decreased approximately 0.6 K. Except for confirming measurements to be made when the coverings are removed from the quadripod, this program is now complete at Venus.

D. Sky Survey

During this period, the antenna positions for this testing have been 180-deg azimuth with elevations between 83.0 and 84.2 deg, in 0.1-deg increments. With the antenna in this range of positions, a total of 609½ hours of data have been collected. During the latter part of the period, a modification was made to the data collection system to install an incremental tape recorder to replace the previously used digital printer.

E. Faraday Rotation Data Collection

During the MVM'73 encounters with Venus and Mercury, data were collected from two receivers and put onto punched paper tape, digital printer, and analog chart recorder. During the encounter with Mercury and for two weeks prior, one of the receivers was receiving signals from ATS-1 while the other received signals from ATS-5.

During the week ending March 17 a receiver purchased from Teledyne Micronetics was installed for evaluation, and the previously loaned receiver was returned to Teledyne. At the close of the two-month period, data continue to be collected on two receivers, one each on ATS-1 and ATS-5, 24 hours per day, 7 days per week.

III. In Support of Section 335

A. Block IV Receiver/Exciter

Personnel from the Development Support Group continued to provide test operation, troubleshooting, and corrective maintenance to this system at DSS 14. Continued doppler counting problems prompted examination of all system coaxial cables with a Time Domain Reflectometer (TDR) and resulted in replacement of several cables having impedance discontinuities.

Other support provided included operation of the system for pre-encounter testing of the associated ranging system, module repair and replacement, and general corrective maintenance culminating in wholly successful equipment operation during MVM'73 encounter with Mercury. A total of 586 manhours of support was provided by the Development Support Group during the two-month period ending April 15, 1974.

B. X-Band Planetary Radar

A 250-kW klystron, which had arced in the electron gun region during testing at DSS 13 and was returned to the manufacturer, was reprocessed and received back at DSS 13.

Significant progress has been made on other areas as the dual klystron setup was completed, dismantled, and shipped to JPL, where it was installed into the final configuration in the Cassegrain Feedcone to be used at DSS 14.

The traveling wave resonator (TWR) has achieved a circulating power of 240 kW, but the need for more cooling and greater excitation power has become apparent from initial testing. Additional cooling, particularly of the input tuners, has been applied, and the beam voltage power supply has been modified to provide up to 25 kV to gain additional power from the klystron used for TWR excitation.

C. DSS 63 100-kW Transmitter Testing

The transformer/rectifier, crowbar cabinet, high-voltage filter choke, and vault control junction box have been

assembled onto the test pad inside of a protective enclosure. The output of the high-voltage power supply was connected to the 1-MW oil-cooled dc load, and a 22-hour test run at 1 MW at 70 kV dc was accomplished.

Contractor personnel have been authorized to aid in testing at DSS 13 and implementation at DSS 63. Three have arrived at DSS 13 and training has commenced. Additionally, two members of the station staff from DSS 63 have arrived to train on the system so as to provide better support when the 100-kW transmitter is installed.

IV. In Support of Section 442

A. Clock Synchronization Transmissions

Five transmissions to DSS 42 and one transmission to DSS 51 were made during this period.

B. DSN Klystron Testing

The DSN High-Power Transmitter Maintenance Facility at DSS 13 performed acceptance class testing on three X-3075 400-kW klystrons for later use at DSS 14. Testing has been temporarily suspended while the dc power supply is used for support of DSS 63 and X-band radar testing.

V. In Support of Section 825

With the approaching encounter of Pioneer 11 with Jupiter, approximately five hours per week of support are being provided. During the period, radiation from the planet Jupiter was observed with the 26-m antenna at DSS 13, wtih the system set to receive 2295 MHz, right circular polarization. Observations of Jupiter and radio star calibrators 3C48, 3C123, 3C286, 3C348, and 3C353 were made for a total of 54 hours.

Reference

1. Jackson, E. B., "DSN Research and Technology Support," in *The Deep Space Network Progress Report 42-20*, pp. 124–127, Jet Propulsion Laboratory, Pasadena, Calif., Apr. 15, 1974.

Table 1. Pulsars selected for test observation at DSS 13

0031−07	1133+16	1929+10
0329+54	1237+25	1933+16
0355+54	1604−00	2021+51
0525+21	1642−03	2045−16
0628−28	1706−16	2111+46
0736−40	1749−28	2218+47
0823+26	1818−04	
0833−45	1911−04	

Table 2. Weak radio sources observed at DSS 13

3C48	3C218	NGC 4736
3C123	3C309.1	NGC 7027
3C138	3C348	PKS 0237-23
3C147	NGC 4258	

Program Structures for Non-proper Programs

R. C. Tausworthe
DSN Data Systems Development Section

Canonic structured programming forms the basis of an attractive software design and production methodology applicable to proper programs (programs having but one entry point and one exit point). Programs developed using this methodology tend to be easier to organize, understand, modify, and manage than are unstructured programs. However, there are notable examples in which programs either are inherently non-proper (usually, with more than one exit, rather than more than one entry), or else suffer when forced to be structured. This article addresses ways of extending the concept of structured programming to cover such cases; it is a report of an ongoing research activity to examine potential Deep Space Network software development standards.

I. Introduction

Canonic program control-logic structures, such as sequence, DOWHILE, and IFTHENELSE proposed by Böhm and Jacopini (Ref. 1) and others (Refs. 2, 3) form the basis of an attractive software design and production methodology, known as "structured programming," applicable to *proper* programs – those that have one point of entry and one exit point. Such programs developed using top-down modular, hierachic structured programming techniques tend to be easier to organize, understand, modify, and manage, especially when the canonic set includes other simple extensions of the three above, such as WHILEDO and CASE (Fig. 1).

However, there are typical cases where the strict adherence to the "one-entry-one-exit" rule for a program or program module is a *hindrance*, rather than a *help*, to effective software development. Structure for the sake of structure should not overrule structure for the sake of clarity.

One notable example of such counter-productivity, occurs when one is designing a program that is capable of detecting the existence of situations for which further processing in the current mode is either useless or unnecessary. Often, in such cases, the most desired, most logical, and most clearly understood course is to divert program control to a recovery mode or back to the user/operator for subsequent decision making and manual operations (Fig. 2).

The alternative to programming such abnormal exits of a module is to introduce structure flags as necessary to force these exits to the normal exit point; but then this flag has to be tested each time a "normal" action in the

program comes up for execution. If an abnormal condition has occurred, the normal action must be bypassed (Fig. 3). Bypassing is necessary until an appropriate nesting level is reached that the appropriate recovery procedure can be invoked in a properly structured way. This not only introduces a clutter of excess, distracting detail to slow down the programmer, but it also creates a somewhat larger, slower program. Hence, besides interfering with programmer effectiveness, strict adherence to canonic proper-program structures has caused the program itself to suffer.

It is also the case in many of the higher level languages that some statements can cause unavoidable, automatic branching to prespecified or default program locations when certain conditions occur. For example, in FORTRAN and PL/1, executing the file-input statement can result in normal input (the program continues at the next statement), an end-of-file condition (the program branches to a prespecified statement), or a file-error condition (the program branches to a separately specified statement). True "structured programming" (using canonic structures) is thus not possible whenever such statements appear.

II. Criteria for Structuring Multi-Exit Modules

The context of structured programming obviously needs to be extended, in such cases, to include constructs that fit the language and that will tend to increase design productivity and program efficiency. But great care must be taken in extending the basic set of structures, not to undo (or potentially undo) the progress that canonic structures have contributed to software development. Mills' (Ref. 3) proof of the correctness theorem depends on the "one-entry-one-exit" character of programs. Permitting modules to have multiple exits (or entries) can, therefore, be a very dangerous policy unless that policy is limited to justifiable situations where correctness is not impaired. I shall judge candidate structures to augment the canonic set relative to the following criteria:

(1) The top-down development and readability of the program design must not be impaired by the extended structures.

(2) The hierarchic, modular form of the program must be maintained using the extended structures.

(3) Program clarity and assessment of correctness on an individual module basis must not be jeopardized.

(4) The situations under which an alternate exit of a module is permissible must be limited to special situations where the need is clear and desirable, or unavoidable.

(5) The new structures must conform to the same codability conventions used for the canonic set, such as modular indentation of lines of code, easily identifiable entry and exit points, and clear connectivity of program modules.

III. Structures for Multi-Exit Modules

Iterations and nestings of canonically structured proper program modules always result in proper programs. Whenever a branching (one entry, multiple exit) node appears in a structure, there also appears a collecting node and one or more process nodes within the structure so arranged that the global view again has only one entry and one exit.

The extension of this philosophy to modules having multiple exits suggests the simple extension to structured programs found in Fig. 4.

The entire structure is a proper module, although module A obviously is not. However, if the function A has been stated explicitly enough that the two exit conditions are determinable, based on entry conditions to A, then proof of correctness is conceptually the same as for an IFTHENELSE structure. I shall use the convention found in Fig. 5 to denote and emphasize the condition for that other exit. The condition or event c under which the exit occurs is directly displayed for more clarity and better understanding.

When there are more than two exits, these can be accommodated by another configuration, analogous to the CASE structure in Fig. 6.

The box A in Fig. 6 represents, for example, the way end-of-file and file-error conditions are actually treated in programming languages such as FORTRAN and PL/1. Using the configuration shown permits file input modules in such languages to take a structured appearance not otherwise achievable.

Normally, I draw the collecting node of CASE and IFTHENELSE constructs directly under the bottom vertex of the decision symbol. However, the exits in Figs. 5 and 6 are unusual exits from a module, so I do not. Normal flow is straight down.

Looping structures can similarly be extended by this technique, as shown in the four configurations in Fig. 7. Structures (a) and (d) in Fig. 7 represent examples of programs which endlessly process streams of input data until the data quality falls below a specified condition *c*, at which time, some alternate procedure is invoked. Structure (b) represents a program *A* in which *c* senses an abnormal condition; *B* is a recovery module which initializes *A* for another try. The structure (c) would find application, for example, when information is being inserted at a terminal by *A* for processing by *B*. If *c* detects an error, the program returns to *A* for correct input; otherwise, it continues.

IV. Hierarchic Expansion of Multi-Exit Modules

All of these configurations certainly satisfy the first four criteria for extensions to the basic proper structures, at least when viewed macroscopically, as Figs. 5, 6, and 7 are. But what happens when a multi-exit function (box) at one level expands (to a flowchart) at the next hierarchic design level?

The ANSI standard (Ref. 4) technique for denoting hierarchic flowchart expansion is by way of *striping* the box to be expanded, as shown in Fig. 8. The striped module is given a procedural name, *NAME*, a cross-reference identifier *x*, and a number *n*, on its current chart. If the current chart identifier is *m*, then the box can be uniquely identified as the Dewey-decimal number *m.n*, and this number can be used for cross-referencing when no ambiguity arises. When that is the case, *x* need not appear at the point of striping.

Using top-down hierarchic-expansion methodology, one starts the design of the module at the next level with a functional description of the module and the conditions under which the several exits occur. He then proceeds to design an algorithm to perform the intended action using the usual canonic structures. In addition, he perhaps finds occasion to use one or all of the configurations of Figs. 5, 6, and 7. At some point, then, he breaks away from proper program constructs, to divert the flow of control to the alternate module exit(s). He does this by replacing a box normally appearing in a structure by an exit symbol, as shown in Fig. 9.

The flowchart which results has one *normal* (structured) exit point, and one or more *extra-normal* (unstructured) exits. It is worthwhile pointing out again that the extra exits may derive from perfectly normal non-pathological events. For example, when reading data from a file, it is a very common practice to read until an end-of-file indication occurs. Hence, the alternate exit from a box labeled "input from file" taken when the end-of-file occurs cannot be said to be an "abnormal" event. I shall refer to it rather as a *paranormal* exit (*para* from the Greek meaning "beside"), to differentiate it from the (normal) exit taken after the more usual, stated function (reading elements from the file) has taken place, and from a truly *abnormal* exit (one in response to an abortive event).

Paranormal events thus lie between the normal and abnormal; they are the simple "alternate exits" which should be allowed in the software designer's bag to permit him, among other things, to create modules which can recover efficiently from minor failures in the program or from erroneous input data.

On the flowchart of a multi-exit module, several occurrences of each paranormal exit might appear, as depicted in Fig. 10. How does such a flowchart stand in relation to the criteria I gave earlier? To me, flow through the chart does not appear disorganized, nor do any of the first four criteria seem violated; some branches just terminate early, back to an activity defined at a previous hierarchic level, that's all. The expansion of a multi-exit symbol as a separate flowchart is thus not objectionable, in my opinion.

However, if a multi-exit chart such as that in Fig. 10 were to replace its flowchart symbol at the previous level in the hierarchy, the new expanded chart would have crossing flowlines. A simplified case of this is illustrated in Fig. 11.

Non-planar flowcharts are particularly annoying to anyone trying to understand a program, because crossing flowlines detract from readability, reduce clarity and understanding, impair assessment of correctness, and attack the program organization generally. Flowcharts with on-page connectors to avoid the crossings are no better. Programming conventions which can lead to such difficulties are of questionable utility and are clearly a violation of the criteria I stated earlier.

The violation comes as the result of substituting the flowchart with paranormal exits back in place of the simple box at the earlier level. Neither of the flowcharts —that with the multi-exit box, nor its expansion at the next design level—is objectionable on a separate basis. For example, there is no objection in Fig. 10 being the next-level embodiment of box *A* in Fig. 6. But, there is

objection to substituting Fig. 10 for box *A* in Fig. 6, because then the flowlines become jumbled.

The exit points of canonic structures, coded or flowcharted, are readily located, because they invariably either appear at the bottom, or else result as the immediate consequence of the loop test, at the top. Logical flow in nested structures having exists somewhere in the middle is naturally going to be harder to read and follow, even if the flowchart remains planar. Hence even if flowlines don't become jumbled as one flowchart replaces its box at the preceding level, the resulting chart is very apt to be less readible, because of the lack of uniformity in substructure exit locations.

These objections are somewhat at variance with the way canonically structured flowcharts at one hierarchic level can replace a striped symbol at the preceding level without violating the criteria given earlier. The way to avert such difficulty is clearly not to redraw flowcharts at one level, substituting flowcharts from the next level for multi-exit striped modules. Fortunately, this restriction is superficial in a top-down *design*, because flowcharts are developed *from* striped symbols, rather than vice-versa.

V. Coding Multi-Exit Structures

I have not addressed how the structures stand in relation to the fifth criterion (codability). Obviously, there are times when the coded procedure corresponding to a striped-module flowchart might need to appear directly in-line for speed efficiency, rather than a coded call to the procedure. In canonic structures, this presents no problem, but in multi-exit structures, there is again apt to be a problem identifying the connectivity of the code. Moreover, if it were deemed objectionable to do such replacement of flowcharts for striped multi-exit modules on a 2-dimensional medium, it seems to me even more objectionable to allow substitution of multi-exit code for procedure calls in the program, a linear medium.

For readability, the following modular coding formats are useful to implement the permissible extended program structures.

Capitalized words in the formats below identify macros for control structures to be translated into whatever language is being used to write the program. The italic symbols identify programming language strings: *c* is a condition (event) which causes the paranormal cessation of the procedure called by statement *s* or of the statement *s* itself; the statements $s_1, \cdots, s_n$ and $s_m, \cdots, s_p$ are nested modules of canonic and extended structures. The skeleton flowline annotations are added merely for readability. Translation of the formats above into programming language statements can be done manually or by an appropriate preprocessor, such as the CRISP processor (Ref. 5).

(1) IF NO *c* DURING *s*

```
:->THEN  s1
:        s2
:        .
:        .
:        .
:        sn
:        END

:->ELSE  sm
         sm+1
         .
         .
         .
         sp
         ENDBLOCK
```

If $c = c_1, c_2 \cdots, c_n$
then use CASE
structures below
for ELSE module,
with ENDBLOCK
for final END:

```
CASE  c1:sm
      sm+1
      .
      .
      .
      sp
      END
```

(2) WHILE NO *c* DURING *s*

```
↑   s1
↑   s2
↑   .
↑   .
↑   .
↑   sn
←←REPEAT
```

(3) UNTIL NO *c* DURING *s*

```
↑   s1
↑   s2
↑   .
↑   .
↑   .
↑   sn
←←REPEAT
```

(4) LOOP

↑ s_1
↑ s_2
↑ ⋮
↑ s_n
←←REPEAT IF c DURING s

(5) LOOP

↑ s_1
↑ s_2
↑ ⋮
↑ s_n
←←REPEAT UNLESS c DURING s

VI. Abnormal Terminations of Structured Programs

The multi-exit structures discussed so far will extend structured-programming techniques to cases where programming to handle events using canonic structures could prove counter-productive. However, there are *abnormal* contingencies encountered during a top-down design that may not have been fully identified at earlier levels as part of a module's normal function. Yet, in order for the program to perform correctly, the abnormal situations must be dealt with, and hopefully, *not* by redesigning the previous levels.

For example, it may be known intuitively ahead of time that some arithmetic operations can result in overflow-errors under certain (perhaps unknown) input conditions. But it may not be knowable, until an actual algorithm is designed, just where the overflows will occur, or what the input conditions that cause them will be.

In other cases, there may be knowable, specifiable contingencies which represent abnormal departures from the program's normal functionings, which the program must respond to (or recover from). A decision table drawn up for this program would likely classify such abnormal conditions into the "ELSE-rule" category--all cases not specifically defined by the program's intended behavior under normal, error-free input.

In some cases, recovery procedures can be instituted by the program itself; in others, operator intervention may be required. Different types of abnormalities will conceptually require entirely separate recovery procedures. For example, a program which generates a report from several files may conceivably be asked to complete the report because some identifiable parts of the report may yet be useful, even though one of the files continues to be read occasionally in error. However, in the same program, execution may be halted and control returned to the operator if one of the files cannot be found.

Abnormal exits to many unstriped modules are often overlooked because the abnormal exit is implied in the code for that module. A flowchart box labeled "A=B+C" would, for example, be coded in FORTRAN as "A=B+C"; but if A and B are large enough, an overflow trap automatically kicks the control to some error-handling procedure. Yet these connections are seldom put on the flowchart. Indeed, if such implicit actions were required to be drawn onto a flowchart, as in Fig. 12, few "structured programs" would exist. And imagine all the confusion trying to follow all the jumbled lines!

A similar statement holds concerning abnormal terminations of striped modules. In order for us to be able to design and program using what *appear* to be structured programming techniques, it is usually necessary for us to suppress the flowchart connections for abnormal situations, at least down to that design level where an abnormal event is sensed explicitly and an explicit branch to the recovery procedure appears. But if program modules—unstriped, as well as striped—may have abnormal contingencies whose connections may not appear in an explicit form at a given design level, then program response can only be fully and readily assessed if the conventions for suppressing the connections are easily remembered, fully understood, and rigorously adhered to.

Of course, it may be entirely possible that a program can invoke a recovery procedure and return to normal processing in a purely structured way. Such cases, even though induced by abnormal events, nevertheless can be handled by the normal and paranormal-exit structures already discussed. It is the others that must be covered by the convention.

The rule for displaying abnormal terminations which, to me, seems most in keeping with the first four criteria given earlier is the following: *Flowlines corresponding to abnormal terminations exiting from modules may be omitted at all hierarchic levels beyond that at which the recovery module appears on a structured flowchart and which also shows the flowline connection from the parent module which contains the nested submodule(s) from which the abnormal exit is made.*

Figure 13 depicts a chart at which a particular abnormal termination first appears. The recovery procedure appears as a module (here named RECOVERY) executed whenever the abnormal error event occurs in later levels. The exploded views of striped submodules of *B* being aborted do not show either the *error* condition or the module termination symbol labeled "RECOVERY" unless there is an explicit need to do so (e.g., when *error* is actually tested as an unstriped module), or unless showing them contributes to readability, understandability, assessment of correctness, etc. As the latter of these represents an optional case, the abnormal exit can appear merely as a comment, as shown in Fig. 14.

VII. Labeling Flowchart Exits

There is obviously a need for correct and consistent labeling of the exit terminals of a module flowchart, so that the reader can tell immediately and with certainty whether it is a normal, paranormal, or abnormal subprogram exit, or a subroutine return. Further, he must be able to locate the procedure next to be executed following the exit easily and unambiguously.

The conventions summarized in Fig. 15 (of which only a subset may actually be operable within a given system) contain an identifier within the terminal symbol, and in some cases, a module number designator which labels the point of continued activity. This number, denoted by *n* in the figure, can be optional whenever *n* is a module appearing on the same chart at the immediately preceding level as the current striped module being terminated, such as is true for cases (c) and (e) of the figure. It may be supplied to aid in locating the next procedure. The number is mandatory, however, for an abnormal exit to an unnamed procedure (case (f)) defined at an earlier level, or to a named procedure (case (g)) when there is more than one named abnormal procedure in the program. The former mandate is clearly one to identify program connectivity unambiguously; the latter is only for ease in locating the referenced procedure in the documentation.

VIII. Coding Module Extra-Normal Exits

A top-down program may be written, as I indicated earlier, in a format whereby each module has its entry at the top and a normal (structured) exit at the bottom. Any exits in between are either calls (transfers) to modular procedures (usually, but not always) farther down in the code, or extra-normal transfers to points within modules at previous design levels, always higher up in the code.

Calls can be classified by the data-space state upon initiation of the called procedure. For example, subroutine calls pass the return address and optional arguments to the subroutine procedure, often in a stack configuration. Coding for the normal exit (in the subroutine case, RETURN) reconfigures the data space for proper resumption of program execution. *The same consideration must be given to extra-normal exits.* (In the subroutine case, these exits must also unstack return addresses and arguments).

Abnormal terminations may transfer back through an arbitrary number of levels, all at once, to a program recovery procedure. Hence, any data-space assumptions in effect at the higher level must be restored prior to the transfer. Paranormal exits may likewise transfer back through a number of levels, but only one flowchart level at a time (although in an optimized object code listing, this could appear as a single jump after appropriate data-space recovery, as above).

Just as it facilitates flowchart readability and understandability to identify normal, paranormal, and abnormal exits separately (but consistently), it is likewise the case with the code corresponding to these exits. Unfortunately, most programming languages do not have separate branching statements for all the cases in Fig. 15. However, coding conventions may be adopted, either in the form of annotations or, better yet, macros, to effect and display the program module connectivity. Table 1 summarizes such a set of conventions.

IX. Conclusion

This paper has demonstrated that the concept of structured programming can be extended to multi-exit structures in a natural way. The methods preserve almost all of the advantages of structured programming: top-down development, hierarchic expansion, program modularity, and assessment of correctness. At the same time, they relax structural constraints to take advantage of more efficient program configurations than are possible with canonic structures.

Acknowledgment

I would like especially to thank Dr. James Layland for his review, comments, and helpful discussions during the preparation of this paper.

References

1. Böhm, C., and Jacopini, G., "Flow Diagrams, Turing Machines and Languages With Only Two Formation Rules," *Communications of the ACM*, Vol. 9, pp. 366-371, 1966.
2. Dijkstra, E. W., "Structured Programming," in *Software Engineering Techniques*, NATO Science Committee, edited by J. N. Burton and B. Randall. Kynoch Press, Birmingham, England, April 1970. Available from Scientific Affairs Div., NATO, Brussels, Belgium.
3. Mills, H. D., "Mathematical Foundations for Structured Programming," IBM Document FSC72-6012, Federal Systems Div., IBM, Gaithersburg, Md., February 1972.
4. "American National Standard Flowchart Symbols and Their Usage in Information Processing," ANSI-X3.5-1970, American National Standards Institute, Inc., New York, N.Y., Sept. 1, 1970.
5. Tausworthe, R. C., "Control Restricted Instructions for Structured Programming—CRISP," to appear in next issue.

Table 1. Module exit conventions

Type	Meaning
SYSTEM	Program termination, return control to system
STOP	Program termination, return control to operator
END *n*	Subprogram normal termination. Control transfers to module *n* at preceding level; *n* is specified optionally
RETURN	Subroutine normal termination. Control returns to calling module
EXIT *event* TO *n*	Paranormal exit. Control passes to *event* case, program module *n* at the preceding level; TO *n* specified optionally
ABORT TO *n*	Abnormal exit to module *n* at earlier level; *n* is mandatory
ABORT TO *ABNAME* AT *n*	Abnormal termination to module named *ABNAME*, numbered *n*; AT *n* is optional

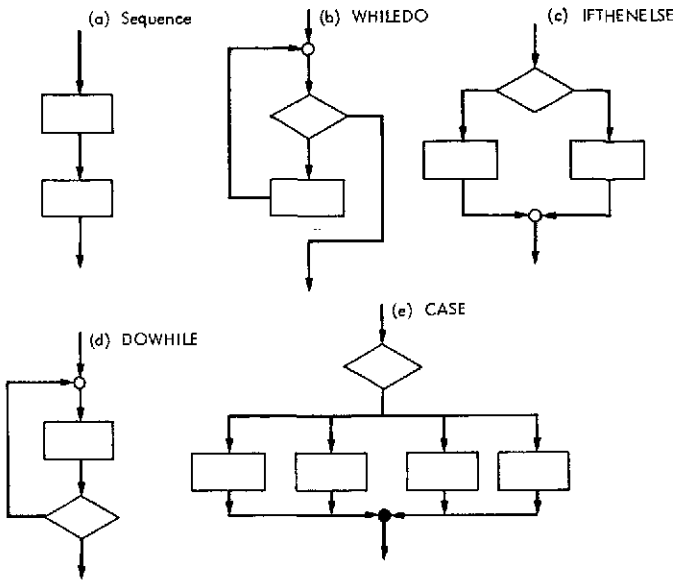

Fig. 1. Canonic program structures

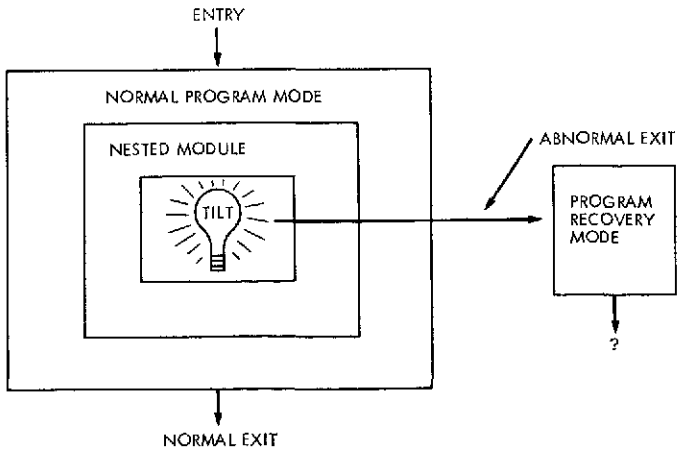

Fig. 2. Abnormal exit from a Nested Structured Program

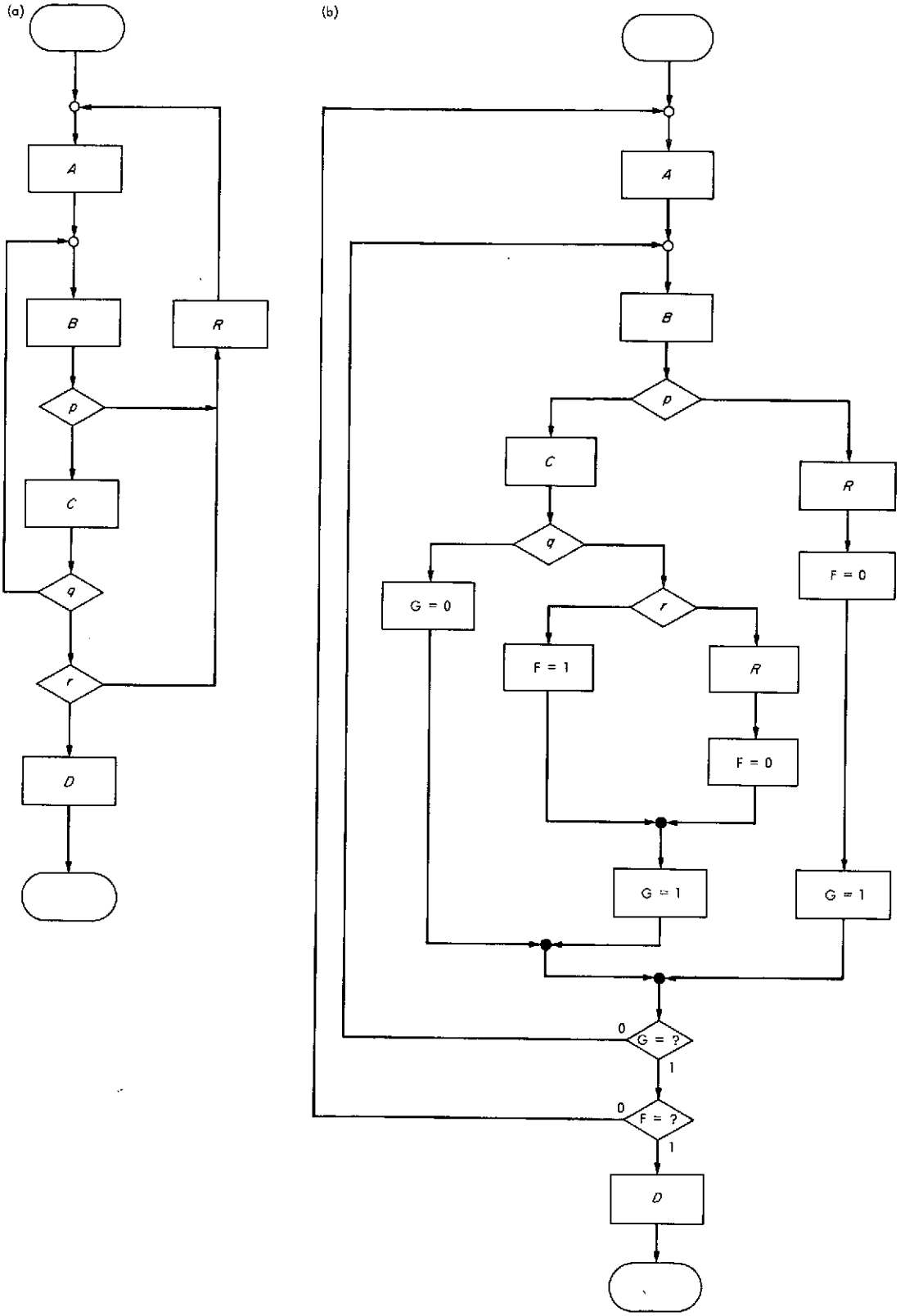

Fig. 3. Abnormal condition (a) unstructured program in which *p* and *r* are tests which indicate further execution is useless; *R* is recovery module which then initiates program restart, (b) structured form of (a)

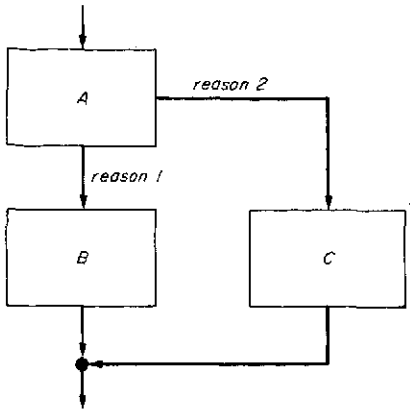

Fig. 4. Multiple exits configured into an IFTHENELSE-like structure

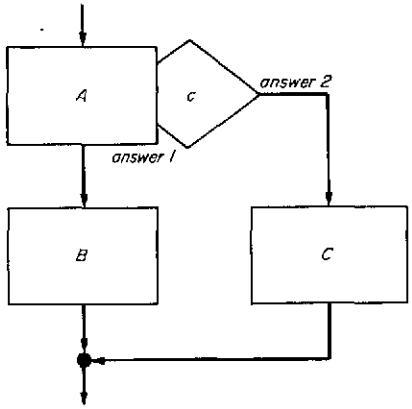

Fig. 5. Multi-exit program configuration with exit condition explicitly labeled

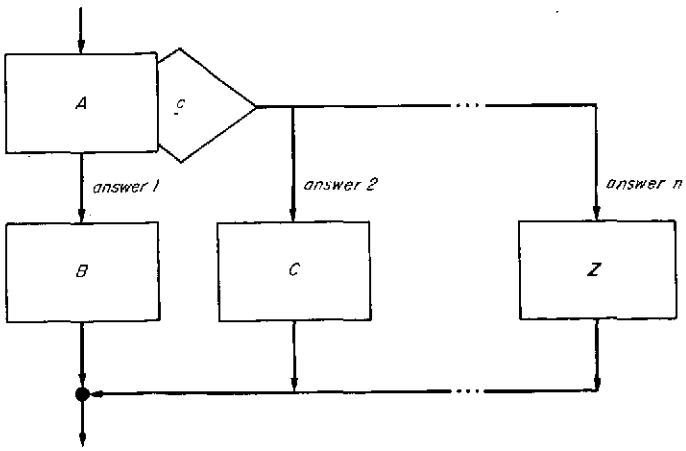

Fig. 6. Multi-exit CASE-like configuration with exit condition explicitly labeled

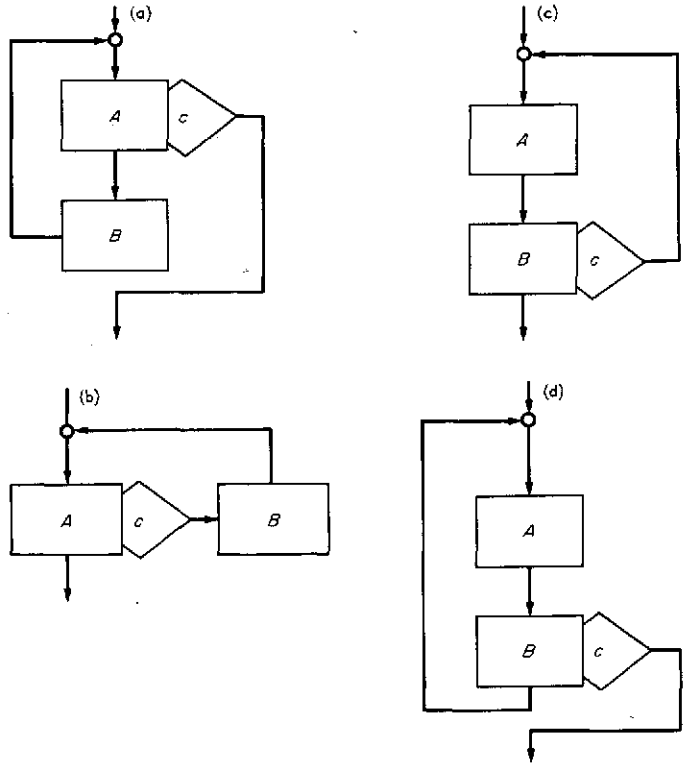

Fig. 7. Looping configuration with multi-exit structures

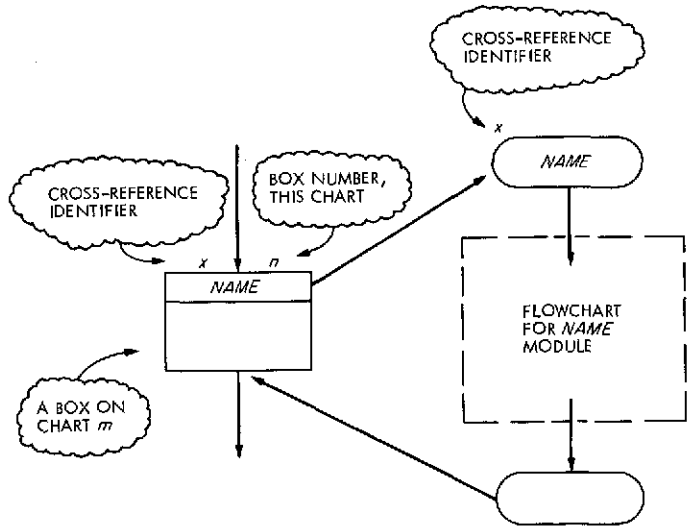

Fig. 8. Hierarchic expansion of striped flowchart symbol

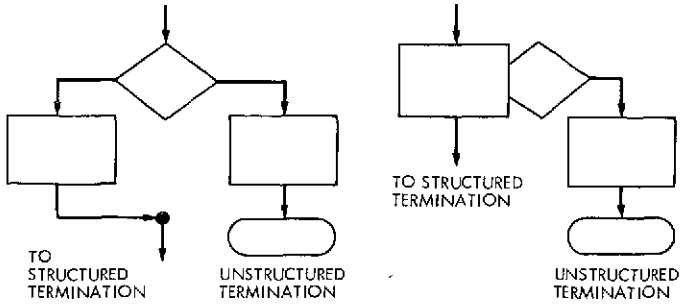

Fig. 9. Modes of generating multiple exits in otherwise structural programs

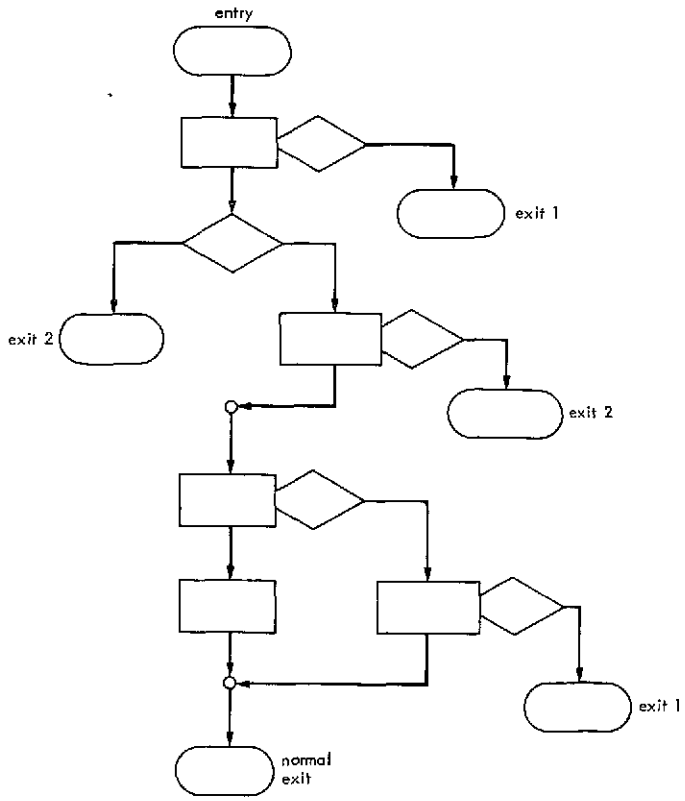

Fig. 10. Possible expansion of a module with two extra-normal exits

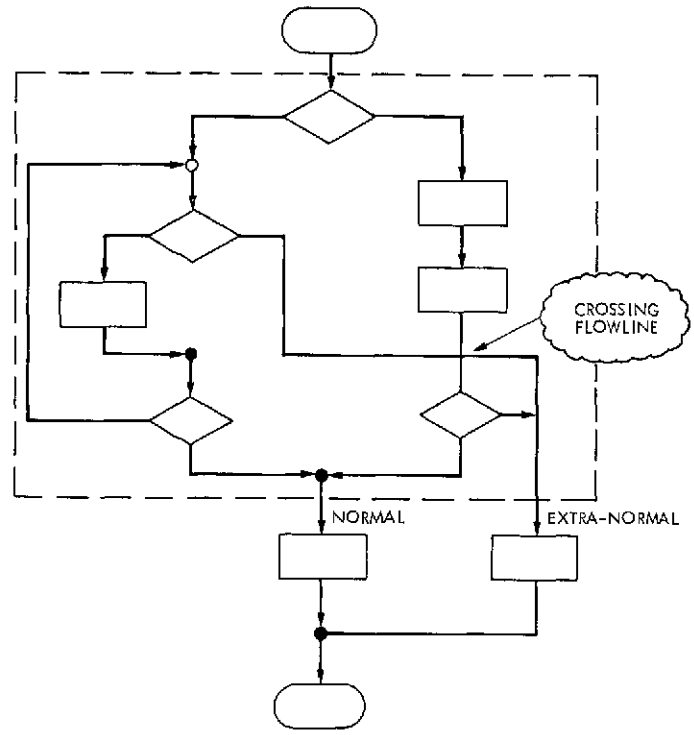

Fig. 11. Crossing flowlines can appear when the flowchart of a multi-exit box replaces the box

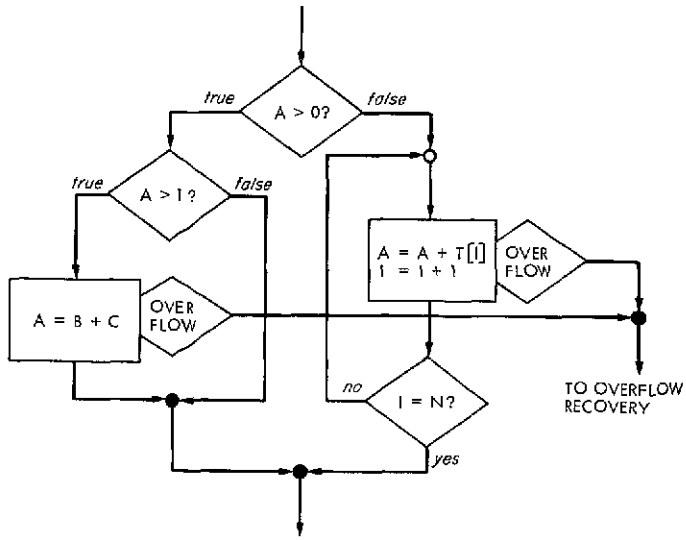

Fig. 12. Implicit abnormal contingencies in a simple "structured" program

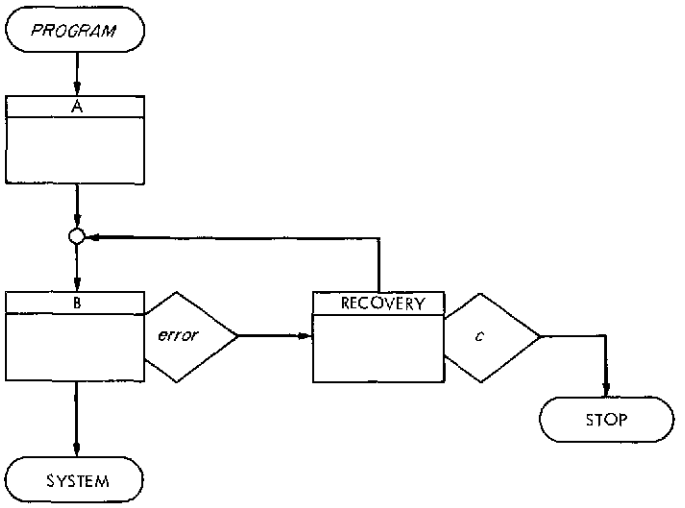

Fig. 13. A Program A THEN B, in which an occurrence of *error* during the execution of B initiates the RECOVERY procedure. If recovery under criterion c is possible, B is tried again; if recovery is not possible, control returns to the operator

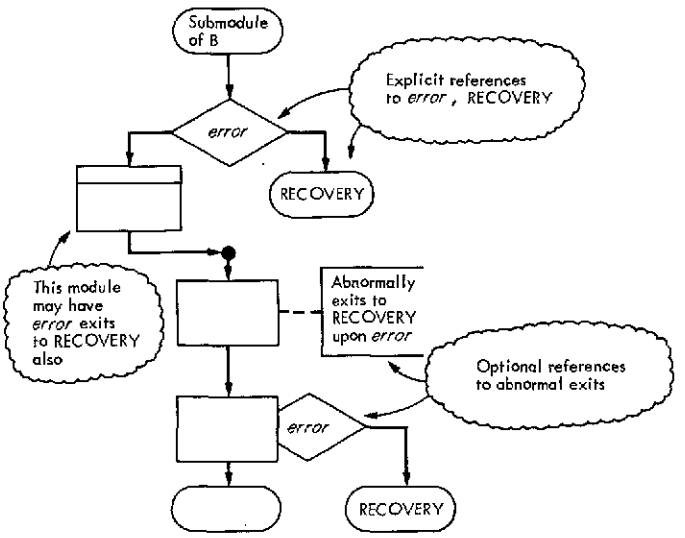

Fig. 14. Notation for abnormal module terminations at levels deeper than RECOVERY

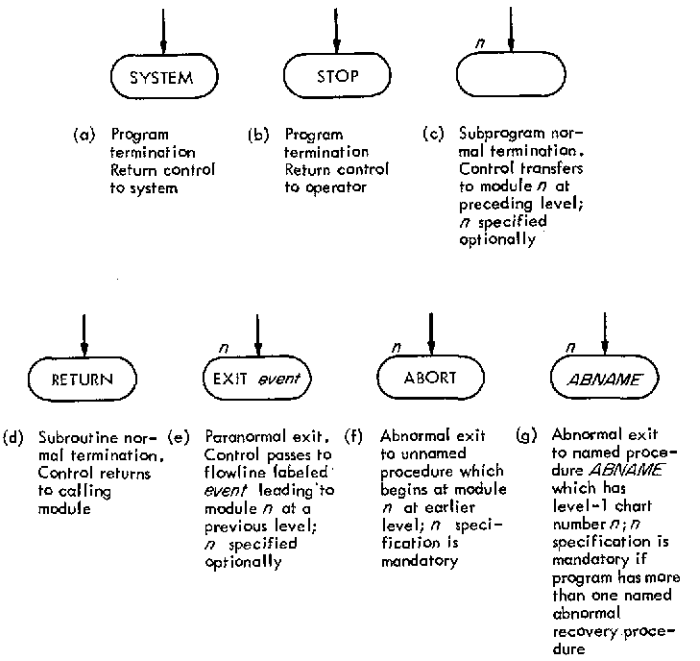

Fig. 15. Module termination symbol annotation conventions

The Star Switch Controller Used in the Network Control System

T. O. Anderson
DSN Data Systems Development Section

This article describes the Star Switch Controller used in the Network Control System (NCS). The NCS requirements are first discussed as are different design philosophies for multi-computer hardware interface systems. The technique adopted is then presented and the functional characteristics discussed.

I. Network Control System Requirements

The Network Control System (NCS) computer-to-computer or computer-to-device communication requires that any one of a set of 16 computers or devices be able to transfer data to any other of the same set. The data transmission is unidirectional and of short duration to allow similar subsequent transmissions between other sets.

Different system design philosophies for a system to meet these requirements were studied, including a serial as well as parallel bus system and a commutator system (Ref. 1).

The following characteristics led to the selection of the commutator or "star" system:

(1) The often used common bus system involves a great deal of modification and addition of control logic to each device, such as addressing and detection logic and bus priority logic.

(2) The ring interface readily lends itself to message broadcasting, but verification of message acceptance by each of the multiple receivers is difficult.

Broadcasting on a star must be accomplished by means of multiple transmission, and verification of message receipt in the star configuration is simple.

(3) The concept of addressing processes, rather than devices, can be implemented in either configuration with equal effort.

(4) The capability of transmitting variable length blocks, which may be desirable for reducing software overhead is not practical in the ring configuration but is easily accommodated in the star configuration.

(5) A message priority system can be implemented easily in a star configuration. For the ring configuration, an overlay priority system would increase both hardware and software complexity.

(6) Both ring and star configurations have central failure points. The serial nature of a ring causes each interface to be a central point of failure, and location of and recovery from failures appears more complex than in the star since it is difficult for any one processor to pinpoint the failure location. The central point of failure in the star configuration is a single controller and switching bus.

II. The Star Switch Controller Application in the Network Control System

Within the NCS two general classes of messages are transmitted across the Star Switch Controller (SSC). The first is the High-Speed Data Block, which is a 1200-bit data block originated by the DSS and each of the subsystems in the network. The second class of message may be of any length and is generated by any of the subsystems shown at the far right of the diagram in Fig. 1 for transmission to any other of these subsystems.

For added system reliability as well as multiple-path transmission, several star switching networks may well be connected in parallel. For a larger number of ports, any one or several ports may again be connected to other stars in a subcommutation scheme. For priority ranking, one may also consider super commutation schemes where one device is connected to two or more ports of a star.

All messages with the exception of High-Speed Data Blocks sent to and received from the DSN consist of two segments: a preamble which describes the message and the message itself. Transfer of control information is accomplished by transmission of a preamble alone. In addition the Standard Interface and the SSC hardware require two words preceding each transmission which define the operation as a data transfer and specify the destination of the message.

III. Functional Description of the Star Switch Controller

Figure 2 shows an abstract diagram of the SSC. The diagram resembles the face of a clock with two hands M and DM. The face is divided into 16 hours. Hand DM resembles a regular hand, while hand M has the arrowhead at the center pointing inwards rather than toward the periphery.

Hand M scans at high speed in search of a request from any one of 16 input ports to transmit. Once such a request has been located the hand stops. A process code is received by the SSC which is decoded using the process/device assignment table stored in memory. Hand DM is then directed to the assigned device and the requested link is established. Upon completion of data transmission, hand M resumes the scanning and the same procedure is repeated. Hand M rotates in one direction only, while hand DM is instantaneously directed to its destination.

If, during a transmission, the recipient device is unable to receive the data within the allotted time, time-out disconnect occurs. The fact that time-out occurred is reported back to the transmitting device as are other error conditions that may arise.

The SSC contains a routing code table stored in a memory. Any device may load or reload this process/device assignment table, either the entire table, sections thereof, or individual entries.

In the latter case, a device is merely introducing itself, as its present port number is part of the entry. Any device may also read out the entire memory contents for verification.

IV. Functional Components

The major functional components of the SSC, which are shown in block diagram form in Fig. 3, are:

(1) The sequencer, which addresses the input multiplexer and together with it forms a scanning device that scans the request-to-transmit lines.

(2) The inbound multiplexer, which selects the next inbound port with an asserted request-to-transmit line.

(3) The memory, which stores the routing table or process/device code conversion table.

(4) The timing control logic, which is used to receive the routing instruction characters and to load and unload the memory (Refs. 2 and 3).

(5) The demultiplexer, which, when addressed by the output from the code converting memory, selects the outbound port.

The Star Switch Controller is illustrated in Fig. 4 and is described in detail in Specification No. ES508535, Revision A (Ref. 4). This unit is being successfully used in the NCS.

References

1. Thurber, K. J., Jensen, E. D., and Jack, L. A., "A Systematic Approach to the Design of Digital Bussing Structures," Fall Joint Computer Conference, p. 719, 1972.

2. Lee, D. K., *Detail Specifications for Deep Space Network Control System, Standard Interface,* JPL Equipment Specification ES508534, Rev. A, May 1973 (JPL internal document).

3. Anderson, T. O., "NCS Standard Computer Interface Hardware, Its Timing and Timing Control Logic," in *The Deep Space Network Progress Report,* Technical Report 32-1526, Vol. XIX, pp. 152–160, Jet Propulsion Laboratory, Pasadena, Calif., Feb. 15, 1974.

4. Anderson, T. O., *Detail Specification for the Star Switch Controller in the Deep Space Network,* JPL Equipment Specification ES508535, Rev. A, Jan. 1974 (JPL internal document).

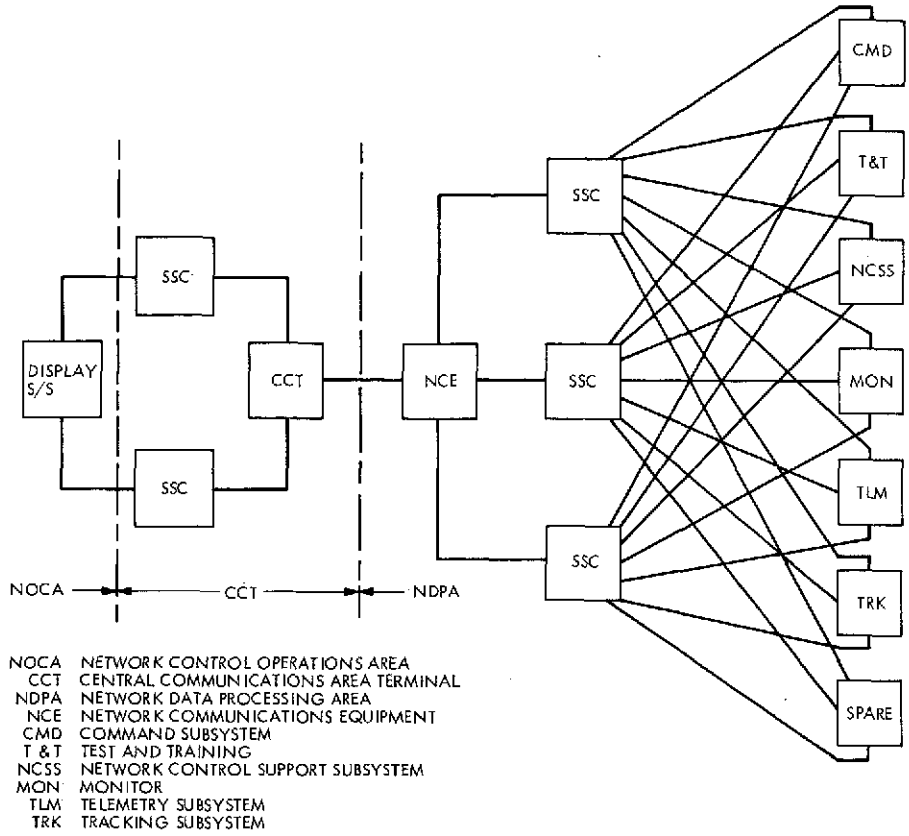

NOCA NETWORK CONTROL OPERATIONS AREA
CCT CENTRAL COMMUNICATIONS AREA TERMINAL
NDPA NETWORK DATA PROCESSING AREA
NCE NETWORK COMMUNICATIONS EQUIPMENT
CMD COMMAND SUBSYSTEM
T & T TEST AND TRAINING
NCSS NETWORK CONTROL SUPPORT SUBSYSTEM
MON MONITOR
TLM TELEMETRY SUBSYSTEM
TRK TRACKING SUBSYSTEM

Fig. 1. Application of the SSC in the NCS

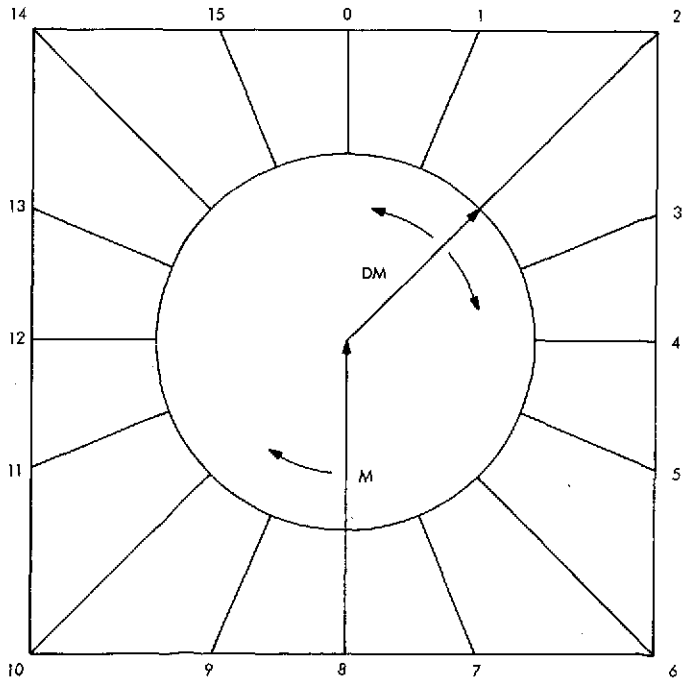

Fig. 2. Abstract diagram of the SSC

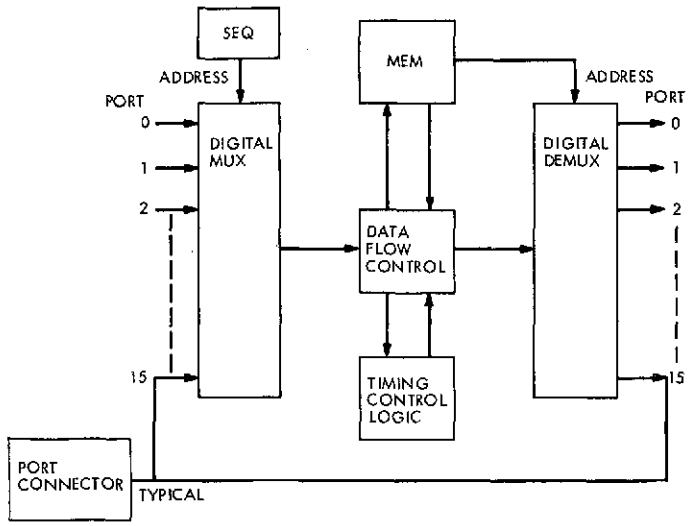

Fig. 3. SSC block diagram

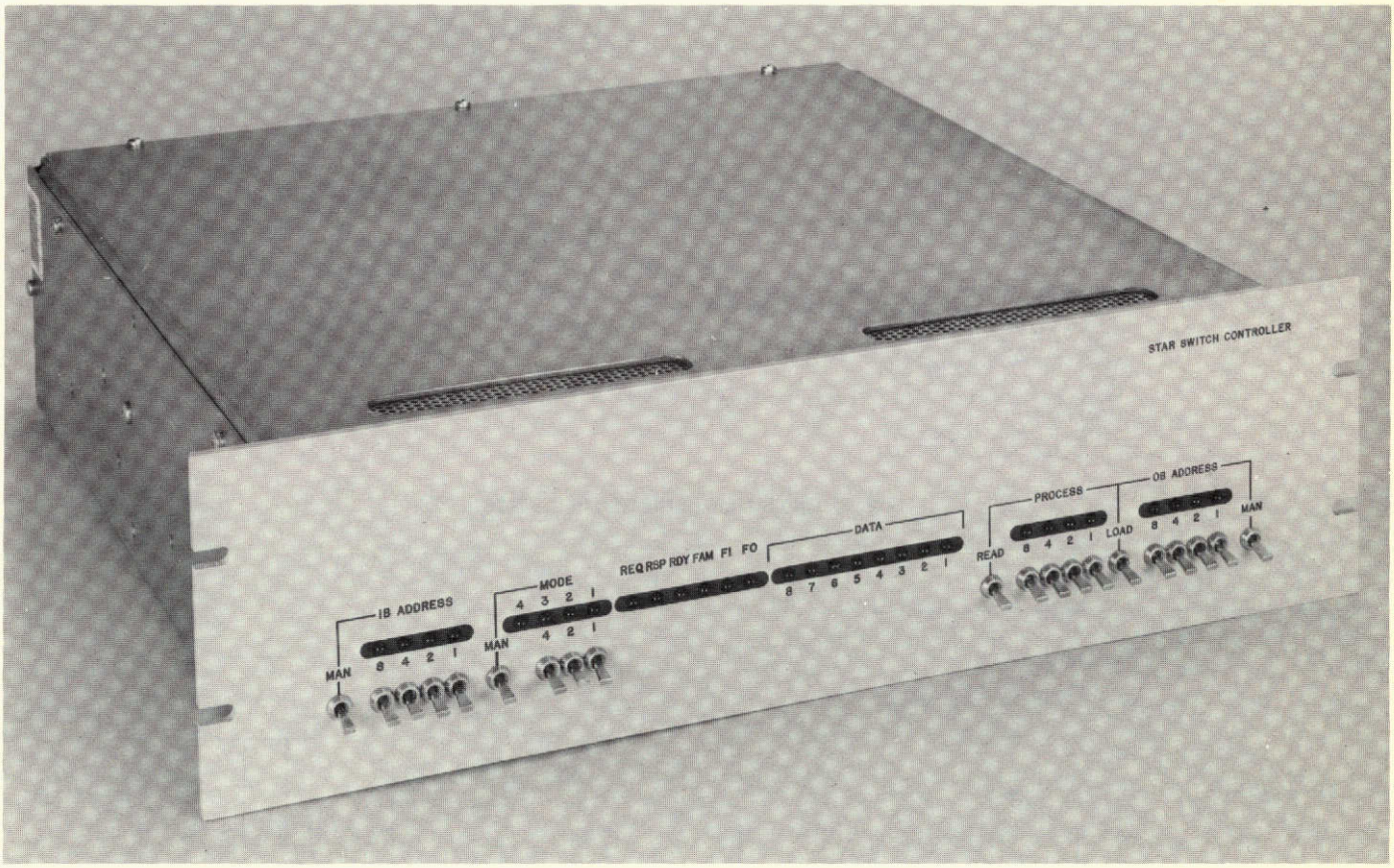

Fig. 4. Star switch controller

Planetary Ranging Operational Software

G. R. Osborn
DSN Data Systems Development Section

The Planetary Ranging Operational Program is now in use at DSSs 12, 43, and 63. It provides ranging capability to several AU. The program also monitors changes in the charged particle density due to diurnal variations in Earth's ionosphere and solar outbursts. The charged particle measurement is used to correct the doppler data. Both outputs contribute to the more precise orbit determination required for multiple encounter and orbiter missions.

I. Introduction

The Planetary Ranging Assembly is operational at DSSs 12, 43, 63, and 71, and CTA 21. It was used in support of MVM'73.

Discrete frequency ranging is presently implemented in the software. The algorithms are essentially the same as those used in the research and development (R & D) discrete spectrum (mu) machine, which was used for MM'71 (Refs. 1 and 2). Continuous spectrum (PN code) ranging will be available for Helios using algorithms similar to those in the R & D continuous spectrum (tau) machine (Refs. 3 and 4). Only discrete spectrum ranging is discussed here.

The program produces two data types, range and differenced range versus integrated doppler (DRVID). The range is measured in light time units with a resolution of about 15 centimeters. The maximum range which can be measured without ambiguity varies with the number of components specified, being about 0.5 light second when all 20 components are used.

DRVID, which is monitored throughout the pass, is used for charged particle calibrations. Diurnal variations in Earth's ionosphere cause a variation in indicated spacecraft range of several meters during a pass. While the range error itself is insignificant, its diurnal variation introduces a systematic bias in apparent spacecraft angular position as derived from the doppler, causing significant navigation errors.

The program runs in a dedicated Interdata ID-4 minicomputer. The assembly language program uses most of the 16-kilobyte memory.

Program control is from a hexadecimal keyboard and a 256-character (8 × 32) display panel. The panel displays eight variables, and a short description of each. During

initialization the variables displayed include the code type, the integration times, and the acquisition time. The operator updates the list and starts the acquisition.

The initialization parameters are used to build a schedule table containing the time and subroutine address for each event in the acquisition sequence. Events are timed to integer seconds. The time each component is transmitted, reception time (one round-trip light time later), and the time the range number is computed are typical events. The program then counts down to acquisition time. No further manual intervention is necessary.

II. Acquisition Sequence

The discrete frequency coders consist of chains of 20 flip-flops, producing 20 square waves having frequencies between approximately 1 Hz and 500 kHz. All but the highest frequency is used to bi-phase modulate the 500-kHz signal. Each component is then a 500-kHz square wave which is periodically inverted. This process keeps most of the ranging power at high frequencies, minimizing interference with the telemetry and command channels.

Since the received waveform is the same as that transmitted, the ranging phase detector output as a function of phase is the autocorrelation function. The autocorrelation function for the first four components is shown in Fig. 1. Only one of the phase detector outputs (the "in-phase") is shown. The other (quadrature) output is similar, except that it has zero crossings where the in-phase output has peaks.

The general form of the C_3 and higher autocorrelation functions is a triangular wave modulated by a lower-frequency triangular wave. The phase of the high-frequency component is sensitive to small displacements, and is used for DRVID during acquisition. The polarity of the low-frequency component is used for range measurement. The components are transmitted sequentially, starting with the highest frequency, C_1 (the clock).

Before the start of clock reception, both coders are driven by the exciter voltage-controlled oscillator (VCO), and run at the same frequency and phase. Doppler rate aiding is applied to the receiver coder at the start of the next second after predicted clock reception. The range number will be valid for the spacecraft position that existed at the instant the rate aiding was applied.

For a receding spacecraft the receiver coder thereafter runs at a lower frequency, the new frequency exactly matching that of the doppler-shifted ranging signal. The phase relationships between the receiver coder and the received signal remain indefinitely as they were at the instant the doppler rate aiding was switched in, and can be measured leisurely.

The phase detector outputs are integrated over 0.25-second intervals by the hardware. The integrator outputs are digitized with two 8-bit analog-to-digital converters, and an interrupt is generated to the computer.

In order to cancel dc offsets in the analog circuitry, the reference signals to the phase detectors are inverted or exchanged each quarter second. The software decommutates the two inputs, and inverts the previously inverted samples. The resulting A and B outputs, when summed over one second, are free of gain and offset errors. These one-second samples are integrated for the time specified during initialization.

The clock phase is computed from the integrated phase detector outputs using the equation

$$\tau = 512\left(1 - \frac{B}{|A| + |B|}\right)\frac{B}{|B|} \qquad (1)$$

where A is the in-phase detector output and B is the quadrature output. The equation produces a number in the range -1024 to 1023 range units, corresponding to -180 to nearly $+180$ degrees in phase.

The clock phase measurement constitutes the low order 11 bits of the range number. The remaining bits depend on the polarity of the other components.

For the C_2 integration, the receiver coder is shifted to place the clock over a positive peak. Figure 1 shows that if the clock is shifted to a positive peak, the C_{2A} component will be at a positive or a negative peak rather than a null, and only channel A polarity need be measured for range acquisition.

The C_2 integration in the example (Fig. 1) produces a negative result. In this case, 2048 or 2^{n+9}, where n is the component number, is subtracted from the range number. Further, in order that the C_3 integration also be on a peak, the receiver coder is shifted by 180 degrees of C_2. This is accomplished by inverting the flip-flop in the divider chain which produces C_2, which advances the receiver coder.

The process is repeated for each additional component C_n: if the channel A output is negative, then 2^{n+9} is subtracted from the range number and that component is inverted in the receiver coder.

This algorithm usually produces a negative range number, which is then evaluated modulo 2^{m+10}, where m is the last component number.

III. DRVID

The doppler rate aiding is only exact for a dispersionless transmission path. Doppler rate aiding is derived from the carrier phase delay, while the phase of the ranging signal depends on the group delay. Changes in the columnar charged-particle density therefore cause a small phase error, which is measured for DRVID.

The program measures DRVID both during and after acquisition. It is apparent that Eq. (1) could be used during acquisition to compute the phase of C_2, as was the case for C_1. Since the period of C_2 is twice that of C_1, the result would have to be doubled to provide DRVID in range units. Different correction factors apply to each component.

A simple numerical calculation shows that the slope of C_2 near 0 deg is ½ that of C_1; C_3 is ¾ that of C_1, and in general

$$M_{C_1} = \frac{2^{n-1}}{2^{n-1}-1} M_{C_n} \tag{2}$$

The channel B output is by definition zero at 0 deg. It is therefore only necessary to multiply by the slope correction factor from Eq. (2) to obtain the corrected B:

$$B' = \frac{2^{n-1}}{2^{n-1}-1} B = B + \frac{B}{2^{n-1}-1}$$

The magnitude of the channel A slope is identical to that of channel B. A geometrical argument leads to:

$$A' = A - \left| \frac{B}{2^{n-1}-1} \right|$$

The resulting A' and B' values are averaged over several components and used with Eq. (1) to compute DRVID during acquisition. The system returns to the clock for DRVID after acquisition, where no correction is required.

The receiver coder is shifted back to the peak whenever it drifts more than 16 range units away, permitting arbitrarily large DRVID excursions to be tracked.

IV. Signal-to-Noise Ratio Estimator

The program provides an estimate of P_r/N_0, the ratio of ranging power to noise power density. The quantity is computed from

$$\frac{P_r}{N_0} = 10 \log_{10} \frac{(|A| + |B|)^2}{\sigma_A^2 + \sigma_B^2} BW$$

The equation is of a different form from that which would be used for sinusoidal signals. The problem is that the total detected power, which is proportional to $A^2 + B^2$, is, for square waves, a function of phase angle. The quantity $(|A| + |B|)^2$ indicates what the detected power would be if the received signal were in phase with the reference, and can be used to estimate P_r/N_0 regardless of phase angle.

BW is the total noise bandwidth. The detection process folds the signal about zero, so the noise bandwidth of the post-detection low-pass filter is doubled to get the RF bandwidth.

The low-pass filtering is mostly due to a single-pole RC network having a time constant of 0.36 second. The digital sampling technique used further reduces the noise bandwidth. The baseband noise bandwidth, considering both analog and digital effects, is 0.51 Hz.

V. Program Outputs

The range number is transmitted to the Mission Control and Computing Center (MCCC) when it becomes available. DRVID and estimated P_r/N_0 are sent periodically throughout the pass. These parameters are also displayed at the DSS Tracking Subsystem (DTS) control panel, along with relative time, correlator outputs, and the component being processed. The displayed parameters can go simultaneously to a teletype if local hard copy is needed.

VI. Summary

Planetary ranging has existed as an R&D effort for several years. New hardware and software have now been installed at selected sites, making ranging to planetary distances a routine operational capability of the DSN.

References

1. Goldstein, R. M., "Ranging With Sequential Components," in *The Deep Space Network*, Space Programs Summary 37-52, Vol. II, pp. 46–49, Jet Propulsion Laboratory, Pasadena, Calif., July 31, 1968.

2. Martin, W. L., "Information Systems: A Binary-Coded Sequential Acquisition Ranging System," in *The Deep Space Network*, Space Programs Summary 37-57, Vol. II, pp. 72–81, Jet Propulsion Laboratory, Pasadena, Calif., May 31, 1969.

3. Tappan, R. W., "DSIF Technical Description, Planetary Ranging Equipment, MM'71 Configuration," TD505943A, Feb. 4, 1972 (JPL internal document).

4. Tausworthe, R. C., "Digital Communication and Tracking: Ranging Measurement," in *The Deep Space Network*, Space Programs Summary 37-42, Vol. III, pp. 52–56, Jet Propulsion Laboratory, Pasadena, Calif., Nov. 30, 1966.

Bibliography

MacDoran, P. F., and Martin, W. L., "DRVID Charged-Particle Measurement With a Binary-Coded Sequential Acquisition Ranging System," in *The Deep Space Network*, Space Programs Summary 37-62, Vol. II, pp. 34–41, Jet Propulsion Laboratory, Pasadena, Calif., May 31, 1970.

Tappan, R. W., "Planetary Ranging," in *The Deep Space Network Progress Report*, Technical Report 32-1526, Vol. XIX, pp. 165–168, Jet Propulsion Laboratory, Pasadena, Calif., Feb. 15, 1974.

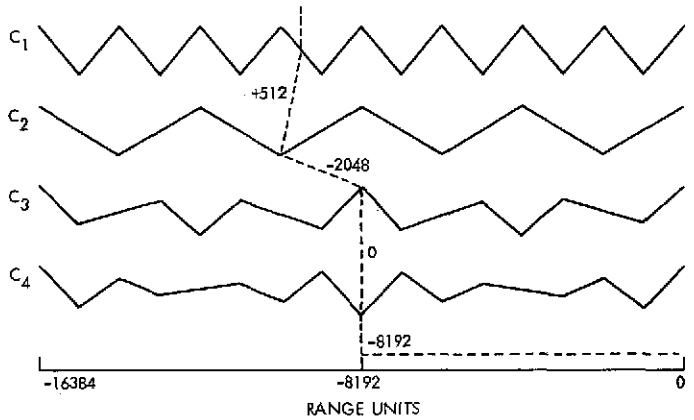

Fig. 1. Acquisition sequence

Data Decoder Assembly Reliability Modifications

R. A. Mancini
DSN Data Systems Development Section

While the Data Decoder Assembly (DDA) has met the required goals of the decoding and processing of telemetry data in the DSN, it has exhibited a higher than desired failure rate. These failures were predominately of an intermittent nature and occurred more consistently in the controlling processor, the Interdata Model 4 (ID4) minicomputer. General lack of mechanical rigidity and the electromechanical construction used on the selector channels were determined to be the main contributors to these intermittent failures. These weaknesses in design initiated the bulk of the problems by causing connector contacts to become intermittent during operation. Mechanical redesign of the ID4 front panel hinges and a design for a cabinet strut stiffener were implemented in the DSN. Newer design, more reliable selector channels were purchased and installed in all ID4s in the DSN. These changes significantly reduced the failure rate; however, there still remains a much lower failure rate, the source of which is being investigated.

I. Introduction

The Data Decoder Assembly (DDA) is part of the Telemetry and Command Data Handling Subsystem of the Deep Space Network (DSN). In operation, the DDA is capable of performing three mutually exclusive functions: sequential decoding of convolutionally encoded data, block decoding of 32/6 or 16/5 biorthogonal block coded data, or high-rate data formatting of encoded or uncoded data for transmission on the wideband data line with simultaneous recording of the data on magnetic tape.

An Interdata Model 4 (ID4) minicomputer is one of nine assemblies mounted in a standard 205.74-cm (81-in.) equipment cabinet which makes up the DDA.

II. Background

Beginning with the first delivery of the JPL configuration of the ID4 computers (used in the Data Decoder Assembly), problems of an intermittent nature have been encountered. It should be pointed out at the beginning

of this report that the JPL configuration (mechanical mountings) of the ID4 was not an Interdata standard.

Interdata bolted their computer chassis into a standard 48.26-cm (19-in.) rack and made all interface cable connections from the front of the rack under the control panel, which was hung from the rack mounting frame on special hooks provided for this purpose.

JPL required that the computer be mounted on slide rails for ease of replacement (at that time sparing was to be done at the computer assembly level). Also, the control panel was hinged to the computer's main chassis to provide access to the motherboards (large component boards of the computer containing modularized computer functions, sometimes requiring several motherboards). Interfacing was required to be through (JPL selected) connectors mounted on the rear of the computer assembly. Also JPL required the use of vinyl sleaving for cables instead of the woven cloth used by Interdata.

Unfortunately, the mechanical design changes required of Interdata were not engineered properly; thus:

(1) The original hinges were not operative until the computer was pulled out on its slides enough to provide clearance for the swing of the hinged front panel.

(2) The chassis was expanded into a double bay configuration but fabricated of the same material as for the single bay and with no stiffening to provide rigidity normally given by the rack framework.

(3) The vinyl sleaving used for cables exerted excessive torque on the daughterboard (component board and or cable plug-ins to motherboard) connectors causing intermittent connections under some conditions.

III. History of Problems

Interdata Model 4 computers were built and delivered to JPL and its Data Decoder Assembly contractor (in Phoenix) between November 1970 and May 1972. During that period, numerous field service visits and reports were made by Interdata to JPL, Phoenix, Goldstone, and Cape Kennedy. A study was made of 85 Interdata field service reports during the period November 10, 1970 to August 24, 1972. Of the 85 reports, there were 20 separate items describing connector or contact problems. These 20 problems were reported on 17 reports.

During the installation periods, connector seating problems associated with the daughter/motherboard connectors were experienced in all Deep Space Stations.

As a result of the high rate of connector mating (seating) problems being reported and the general experience with the Interdata equipment at CTA 21, an investigation was initiated to define and document these problems for more thorough study.

All Deep Space Stations were asked to document specific failures in the ID4 (only) and forward the information in two groupings: specific failures (design faults, timing adjustments, noisy data lines, and components) and nonspecific failures (reseated motherboards and daughterboards, reloaded computer, etc.). Also the related downtime was requested. The responses from the DSN indicated a number of connector-related problems corrected by the reseating of motherboards and daughterboards.

The ID4 computer at that time contained 7776 contacts for all daughterboards, in addition to the motherboard backpanel and external interfacing connections.

Frame twisting of the computer causing intermittent failures was noted when pulling the ID4 out on its slide rails.

IV. Corrective Action Implemented

Based on the information accumulated in studying this intermittent failure problem, various corrective actions were taken.

A. New Hinges

The front panel hinges were redesigned to allow the panel to open for maintenance and troubleshooting with the computer bolted to the rack frame. This allows the rack stiffness to support the inadequate computer cabinet construction. These new hinges were installed in all ID4s in the DSN, and all new ID4s purchased for Mariner Venus/Mercury 1973 (MVM'73) and Viking requirements came with these new hinges installed.

B. Interdata Four Cabinet Strut

To preclude chassis distortion when the computer is pulled out on its slides, a stiffening strut was designed

and implemented in all ID4s in the DSN, and in all new ID4s purchased for MVM'73 and Viking requirements. This strut fits across the front face of the computer chassis (or cabinet) and provides rigidity to what was effectively an open box face. With these struts installed, connector mating intermittent problems have been significantly reduced since the ID4 cabinet no longer distorts when the computer is pulled out on the slide rails.

C. New Selector Channels

A new selector channel design, which significantly reduced the number of contacts, was evaluated for replacement of the existing failure-prone selector channels. The new selector channels are of all integrated circuit (IC) construction mounted on two printed-circuit motherboards with wire-wrap interconnections, whereas the old selector channel was constructed of IC and discrete components mounted on 109 daughterboards, which were in turn mounted on three motherboards. The circuit interconnections were by means of wire-wrap also. By using these new selector channels, the number of electromechanical connections was reduced by 5232 in Configuration II DDAs and by 3488 in Configuration I DDAs. An additional feature of the new selector channel was the correction of a pulse timing condition in the address sequence which caused data to be stored and or retreived from erroneous locations in ID4 memory. The new selector channel eliminated the timing problem through the exclusive use of integrated circuits reducing the propagation delay of discrete component construction. All ID4s in the DSN were retrofitted with the new selector channels.

V. Results

The implementation of these DDA reliability improvement modifications has significantly reduced the number of failures from marginal connections in the ID4.

VI. Remaining Problems

There are still a number of daughterboard cable connectors being used in the computer, and engineering has been looking into the possibility of replacing these daughterboard connectors with a more reliable type of connector, especially in the daisy chain high-speed memory bus associated with the selector channel operations.

Also, within the DDA, there are other points of substandard reliability. Several sets of coupler boards used in the DDA interface were fabricated with IC receptacles of questionable reliability (CTA 21 has one set of these and has experienced many instances of ICs loosening in their sockets). The DDA Interface Backplane Assembly is possibly over-flexible and appears to cause connector seating problems of the coupler chassis which mount on it.

The AMP, Inc., connectors used on the DDA Backplane Assembly and on the computer (ID4) interface connector panel have a tendency to be pushed or pulled out of their mounting holes if they are not assembled properly.

The ID4 low-voltage power supply fuse blows too frequently because of excessive heating in the area where it is mounted. An Engineering Change Order (ECO) is in preparation to remedy this problem.

Tracking Operations During the Mariner 10 Venus Encounter

A. L. Berman and G. L. Spradlin
Network Operations Office

Tracking operations during the Mariner 10 Venus encounter phase were strongly impacted by the first critical phase usage of the Block IV S- and X-band receivers, the relatively new digitally controlled oscillators, and the large uncertainties associated with the Venusian atmosphere. This report describes the pre-encounter planning and subsequent analysis of tracking operations during the Mariner 10 Venus Encounter phase.

I. Introduction

On February 5, 1974, at 17:01:04 GMT (spacecraft time), the Mariner 10 spacecraft reached closest approach to the planet Venus. The encounter was visible only to the Goldstone complex, thus limiting participation to DSS 14 (the prime station) and DSS 12 (the backup station), and was noteworthy from a tracking system standpoint in that it marked the first use of the Block IV S- and X-band receivers (at DSS 14) during a critical phase, planetary encounter. Briefly described (for greater detail, refer to Ref. 1), the Block IV receiver is a quadruple conversion, superheterodyne, phase-locked receiver capable of either S- and/or X-band operation. Increased capabilities of the Block IV receiver over the Block III receiver are as follows:

(1) Improved single pass phase and modulation delay stability.

(2) Increased receiver sensitivity.

(3) Increased modulation bandwidth.

(4) Programmable oscillators (DCOs).

(5) S- and X-band operation.

(6) Automatic control capability.

(7) More efficient packaging.

(8) Increased reliability.

For the Venus encounter, the mode used at DSS 14 consisted of the Block III exciter as the transmitter, with one Block IV receiver at S-band, with a coherent ratio of 240/221, and the other Block IV receiver at X-band, with a coherent ratio of 880/221. Combined with the two Block III receivers, this made a total of four receivers at DSS 14. Each of these receivers was equipped with a

digitally controlled oscillator (DCO), which had to be programmed separately. The DCOs were still relatively new, having been used only once previously in a critical encounter phase (Pioneer 10 Jupiter encounter, December 5, 1973) and so remained a vital area of concern. Besides the burden of supplying DCO level predictions manually from JPL to DSS 14 for four separate receivers, the Block IV receivers posed an additional difficulty in that both the S- band and X-band doppler data are interleaved into the same pseudo-residual stream. Since the doppler residuals for S-band and X-band data are radically different (by a factor of 11/3), near real-time interpretation of doppler residuals at the Network Operations Control Area (NOCA) during periods of rapidly changing residuals, such as those occurring at planetary encounters, is made extremely difficult. Finally, a very important facet of the Venus encounter was the extremely large refractive effect of the Venusian atmosphere during the period between geometric enter and exit occultation (at its peak, this refraction amounted to approximately 13,000 Hz, two-way S-band). This large refractive effect evidenced itself very strongly during the pre-encounter tracking operations planning phase in three areas:

(1) As the signal became increasingly refracted, it also became increasingly attenuated, and, as no information existed regarding the accuracy of what little attenuation information was available, there was a large uncertainty as to when one would drop and subsequently acquire both spacecraft uplink and downlink.

(2) No information was available regarding the accuracy of the atmospheric doppler predictions, impacting the selection of an acquisition sweep range.

(3) The IBM-360 Prediction Program does not model planetary atmospheric refraction, so the refraction predictions had to be manually factored into otherwise computerized prediction data for the various encounter strategy studies.

II. Uplink Tuning Strategy

The original strategy called for both enter and exit occultation to occur in the one-way mode. However, some days before encounter, additional testing of the spacecraft auxiliary oscillator disclosed an unacceptable short-term instability, so the decision was made to enter occultation in the two-way mode. This decision immediately introduced a complication with the usage of the open-loop receivers. It was quite conceivable that the uplink could be lost one round-trip light time (RTLT) or more before loss of the downlink, such that part of the open-loop data would be two-way and part one-way (this in fact happened, and will be amplified in a later section). To avoid possibly losing the one-way segment of data (since the bandwidth of the open-loop receivers is limited), it was desirable to see if the one-way and two-way downlinks could be forced to be the same frequency at the time of expected two-way/one-way transition. This was accomplished as follows:

Define: D1 = one-way downlink
D2 = two-way downlink
TSF = Track Synthesizer Frequency (transmitted frequency)
XMTREF = spacecraft best lock
TFREQ = spacecraft auxiliary oscillator
XA = spacecraft best lock including doppler
$\dot{r}$ = spacecraft range rate
c = velocity of light
R = received time
T = transmitted time

Now:

$$\mathrm{D1}_R = 96\frac{240}{221}\mathrm{TSF}_R - \mathrm{TFREQ}\left(1 - \frac{\dot{r}}{c}\right) + 10^6$$

$$\mathrm{D2}_R = 96\frac{240}{221}\mathrm{TSF}_R - 96\frac{240}{221}\mathrm{TSF}_T\left(1 - \frac{2\dot{r}}{c}\right) + 10^6$$

By requiring $\mathrm{D1}_R = \mathrm{D2}_R$, one has:

$$-\mathrm{TFREQ}\left(1 - \frac{\dot{r}}{c}\right) = -96\frac{240}{221}\mathrm{TSF}_T\left(1 - \frac{2\dot{r}}{c}\right)$$

or

$$\mathrm{TSF}_T = \frac{221}{96\,(240)}\mathrm{TFREQ}\,\frac{1 - \frac{\dot{r}}{c}}{1 - \frac{2\dot{r}}{c}}$$

Now for $1 \gg \dot{r}/c$

$$\frac{1 - \frac{\dot{r}}{c}}{1 - \frac{2\dot{r}}{c}} \approx 1 + \frac{\dot{r}}{c}$$

so that:

$$\mathrm{TSF}_T \approx \frac{221}{96\,(240)}\,\mathrm{TFREQ}\left(1+\frac{\dot{r}}{c}\right)$$

Furthermore:

$$\mathrm{XA}_T = \mathrm{XMTREF}\left(1+\frac{\dot{r}}{c}\right)$$

so that one finally arrives at the necessary condition upon the transmitted frequency:

$$\mathrm{TSF}_T \approx \frac{221}{96\,(240)}\,\mathrm{TFREQ}\left\{\frac{\mathrm{XA}_T}{\mathrm{XMTREF}}\right\}$$

Whether this condition is feasible for any given spacecraft depends on the values of TFREQ and XMTREF; in this case it was feasible, but would cause the spacecraft to be left approximately 80 Hz (at voltage-controlled oscillator (VCO) level) above XA at approximately the time of loss of uplink at enter occultation. However, this immediately impacted the uplink acquisition strategy at exit. In general, the spacecraft is left at XA at enter occultation (because one has the best chance of knowing where the spacecraft is at exit) and then a simple sweep around XA at exit is performed to reacquire the uplink. Since the spacecraft was being left quite far from XA, one would have to calculate (rather imprecisely) where the spacecraft had drifted to, and then perform a much wider sweep because of the uncertainties introduced by the spacecraft drift. The calculations were as follows:

TSF − XA (at approximately drop lock)

$\cong$ 80 Hz

Δt (from drop lock to reacquisition)

$\approx$ 1200 seconds

Mariner 10 receiver relaxation constant

$= t_0 \approx$ 3600 seconds

so that the drift back to best lock would be:

$$\Delta = \Delta_0\, e^{-\Delta t/t_0}$$
$$\cong (80\ \mathrm{Hz})\, e^{-1200/3600}$$
$$\cong 57\ \mathrm{Hz}$$

It was therefore decided to execute a two-way acquisition sweep of (XA + 60 Hz) ±60 Hz. This sweep successfully acquired the spacecraft and will be dealt with in greater detail later in this report. The uplink frequency strategy is detailed in Fig. 1, while Fig. 2 describes the one-way and two-way doppler during the occultation period.

III. DSS 14 Reacquisition Strategy at Exit Occultation

A fast reacquisition of the downlink by the closed-loop receivers at exit occultation was a prime goal, and it was here that the heaviest impact of the large Venusian atmospheric refraction was felt. Given the large uncertainties in signal strength and doppler as a function of time, the DCO Automatic Acquisition Mode was an obvious choice. The selection of sweep rate and sweep range, however, was a far more difficult problem. The situation one was faced with was a signal emerging at threshold (~ -175 dBm) and slowly, over a period of minutes, increasing to its full unrefracted value (~ -130 dBm). To acquire at very low signal strength, one must greatly lower the sweep rate, but in so doing, it takes much longer to sweep out the uncertainty band, thus lowering the chances of rapid acquisition. The Radio Science Occultation Team finally decided on choosing a sweep rate which would be conservative for a signal strength of −150 dBm, and after considerable testing at DSS 14, the value of ±1000 Hz/s was chosen, in conjunction with a tracking loop filter setting of 100 Hz (wide). A sweep range of D1 − 3000 Hz to D1 + 5000 Hz was selected, where D1 was the predicted one-way doppler (with atmospheric refraction included) at the time of predicted −150 dBm downlink signal strength. This sweep range was selected as it covered the expected uncertainties from all sources as well as allowing for the increasing doppler if the reacquisition of the downlink was not as rapid as had been expected.

IV. Analysis of Tracking Operations at DSS 14 During Venus Occultation

A. Accuracy of Atmospherically Refracted Doppler Predictions

Information regarding atmospheric refraction of doppler was provided by Dr. G. Fjeldbo of the Tracking and Orbit Determination Section (391). These data were made available as a plot of the expected X-band doppler shift due to atmospheric refraction superimposed upon the nominal transparent planet X-band doppler curve. Post-encounter analysis of the doppler residuals as computed by the IBM-360 Pseudo-Residual Program reveals that these atmospheric corrections were quite accurate. The

Pseudo-Residual Program computes doppler residuals by subtracting from a received actual doppler data point a value obtained from the IBM-360 Predicts Program. Since these predicts do not contain atmospherically refracted doppler corrections, the doppler residuals directly reflect the magnitude of the doppler shift due to the atmosphere of Venus, as well as trajectory and frequency inaccuracies. A plot of the doppler residuals computed by the Pseudo-Residual Program on data received from the Block IV S-band receiver during the enter occultation period can be seen in Fig. 3. Superimposed on the plot of these data is a plot of predicted atmospheric effect. As can be seen from Fig. 3, biases due to trajectory and/or frequency inaccuracies were very small (note the period prior to encountering the atmosphere), and the computed doppler residual compares very favorably with the predicted doppler shift due to the atmospheric refraction.

B. Loss of the Uplink and the Downlink at Enter Occultation

Referring to Fig. 3, it can be seen that two-way lock with the spacecraft was maintained for approximately 6 min beyond geometric occultation. At that time, the spacecraft, being unable to maintain lock on the uplink, began transmitting using the on-board auxiliary oscillator. With the out-of-lock condition, the Block IV S-band receiver began to drift, unexpectedly resulting in the receiver locking to the auxiliary oscillator-generated downlink. The Block IV S-band receiver maintained one-way lock for approximately 40 s before the signal became too weak to sustain receiver lock. The offset that can be seen between the predicted one-way doppler residuals and the actual values indicated on the plot is the result of inaccuracy in predicting the spacecraft auxiliary oscillator frequency, this difference being approximately 580 Hz.

Following the loss of receiver lock one-way, the Block IV S-band receiver again began to drift as a result of the receiver VCO being stressed off nominal rest frequency. Figure 4 is a plot of the observed doppler during the period of receiver drift. By fitting a curve through these points, it was determined that the receiver time constant was approximately 675 s. This compares reasonably with a theoretical (assuming the narrow (30 Hz) tracking loop filter) receiver time constant of approximately 650 s. The exponential drift of the receiver and the relatively long time constant indicate that the Block IV receiver loop was not shorted (which would have immediately removed the stress) and that the tracking loop filter in use was 30 Hz (resulting in the relatively long time constant). It should be noted that it had been planned to switch to the wide (100 Hz) tracking loop filter following loss of lock, but that apparently during the excitement and confusion resulting from the unexpectedly lengthy ground receiver lock at enter, this sequence of events (SOE) item was not executed. Had the switch to the wide (100 Hz) tracking loop filter taken place, the receiver time constant would have been reduced to approximately 35 s. At loss of one-way lock the receiver VCO was stressed approximately 15.7 kHz (S-band) off nominal rest frequency. During the approximate 465 s the receiver was allowed to drift, this stress had decayed to approximately 7.9 kHz off receiver VCO rest frequency. During this interval the receiver DCO was being set up for re-acquisition of the spacecraft as it emerged at exit occultation.

C. Acquisition of the One-Way Downlink at Exit Occultation

The receiver tuning pattern executed by DSS 14 can be seen in Fig. 5. The data points plotted are the doppler residuals as computed by the Pseudo-Residual Program, but modified such that zero represents the predicted one-way doppler. The acquisition search can plainly be seen to be in the wrong frequency region (due to failure to short the VCO). However, even if the search had been in the correct frequency region, acquisition would have been precluded by the incorrect tracking loop filter setting.

After several minutes of sweeping, the data indicate that DSS 14 altered the sweep pattern and did cross the expected lock up frequency. However, since the tracking loop bandwidth had not been changed to the prescribed wide (100 Hz) tracking loop filter, the sweeps were too fast for the receivers to acquire the downlink. After several minutes of searching in the widened sweep pattern, DSS 14 did acquire the downlink. This occurred at approximately 17:28:58 GMT and, as is apparent from the plot, only after the sweep rate had been reduced (to approximately ⅛) to a rate compatible with the still-in-use narrow-band (30 Hz) tracking loop filter. It should be noted at this point that the Block III prime and backup receivers using the correct tracking loop filter, an identical sweep region, and with the receiver VCO stress removed acquired at approximately 17:26:00 GMT.

The Block IV X-band receiver acquired the two-way downlink at approximately 17:40:58 GMT. Due to the intensified effort to lock the Block IV S-band receiver and the complications introduced due to the differences between the S-band and X-band receivers, the lock up of the X-band receiver was delayed until some time after lock of the S-band receiver had been achieved.

The doppler residuals seen in Fig. 6 are of the exit occultation period. Again it can be seen that the predicted residuals and the actual residuals reflect the effects of atmospheric refraction, with the offset being due to the previously mentioned inaccuracy in the predicted auxiliary oscillator frequency.

D. Acquisition of the Uplink at Exit Occultation

At approximately 17:32:50 GMT, the downlink switched from the one-way to the two-way doppler mode. This switch occurred without loss of lock as the one-way doppler and two-way doppler were nearly equal at this time. As mentioned in an earlier section, the uplink frequency at the expected loss of signal time at enter occultation was chosen to cause the one-way doppler and the two-way doppler frequencies to be as close together as possible to optimize the open-loop receivers. To demonstrate that the one-way and the two-way doppler frequencies were also nearly equal at the time of the two-way acquisition, it is necessary to determine how far off the spacecraft nominal rest frequency (XA) the spacecraft receiver was when loss of two-way lock occurred at enter occultation. From Fig. 3 it is apparent that the spacecraft dropped the uplink at approximately 17:15:28 GMT ground received time or about 17:10:34 GMT ground transmit time. The value of XA at this time, corrected for atmospheric refraction, was 22014595.6 Hz. The transmitted frequency (TSF) at the time the spacecraft dropped the uplink was 22014680.0 Hz. Therefore, at loss of two-way lock, the spacecraft receiver was stressed off XA by +84.4 Hz.

During the out-of-two-way lock period, the spacecraft receiver drifted back toward XA. Using the equation that describes this relaxation, the spacecraft rest frequency at two-way reacquisition time can be determined as follows:

$$\Delta = \Delta_0 \text{ (at start of drift) } e^{-\Delta t/t_0}$$

where

Δt = period of drift

t_0 = spacecraft receiver time constant

Δ = (actual spacecraft receiver) − XA

Since the spacecraft dropped lock at 17:10:34 GMT and reacquisition occurred at 17:27:56 GMT (ground transmit times), $\Delta t = 1042$ s. From spacecraft measurements:

$$t_0 \approx 3600 \text{ seconds}$$

Therefore,

$$\Delta \approx (84.4 \text{ Hz})\, e^{-(1042/3600)}$$

$$\Delta \approx 63.2 \text{ Hz}$$

Since the predicted XA at this time was:

$$\text{XA} = 22014448.8 \text{ Hz}$$

the expected spacecraft best lock (XA_A) at this time would be:

$$\begin{aligned}\text{XA}_A &\approx \text{XA} + \Delta \\ &\approx 22014448.8 \text{ Hz} + 63.2 \text{ Hz} \\ &\approx 22014512.0 \text{ Hz}\end{aligned}$$

The actual transmit frequency (TSF_A) at the spacecraft reacquisition time is found as follows:

$$\text{TSF}_A = \text{TSF}_1 + (\text{ramp rate}) \times (\text{time})$$

where

$$\begin{aligned}\text{TSF}_1 &= \text{pre-ramp TSF} = 22014450.0 \text{ Hz} \\ \text{ramp rate} &= 2 \text{ Hz/s} \\ \text{time} &= 32.8 \text{ s}\end{aligned}$$

Thus

$$\text{TSF}_A = 22014515.6 \text{ Hz}$$

The difference between the expected lock-up frequency and the actual lock-up frequency is:

$$\begin{aligned}\text{TSF}_A - \text{XA}_A &= 22014515.6 \text{ Hz} - 22014512.0 \text{ Hz} \\ &= 3.6 \text{ Hz (at VCO level)}\end{aligned}$$

thereby indicating good agreement between expected and actual. Finally, using the equation developed earlier to determine the transmitted frequency (TSF_B) that forces the one-way doppler frequency and the two-way doppler frequency to be equal, we have as follows:

$$\text{TSF}_B = \frac{221}{96\,(240)}\,\text{TFREQ}\left\{\frac{\text{XA}}{\text{XMTREF}}\right\}$$

where

$$\begin{aligned}\text{TFREQ} &= 2294999220.0 \text{ Hz} \\ \text{XA} &= 22014448.8 \text{ Hz} \\ \text{XMTREF} &= 22013600.0 \text{ Hz}\end{aligned}$$

Thus,

$$TSF_B = 22014513.2 \text{ Hz}$$

The difference between the one-way and the two-way doppler frequencies at two-way reacquisition time is found to be:

$$96\frac{240}{221}\{TSF_A - TSF_B\} = 96\frac{240}{221}\{22014515.6 - 22014513.2\} \text{ Hz}$$
$$= 251 \text{ Hz (S-band)}$$

With so small a difference between the one-way and the two-way doppler frequencies, the switch from the one-way mode to the two-way mode occurred without loss of lock. Within 60 s the station had been informed of this condition and had thrown the two-way data mode switch. This can be seen in Fig. 6 at approximately 17:34:20 GMT, at which point the two-way residuals reflect only biases due to prediction inaccuracies.

E. Summary of DSS 14 Lock Status During Venus Occultation

Table 1 provides a summary of the receiver lock status for the DSS 14 Block III prime and backup and Block IV S-band and X-band receivers. The in/out of lock times are derived from the monitor automatic gain control (AGC) data.

V. Accuracy of Orbital Solutions as Encounter Is Approached

Table 2 presents the accuracies of (as compared to the actual data at encounter) the last four Orbital Determination Solutions as provided for encounter planning. Probe Ephemeris Tapes (PETs) M778 and M774 were provided several weeks prior to encounter, while PETs M781 and M780 were provided in the last days before encounter. In all cases the residuals provided represent the Δ between the referenced PET and the final observed doppler and time. Two generalizations (at least for this encounter) can be formulated here:

(1) The 3-σ uncertainties provided by the Navigation Team for encounter planning were approximately 1500 Hz (S-band, two-way) for doppler and 40 s for time events. Using the four referenced solutions, the navigation-provided uncertainties would have to be considered quite conservative, which is as it should be.

(2) There is a noticeable improvement between the PETs (M778 and M774) provided weeks ahead of the encounter versus those (M781 and M780) provided in the last days before encounter. However, there is, for instance, no clear cut improvement in going from M780 to M781 (the final PET provided). Therefore, the idea of changing many tracking parameters in the last hours before an encounter might be considered more of a possible, but unlikely contingency, rather than a planned for and totally expected procedure.

VI. Summary of Tracking Operations During the Venus Encounter Phase

Tracking operations during the Venus encounter phase were extremely successful on balance, especially in light of the considerable difficulties posed by the confluence of radically new equipment at DSS 14 (the Block IV receivers) and the large uncertainties associated with the Venusian atmospheric effects on telecommunications. The one minor problem during this phase was the late acquisition by the Block IV receivers at exit occultation, which is explained in large part by the unexpectedly lengthy lock at enter occultation and a degree of unfamiliarity with the new equipment. Furthermore, the late acquisition entailed no loss of data since:

(1) The DSS 14 Block III receivers locked up extremely early in the exit occultation, successfully receiving all spacecraft data.

(2) The DSS 14 open-loop receivers successfully acquired data during both enter and exit occultations, thus satisfying radio science requirements.

Reference

1. Donnelly, H., Shallbetter, A. C., and Weller, R. E., "Block IV Receiver–Exciter Development," in *The Deep Space Network*, Space Programs Summary 37-66, Vol. II, pp. 115–124, Jet Propulsion Laboratory, Pasadena, Calif., Nov. 30, 1970.

Table 1. Summary of DSS receiver events

Event	Ground received time (Feb. 5, 1974), GMT
Enter atmosphere[a]	17:09:10
Enter geometric occultation[a]	17:09:23
Block IV X-band out of lock	17:10:45
Block III prime and backup out of lock	17:14:58
Block IV S-band out of lock (two-way)	17:15:35
Block IV S-band out of lock (one-way)	17:16:30
Block III backup in lock	17:25:48
Block III prime in lock	17:26:03
Block IV S-band in lock	17:28:58
Exit geometric occultation[a]	17:30:17
Exit atmosphere[a]	17:30:28
Two-way[a]	17:32:50
Block IV X-band in lock	17:40:58

[a]These are best estimates from actual encounter data.

Table 2. Accuracy of orbit determination solutions generated prior to Venus encounter

Time	Observed doppler, Hz	Δ from observed, Hz			
		M781	M780	M778[a]	M774[a]
16:00 GMT	1214895.35	−2.5	−3.65	−11.52	−11.07
Closest approach	1214073.47	+3.1	+74.42	+72.55	+88.16
Enter occultation	1204820.21	−4.1	−10.38	−45.23	+58.56
Exit occultation	1191292.72	−33.8	−13.61	+7.37	+63.79
18:00 GMT	1167523.96	−41.2	−11.93	+33.94	+88.00

[a]PETs M778 and M774 were based upon pre-gas leak solutions.

Event	Ground observed, GMT	Δ from observed, s			
		M781	M780	M778	M774
Closest approach	17:03:31.344	+3.656	+1.126	+3.226	+3.816
Enter occultation	17:09:22.585	−0.585	+0.415	+4.415	+6.415
Exit occultation	17:30:16.842	+1.158	+2.158	+6.158	+6.158

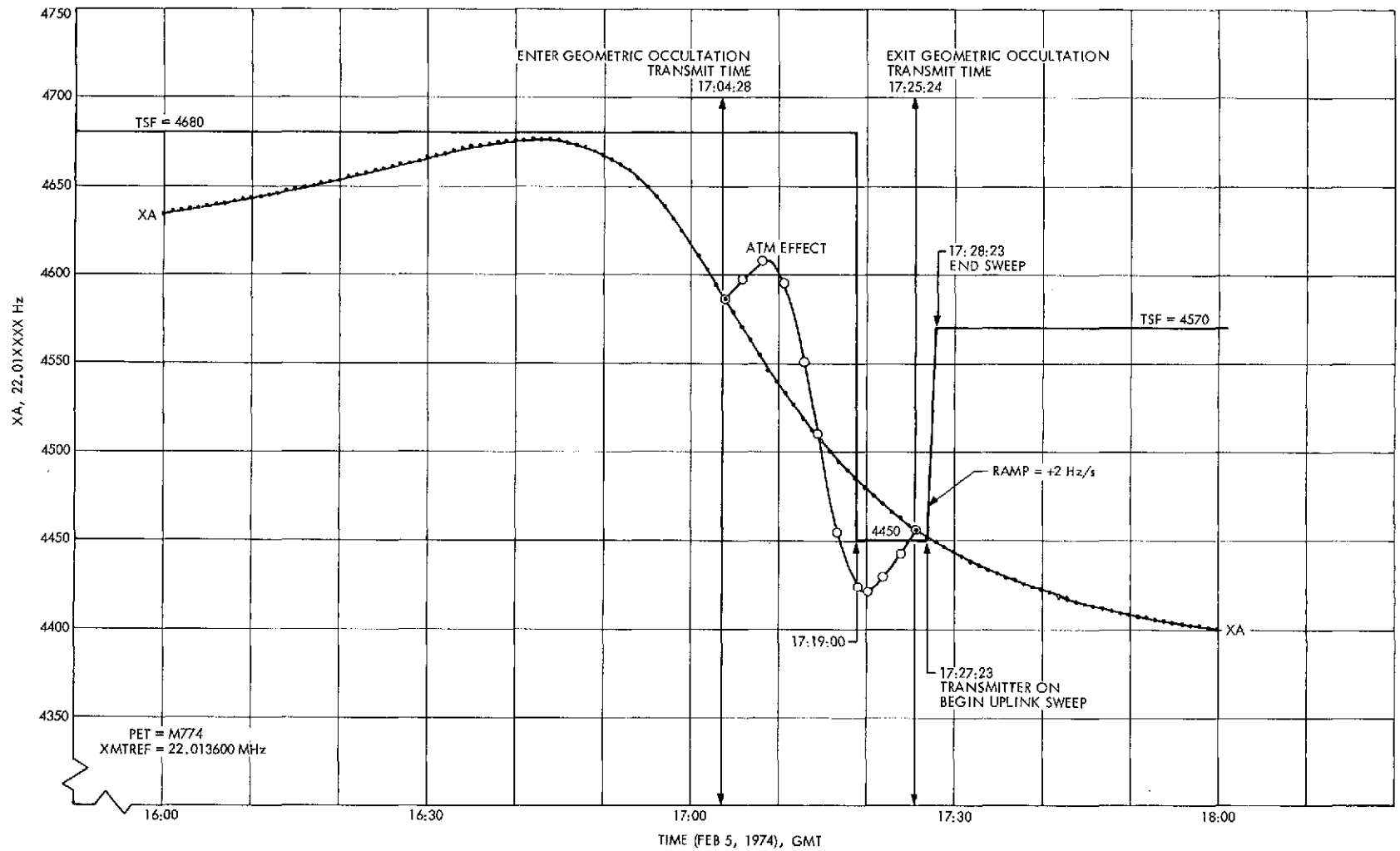

Fig. 1. XA and tuning pattern for Venus encounter (DSS 14)

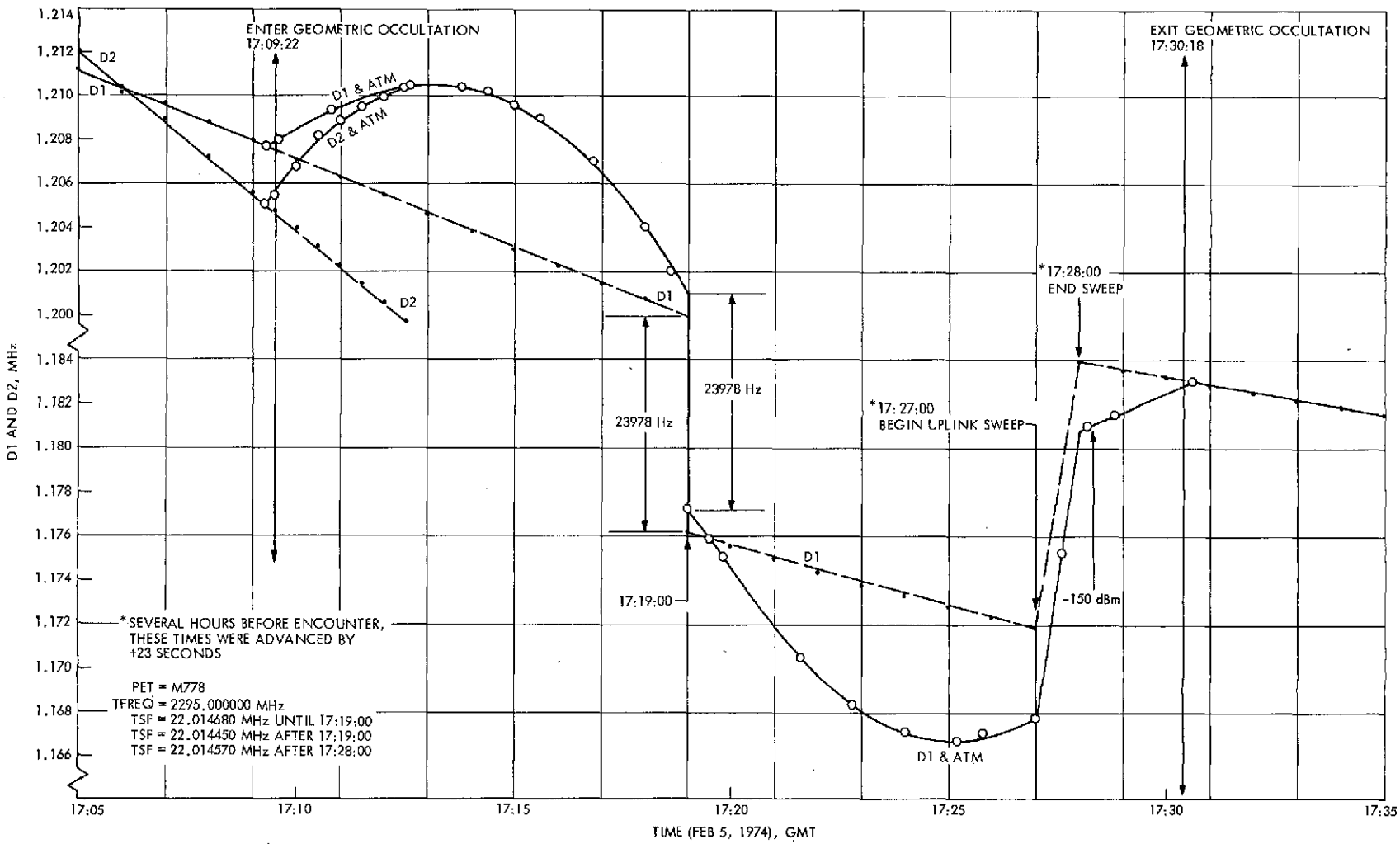

Fig. 2. D1 and D2 plus atmospheric correction for Venus encounter (DSS 14)

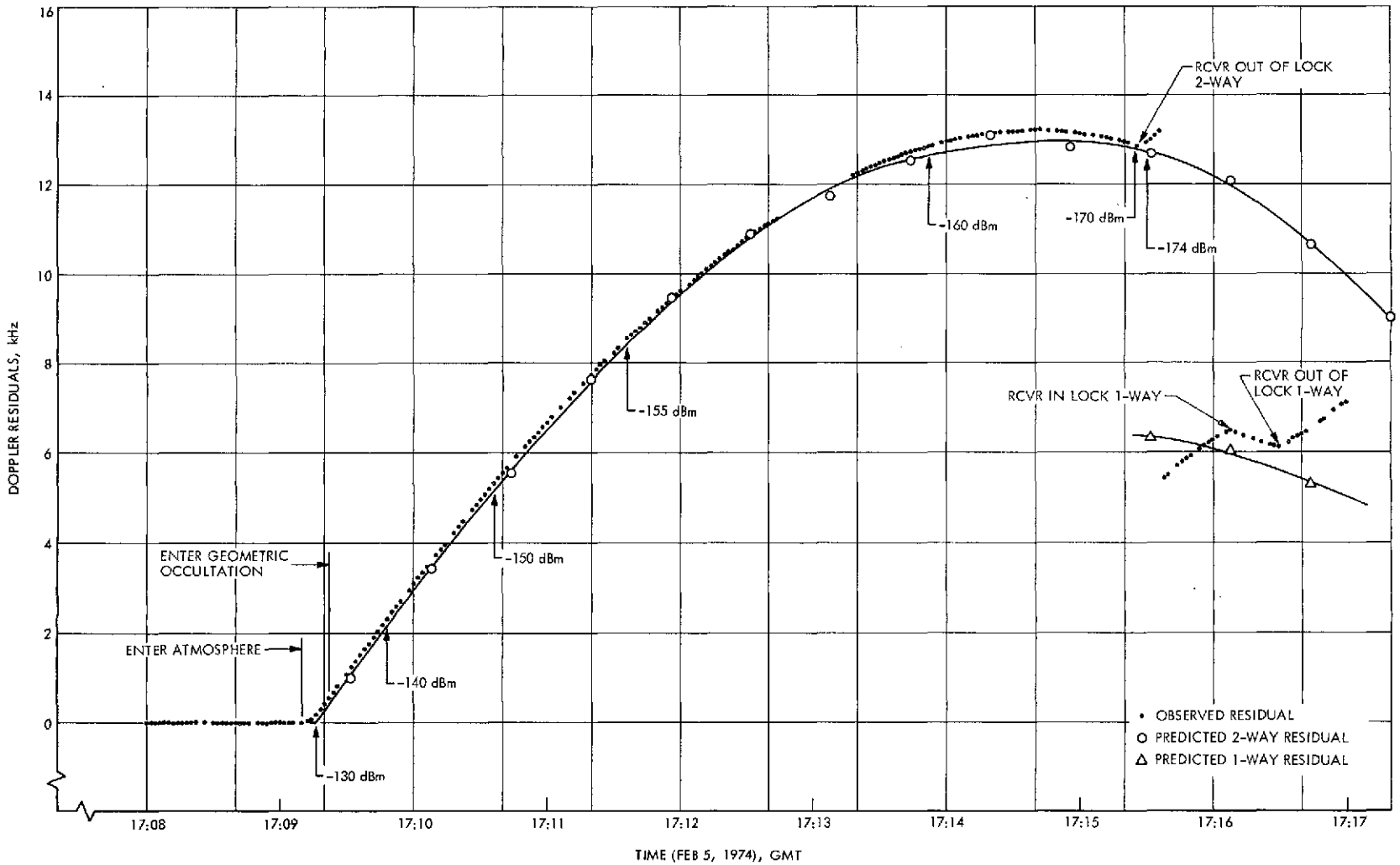

Fig. 3. Enter occultation doppler residuals for Venus encounter (DSS 14 Block IV S-band)

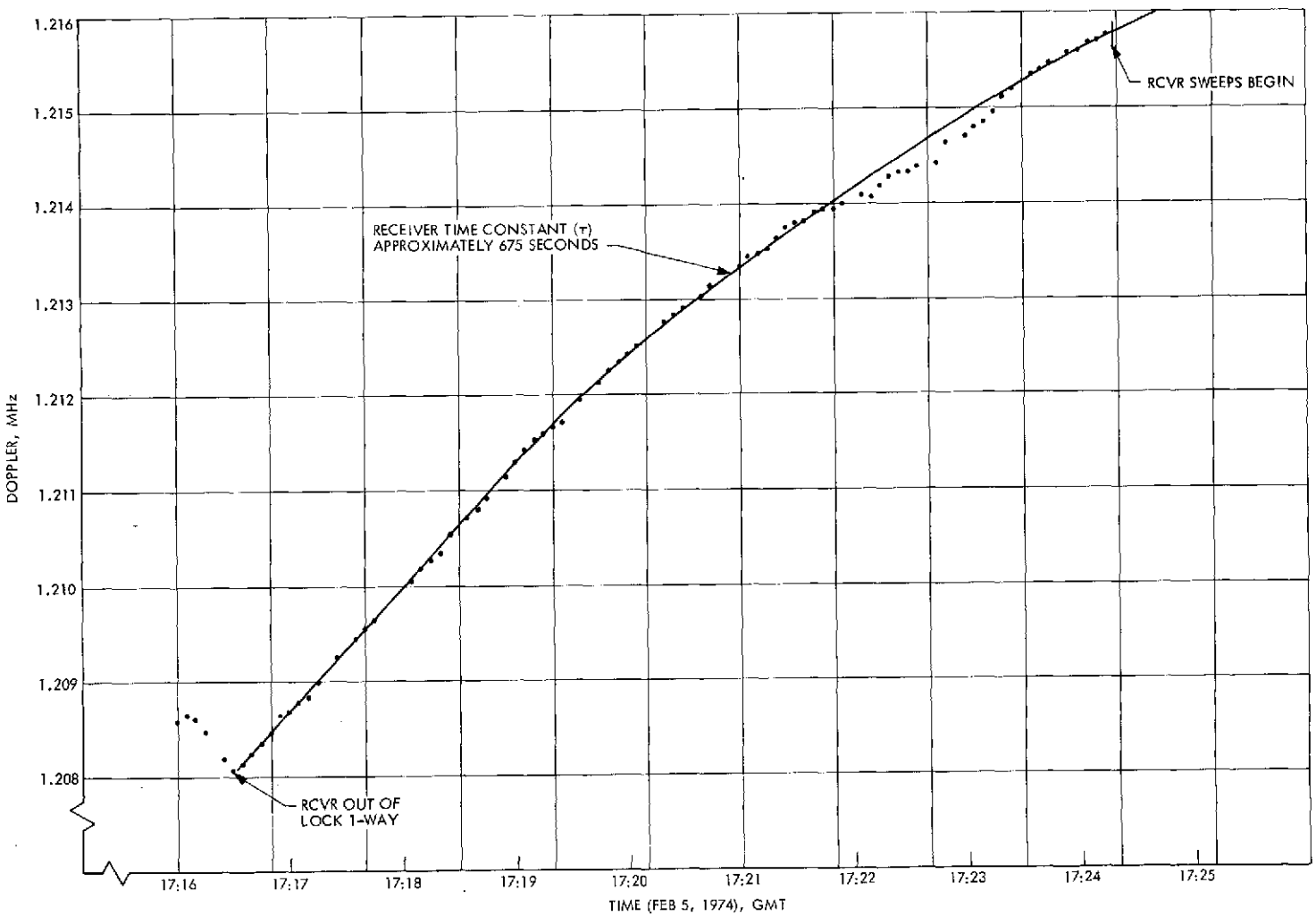

Fig. 4. Receiver stress relaxation DSS 14 Block IV S-band for Venus occultation

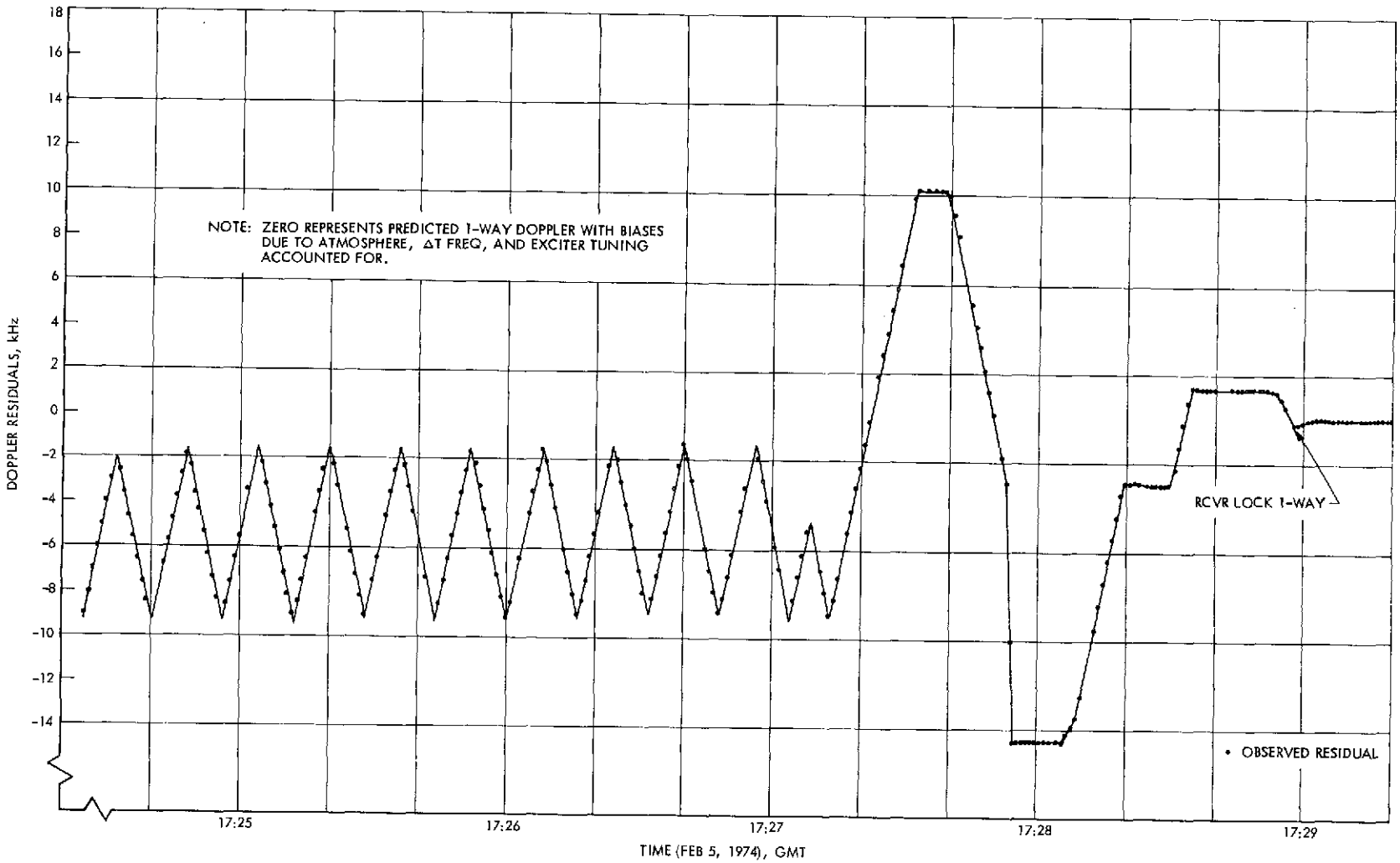

Fig. 5. DSS 14 Block IV S-band receiver turning pattern for Venus exit occultation

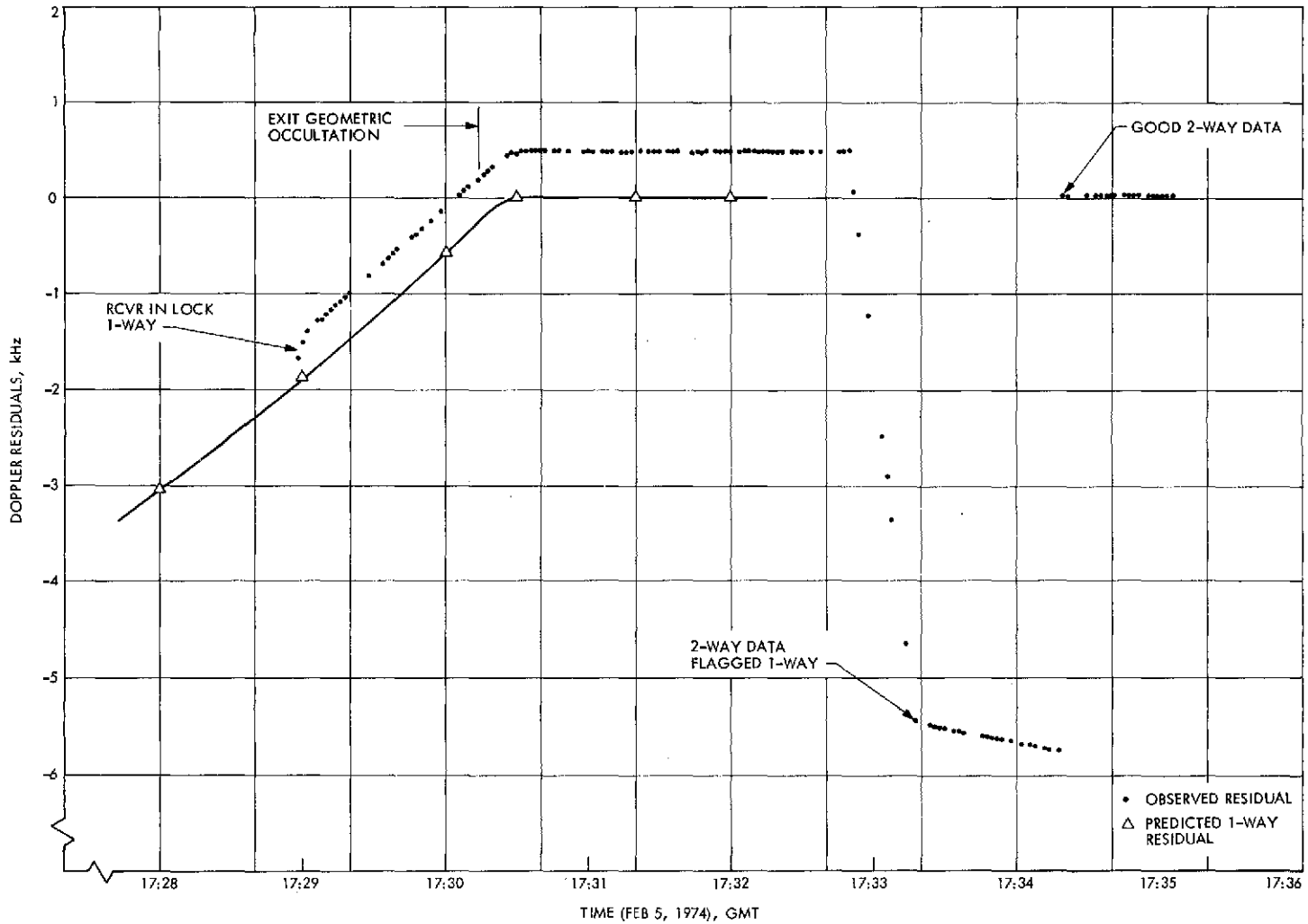

Fig. 6. Exit occultation dopper residuals for Venus encounter (DSS 14 Block IV S-band)

Software Modification to the Traceability and Reporting System

M. Puchalski
Network Operations Section

The Traceability and Reporting System (TRS) is a Network Information Control function that stores, maintains, and reports on data collected during each tracking period. This article explains the TRS, the improvements made on the software, and the reasons for the software modifications.

I. Introduction

The Network Information Control (NIC) function is organized as part of the Network Operations Control Group and supports the DSN by:

(1) Providing an effective index to all information concerning station tracking periods for each mission

(2) Providing quick-look information concerning station tracking periods for each mission

(3) Supplying monthly operations summaries of selected data to DSN management

(4) Maintaining data bases capable of providing special reports as required by management

(5) Providing coordination for shipment of all DSN data records

This article provides an explanation for the Traceability and Reporting System (TRS).

II. Traceability and Supporting System

The function of the TRS is to provide investigators, analysts, and end users with information which has been collected by the Network Operations Group. To accomplish this task, three files are maintained for data storage and report generation. One file is stored on microfilm and contains passfolder information. Passfolders contain all the DSN data logs, summaries, and other information gathered and compiled by the Operations Support Analysts concerning a single Deep Space Station (DSS) spacecraft tracking period. The other two files are stored on magnetic tape from the IBM 360/75 computer system. The first of these two computer-processed data bases contains index information leading to the location of specific passfolder information contained in the microfilm file. The other data base contains passfolder summary information. This summary data consists of information that is most desired by users for analytic and decision-making purposes and is readily available for the generation of monthly reports and special requests.

Both the passfolder and the summary input form (Fig. 1) are prepared by the Realtime Network Operations Analysts and forwarded to NIC at the end of each tracking pass. On receipt of those materials NIC then initializes the DSN Operational Data Control (ODC) input-index form (Fig. 2). A passfolder key is then assigned and recorded on the input-index and summary forms, and the transaction is recorded in the passfolder log. The passfolder log serves as a referral to any passfolders that have been forwarded to the microfilm lab. After posting has been made in the log, the passfolder is sent out for microfilming, while the summary keypunch sheet is keypunched and entered to the summary data base. The microfilm lab enters the roll and frame numbers on the DSN Operational Data Control input-index form that is filmed along with each passfolder. Once filmed, passfolders are returned to NIC where the microfilm is stored, and each passfolder roll and frame number is posted to its corresponding entry in the passfolder log. The ODC input-index form is then keypunched to data cards, which are entered to the index data base. Passfolders are then returned to the Network Operations Analysts for post-pass and nonreal-time analysis.

The purpose of the TRS is to provide users with valid and timely data for analytic and decision making functions. The interaction between the microfilm and computer data bases is designed to accomplish this goal while maintaining a satisfactory level of cost. To insure that users receive accurate data (reports) a system that provides for continuous data validation through the TRS has been developed. The validations system begins as the passfolder first arrives in NIC where it is checked for completeness. Any passfolder or summary that does not contain all the required information is returned to the Operations Support Analysts for completion. NIC does not attempt to interpret data, but familiarity raises questions on entries that do not appear consistent with past data. Data are again verified as they are input to each of the computer data bases. This checking is performed by the software that does the file updating. The software checks all constants and variables that have a fixed number of entries for consistency, it also confirms that all the data have been entered. All records not meeting these validity constraints will be rejected and printed in an error report. Corrections can then be made by referring to the microfilmed passfolder records or the Operations Support Analysts. All input cards are listed and checked visually for keypunch errors. The final check entails comparing the index and summary data bases to confirm that all records have been entered correctly. This is accomplished each month by software that reports all discrepancies that may exist.

III. File Management

In designing an effective computer file from which users can draw meaningful information, the file originator must first establish and understand all user requirements. Without this initial groundwork the tendency is usually to have created a file which contains too many or not enough data. An information system that contains a great deal more data than are necessary for its users can create problems that lead not only to added expense but also to decreasing the reporting accuracy of the system. The former summary data base serves as an excellent example of these problems. Previously, all information that was stored on microfilm from the DSN Network Analysis Area (NAA) Composite Pass Summary Report (Fig. 1) was also stored in the summary file. It had been brought to NIC's attention that the monthly Operations Report which was produced from this file contained far too many errors to be considered acceptable. Corrections needed for this report required several days at great expense in man hours and computer runs to produce an acceptable report. A study to determine the major causes of these errors concluded that the size and format of the Composite Summary Report made it difficult to keypunch and verify the input data. To correct the problem it was first necessary to establish the requirements for the summary. This was accomplished by soliciting user response. Once determined, a new file was designed that included only that information necessary for user satisfaction. Next it was necessary to design an input format which would facilitate keypunching and verification routines. This was accomplished by initializing a multi-card data input record (Fig. 2) that not only speeds and aids the keypunching function but also provides a card listing that is easily verified for content by a manual scan of the data. Since this new file was created, report errors have decreased and have continued to decrease to an acceptable level. Time and cost savings have been reflected in a 2/3 decrease for input keypunching and verification as well as a 50% decrease for file maintenance and reporting.

IV. Software

The NIC data bases are maintained by the Mark IV File Management System. It has been our experience that Mark IV is one of the best systems for manipulating files and does so in an efficient and economical manner. The Mark IV software allows the user to create, delete, and

alter records as required. Both the index and summary file maintenance software feature editing routines which verify, correct, or reject each parameter of a record transaction. Mark IV allows the user to obtain a report on desired information in the same computer run for which a file is being updated. Reports generated for use by NIC which do not require a formal output format are handled adequately by Mark IV. Conversely, special reports generated for requestors requiring specific formats have been not only difficult to obtain with Mark IV but also costly.

One example was encountered while attempting to produce the DSN Monthly Operations Report, which requires a special format that is later microfilmed and published in the DSN Operations Report. In this case, it was discovered that the Mark IV system residing in the IBM 360/75 computer did not contain a large enough buffer capacity to produce the required format. The best alternative software for outputting to this format proved to be through the use of the PL1 language which is an excellent report generator from the standpoint of efficiency as well as cost.

Another example reflecting the cost savings accrued by using an alternative program language occurred when it was felt that the Mark IV request that compared the index and summary data bases for consistency was too costly and did not give enough information to satisfy NIC. Comparing data fields from separate files through the use of the Mark IV coordinated file feature required too great a tradeoff between obtaining the greatest amount of information with the least cost. This meant that to get the required data resulted in a sizeable increase in cost, and conversely, decreased cost meant decreasing desired output. The problem was solved by generating a Fortran language program that gives all the needed information and results in a cost reduction of approximately 90% over the previously used Mark IV software.

V. Conclusion

NIC's experience with software has been that familiarity with more than one type of program language has resulted in the necessary flexibility required to meet its objectives.

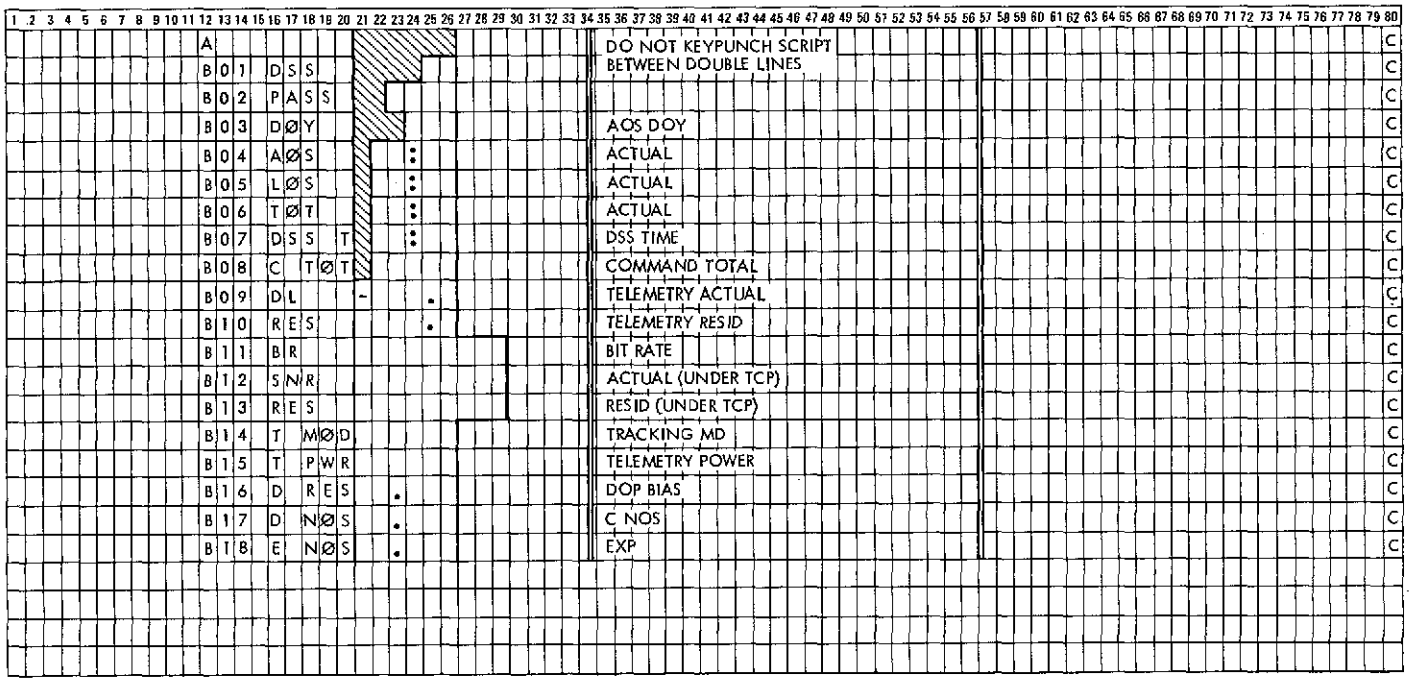

Fig. 1. Summary input form

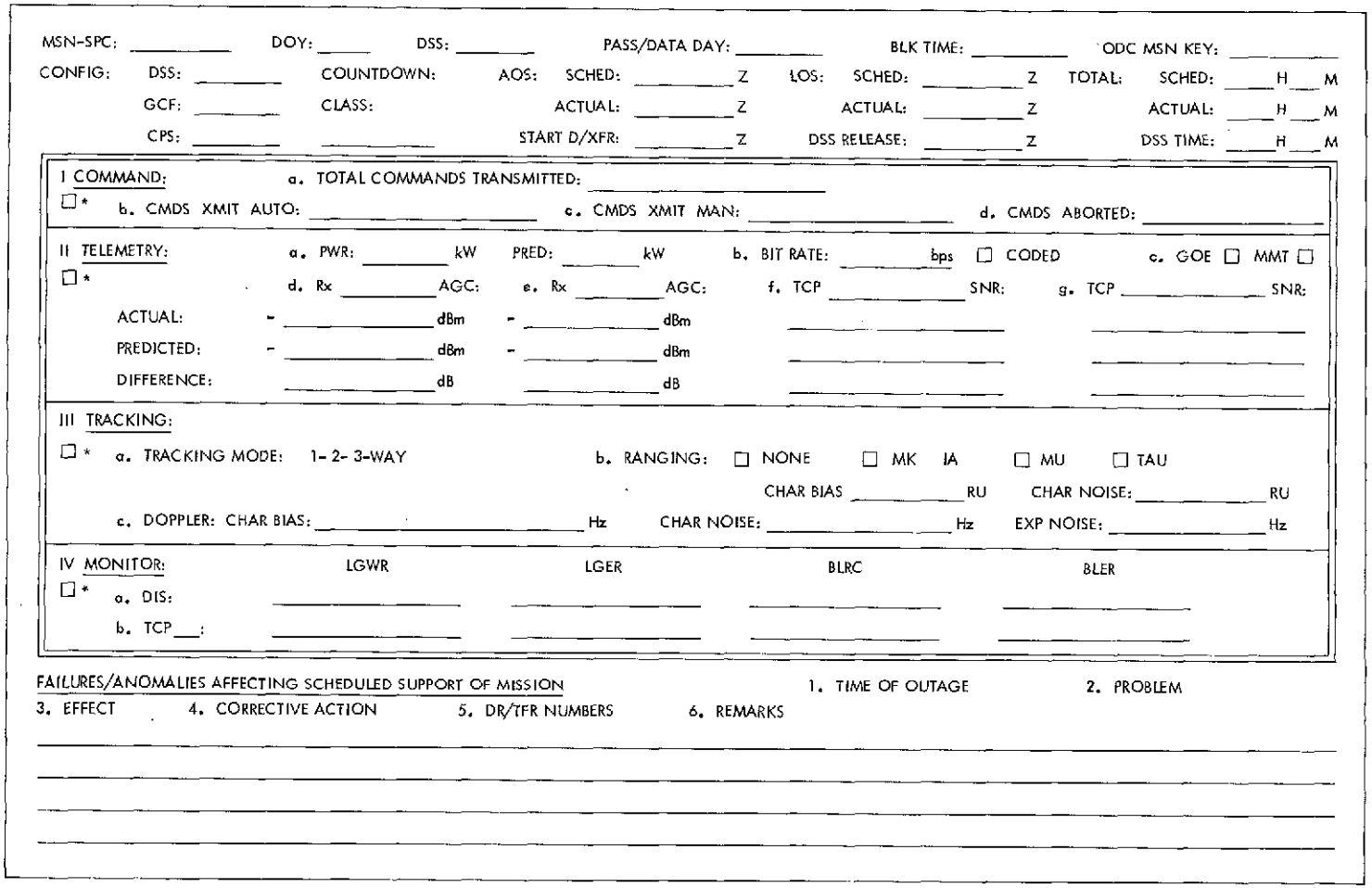

MSN-SPC: _____ DOY: _____ DSS: _____ PASS/DATA DAY: _____ BLK TIME: _____ ODC MSN KEY: _____

CONFIG: DSS: _____ COUNTDOWN: AOS: SCHED: _____ Z LOS: SCHED: _____ Z TOTAL: SCHED: ____ H ____ M

GCF: _____ CLASS: ACTUAL: _____ Z ACTUAL: _____ Z ACTUAL: ____ H ____ M

CPS: _____ _____ START D/XFR: _____ Z DSS RELEASE: _____ Z DSS TIME: ____ H ____ M

I COMMAND: a. TOTAL COMMANDS TRANSMITTED: _____

☐* b. CMDS XMIT AUTO: _____ c. CMDS XMIT MAN: _____ d. CMDS ABORTED: _____

II TELEMETRY: a. PWR: _____ kW PRED: _____ kW b. BIT RATE: _____ bps ☐ CODED c. GOE ☐ MMT ☐

☐* d. Rx _____ AGC: e. Rx _____ AGC: f. TCP _____ SNR: g. TCP _____ SNR:

ACTUAL: – _____ dBm – _____ dBm _____ _____

PREDICTED: – _____ dBm – _____ dBm _____ _____

DIFFERENCE: _____ dB _____ dB _____ _____

III TRACKING:

☐* a. TRACKING MODE: 1- 2- 3-WAY b. RANGING: ☐ NONE ☐ MK IA ☐ MU ☐ TAU

CHAR BIAS _____ RU CHAR NOISE: _____ RU

c. DOPPLER: CHAR BIAS: _____ Hz CHAR NOISE: _____ Hz EXP NOISE: _____ Hz

IV MONITOR:	LGWR	LGER	BLRC	BLER
☐* a. DIS:				
b. TCP___:				

FAILURES/ANOMALIES AFFECTING SCHEDULED SUPPORT OF MISSION 1. TIME OF OUTAGE 2. PROBLEM

3. EFFECT 4. CORRECTIVE ACTION 5. DR/TFR NUMBERS 6. REMARKS

Fig. 2. Composite pass summary report

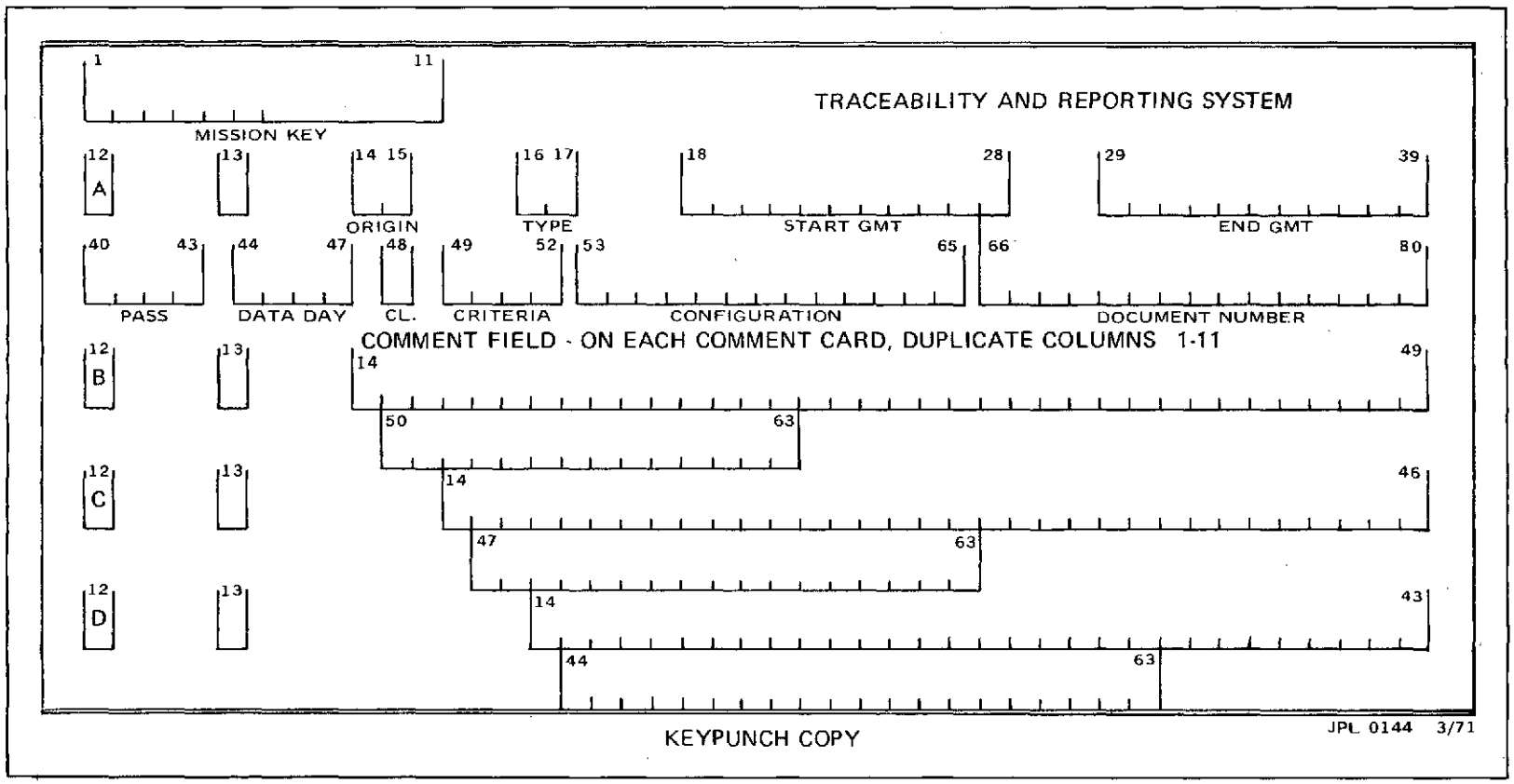

Fig. 3. DSN operational data control input index

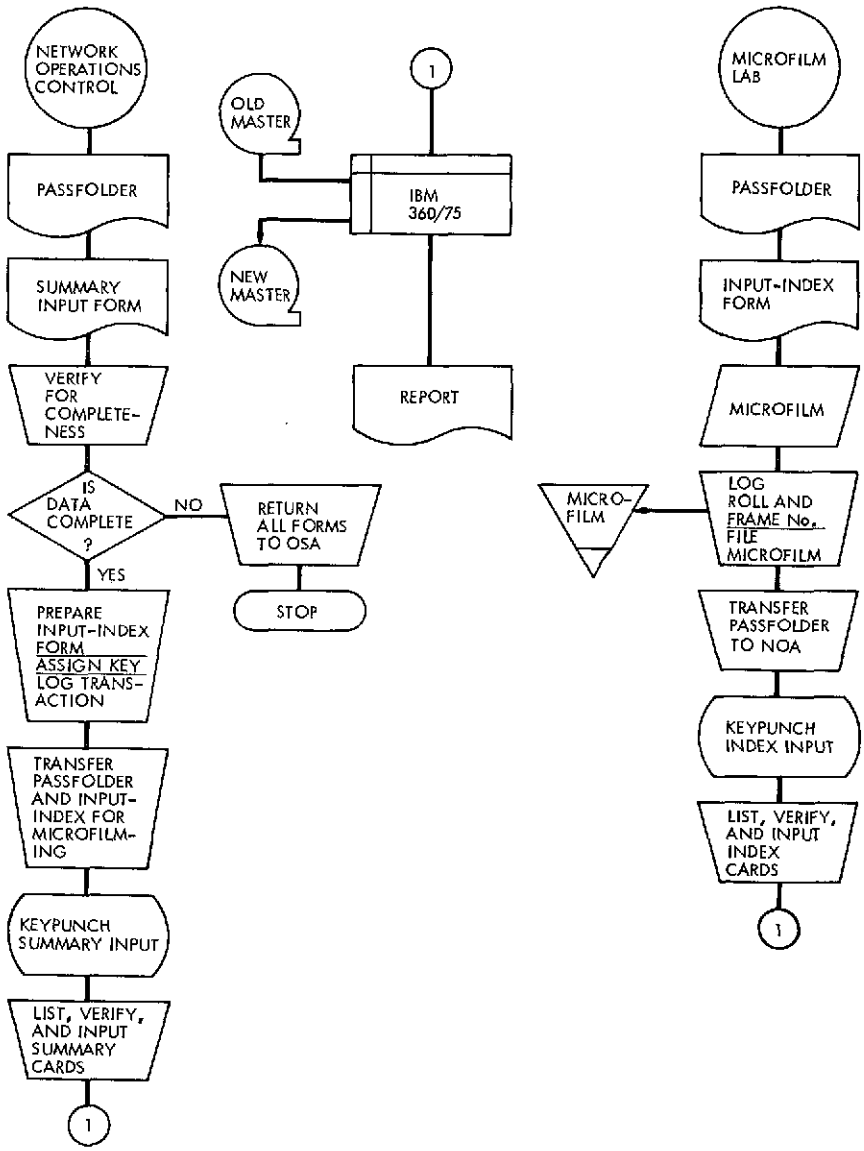

Fig. 4. TRS systems report

System Performance Tests for the Network Control System

F. B. Leppla
Network Operations Section

This article presents a description of the system performance tests executed during the implementation and transfer to Operations of the Network Control System, Block I, Phases 1 and 2.

I. Introduction

System Performance Tests (SPTs) are executed throughout the DSN whenever modifications that may affect system performance are made. Also, SPTs are required for the verification of performance of new equipment and capabilities.

The purpose of this article is to describe the effort that was undertaken in executing SPTs for the Block I Network Control System (NCS). The philosophy and the objectives of the SPTs will be discussed so as to demonstrate the benefits gained by performing these tests. A description of the NCS SPTs will be presented along with a description of the test procedure and test software.

The NCS is being implemented in three major steps defined as Block I, Block II, and Block III. Each of these Blocks is further broken down into phases. This article describes the SPTs performed for NCS Block I Phases 1 and 2.

II. Objectives of System Performance Testing

The development of test procedures and test software, and the execution of the NCS SPTs are performed to accomplish certain objectives. The overall objective is to guarantee that the NCS can meet specified operational capabilities. These capabilities are defined in various documents; those of particular importance are given in Refs. 1 through 3. The SPT must verify that the NCS configuration and interface requirements are satisfied. They also evaluate the ability of the NCS to meet data rate performance requirements.

An additional object of SPTs is to aid in the training of NCS and DSN Operations personnel. The SPTs are performed with configurations as near as possible to configurations utilized for real time tracking of spacecraft. By using the test procedures, NCS and DSN Operations personnel can gain experience in operating the NCS hardware and software.

One additional feature of the NCS SPT is that the test procedure may be used to isolate system problems. This capability may aid in the resolution of discrepancy reports written against the NCS during operational periods.

III. Test Configuration

Shown in Fig. 1 is the basic NCS Block I hardware configuration. The normal mode of operational support is as follows:

(1) One Sigma-5 on-line processing real-time data. This Sigma-5 is connected to the remote peripheral devices located in the Network Operations Control Area (NOCA).

(2) Off-line Sigma-5 processing and preparing data for transmission to the Network

(3) One PDP-8 computer operating as a real-time multiplexer and demultiplexer. The second PDP-8 operating as a hot-backup

The operational software required for the NCS Block I Phase 1 implementation consists of three computer programs. They are:

(1) DOI-5056-OP PDP-8 Real Time Program

(2) DOI-5057-OP Sigma-5 Real Time Program

(3) DOI-5058-OP Sigma-5 Off-Line Program

For Phase II, Items 2 and 3 above are replaced with:

(4) DOI-5059-OP Sigma-5 Real-Time Program

(5) DOI-5060-OP Sigma-5 Off-Line Program

The NCS SPT is divided into three basic tests. They will be explained in more detail later. The first portion of the SPT consists of a short loop configuration as shown in Fig. 2. The second portion is a long loop configuration with one DSS operating its Monitor, Tracking (TRK), Telemetry (TLM) and Command (CMD) Subsystems in a normal tracking mode. The Simulation Conversion Assembly (SCA) is used to generate fixed pattern telemetry data. The third and final portion of the SPT is a combination of the first two portions with multiple DSSs on-line as well as a short-loop link operating simultaneously.

The software required at the DSS to support the NCS SPT is:

(1) DOI-5046-OP Digital Instrumentation Subsystem (DIS) Monitor Program

(2) DOI-5035-OP-F Pioneer 10 Terminal Countdown Demonstration Test (TCD) Program

(3) DOI-5050-OP-A MVM'73 TCD Program

(4) DOI-5050-OP-B Pioneer and Helios TCD Program

(5) DOI-5089-OP-C SCA Program

IV. NCS SPT Test Software

SPTs for other systems such as CMD and TLM use test software in conjunction with the normal operational software for analytical purposes. This is possible since additional on-site computers are available for real-time testing.

Within NCS Block I, test software may not reside within the operational software. A limited self-test capability exists which consists of generation of HSD Blocks and transmission in a short loop mode. This capability simulates one Deep Space Station (DSS) and is primarily used for software development.

A computer program has been developed which allows the test personnel to formulate SPT procedures files. These files may then be transmitted to DSSs via high-speed data (HSD) and listed on high-speed printers. The general goal of this implementation was to provide a method for rapid update of SPT procedures and distribution to the Network Operations personnel.

V. Test Descriptions

The NCS System Performance Test is divided into three basic tests. They are described below:

A. Short Loop Test

This test verifies the operation and capabilities of the NCS in a short loop mode. This test is executed as the first part of the SPT, in order to verify operation prior to scheduling HSD lines and DSS resources.

TRK, TLM, and CMD test data transmission files are generated by the off-line Sigma-5. These data types are transmitted and received by the NCS. Ground communications (GC) accountability is verified, as well as the capability of test data generation. The peripheral equipment control and capabilities are exercised; computer

system recovery is verified; and backup computer and communication configurations are also verified.

The time required to perform this portion of the SPT is twelve hours.

B. Long Loop Test

This test verifies the operation of the NCS in a long loop mode with one DSS at a time. The primary goal is to prove that the DSS interfaces are, indeed, correct.

Transmission files are created for sequence of events (SOE), schedule (SKED), tracking predicts, and commands (for Mark III-71 and Mark III-74 versions) by the off-line Sigma-5. These data types are transmitted to the DSS. Real TRK, TLM, CMD, and monitor data reception is validated for various data rates. GC data accountability is tested. Commands are transmitted to TCD A and TCD B for Pioneer, Mariner, and Helios configurations. The capability of transmitting command data simultaneously with other data types is exercised. The input/output portions of NCS software are tested thoroughly.

The time required to perform this part of the SPT is six hours for each DSS.

C. Full Load Test

The last test performed in the SPT is the full load test. The goal is to prove that the NCS can operate with multiple DSSs on-line in a normal Network configuration.

The test capabilities described above for the short and long loop tests are combined to exercise the NCS with multiple DSS, spacecraft, and data rate combinations. Excessive data rates and erroneous information are input to the NCS to determine error detection properties.

The time required to perform this test is twelve hours.

VI. Test Status and Results

NCS Block I Phase 1 SPTs were executed from Dec. 15, 1973 through Jan. 15, 1974. The Phase 2 SPTs were begun on Feb. 4, 1974 with Compatibility Test Area, CTA-21. Due to high activity within the Network, the complete NCS SPT has not been completed for the Phase 2 software.

The tests for Phase 1 were run by system support personnel from Network Operations. The Phase 2 tests were run by real-time operations analysis personnel under direction of the System Support Group.

In a number of cases the SPTs uncovered software anomalies. These have been reported to the software development organization. Also, a number of improvements have been suggested and are under consideration for future software releases.

Overall, the hardware and software performance as demonstrated by the NCS SPTs has been acceptable. The SPTs have proven to be a valuable tool in the performance evaluation of the Network Control System. In addition, training has been accomplished for numerous operating personnel.

As new versions of NCS software become available with new or revised capabilities, the SPTs will be updated accordingly and executed as required.

References

1. *Deep Space Network System Requirements Block I Network Control System*, Document No. 822-10, Jet Propulsion Laboratory, Pasadena, Calif., Oct. 15, 1973.
2. *Deep Space Network System Requirements Detailed Interface Design*, Document No. 820-13, Feb. 1, 1971 (JPL internal document).
3. Maclay, J., *Block I NCS Network SPT Requirements and Acceptance Criteria*, IOM NSE-74-2, Jet Propulsion Laboratory, Pasadena, Calif., Jan. 3, 1974 (JPL internal document).

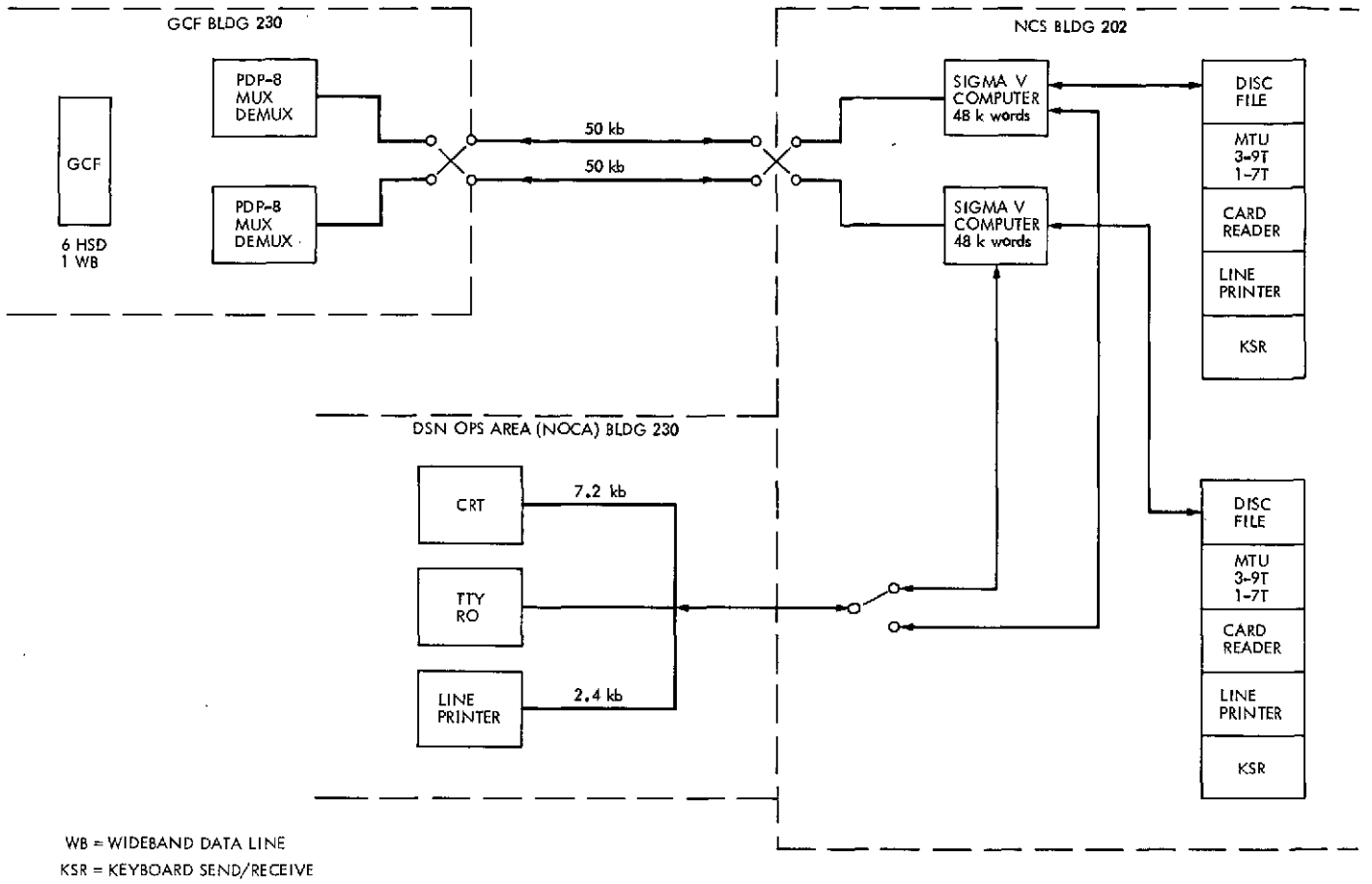

Fig. 1. NCS Block I configuration

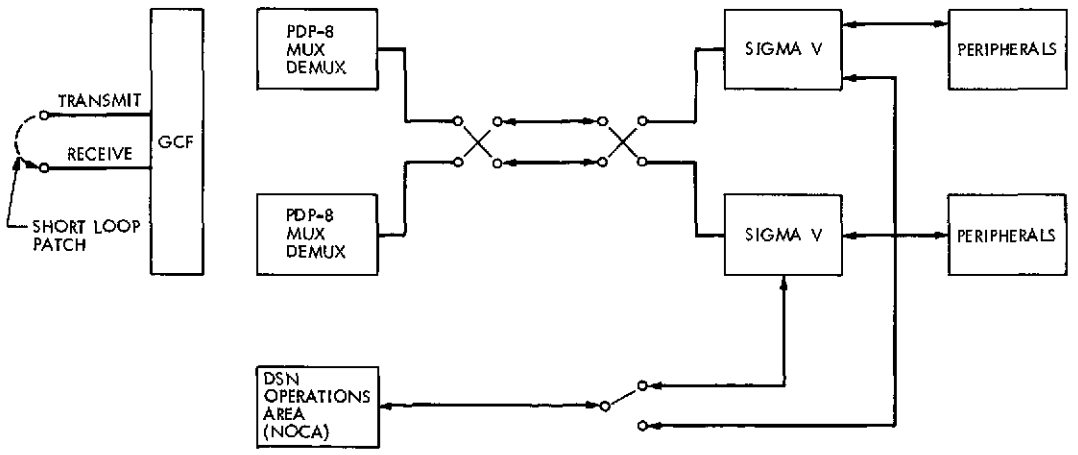

Fig. 2. NCS Block I short-loop test configuration

Minimum Cost Assignment of Crews to Meet Tracking Requirements

C. A. Greenhall[1]
TDA Planning Section

A model of the tracking constraints, maintenance constraints, labor constraints, and labor costs of a DSN complex is made. The problem of minimizing the labor cost while satisfying the constraints is solved. Minimum cost schedules for all cases of interest are given. Modifications of the model are suggested.

I. Introduction

This report gives a solution, subject to simplified assumptions, to the management science problem of scheduling the spacecraft tracking, station maintenance, and crew shifts at a DSN tracking complex. Section II defines the problem precisely, but here is an overview: assume we have a complex with 1 to 4 stations. There are 0 to 5 spacecraft to be tracked at that complex. Each spacecraft pass lasts 12 hours and must be tracked in its entirety by one and only one station, or not at all. (Four hours of pre- and post-calibration are included.) In this version of the problem, rises and sets are synchronized with each other modulo 12 hours and are constant from day to day. Each station requires 16 hours per week of maintenance subject to certain constraints, and must be open at least 40 hours a week. Work crews (whose number is not predetermined) are to be assigned the above duties. Their schedules are governed by constraints imposed by labor laws, sound personnel practice, and the mechanics of the situation. The problem is to schedule tracking, maintenance, and crew assignments in such a way that the labor cost is minimized, while meeting the various constraints.

The general case of the problem is labeled Case (i, j), n; this means that there are n stations, i spacecraft up during one 12-hour period of each day, and j spacecraft up during the other 12-hour period. We can always assume $j \leq i$. The restriction $0 \leq i + j \leq 5$ gives rise to 12 spacecraft configurations: (0,0), (1,0), (2,0), (1,1), (3,0), (2,1), (4,0), (3,1), (2,2), (5,0), (4,1), (3,2). Since there are 1, 2, 3, or 4 stations, the problem has $4(12) = 48$ different cases. In order to generalize, however, we will also consider cases with more than 5 spacecraft or 4 stations. From now on, the original cases of the problem will be called the "lower 48 cases."

Minimum cost schedules for all the lower 48 cases are given in Appendix C. But the purpose of this report is not just to solve these particular problems, for the constraints are perhaps not yet realisic enough for these schedules to be usable in the field without modification. Rather, the

[1]Consultant.

solution techniques will prove adaptable to similar DSN scheduling problems, but in realistic situations.

After stating the problem (Section II), we show that solutions always exist (Section III). Section IV gives an algorithm that computes a lower bound for the cost of a most economical schedule. The bound is actually attained in the lower 48 cases by the schedules in Appendix C. Construction of schedules is still partly *ad hoc*, but it is possible to give some guidelines (Section V). In any case, *some* schedule can be made, whether or not it is a cheapest one; its cost then certainly provides an upper bound for the minimum cost.

II. Description of the Model

A. Constraints

There is a DSN complex with n stations, $n \geq 1$. There are $i + j$ spacecraft up, $0 \leq j \leq i$. The first i spacecraft rise at midnight and set at noon. The other j rise at noon and set at midnight. We will call this Case (i, j), n.

(1) All schedules are periodic with period one week.

(2) The complex is manned by an indeterminate number of crews, each crew to be treated as a single indivisible unit. A crew works only 8- or 10-hour shifts. Possible work weeks are 40, 42, 44, 46, or 48 hours. Any crew can work at any station, but a crew must not switch stations during a shift. No more than two crews can be at one station at the same time. Starting times for consecutive shifts of the same crew must be at least 24 hours apart.

If work (tracking or maintenance) is being done at a station, then at least one crew is present. We allow crews to be on duty at a station but not working (in this mathematical sense).

(3) Each station must be open, with a crew, at least 40 hours a week.

(4) If a particular spacecraft is tracked at all during a pass, then it is to be tracked by one, and only one, station during its entire 12-hour pass. Any one station is allowed to track no more than 13 passes a week. (Fourteen are available but are regarded as an overload.)

(5) Each station must receive at least 16 "units" of maintenance a week. (The notion "unit" will be identified subsequently.) At each station, at least 12 hours must be spent on maintenance while the station is not tracking.

If the station is not tracking, and a single crew does maintenance (another crew could be present but idle), then each crew hour accomplishes 1 unit of maintenance. We say that the crew works with efficiency 1.

If tracking and maintenance are simultaneous at a station, then two crews are present, one tracking, the other doing maintenance. The crew that is doing maintenance has efficiency 2/3, that is, each crew hour accomplishes 2/3 units of maintenance. (The crew doing the tracking has priority, and is allowed to interfere with the maintenance crew; the latter's efficiency is therefore reduced.)

If two crews are at a station and both are doing maintenance, then no tracking occurs, and each crew has efficiency 2/3 again, so that both crews working for an hour accomplish 4/3 unit of maintenance. (The crews work at less than double efficiency because they interfere with each other.)

(6) Maintenance on each station must be done in "blocks." A block is a time interval of uninterrupted maintenance composed of x hours at efficiency 1, y hours by a single crew at efficiency 2/3, and z hours by two crews at efficiency 2/3, where $x + (2/3)\,y + z \geq 4$. (Observe that we have z, not $(4/3)z$. In this case, $x + (2/3)y + (4/3)z$ units of maintenance get done. (It has been found that this job cannot adequately be done in short time blocks. The multiplier 4/3 is removed from z in order that a block always be at least 4 *hours*, not just 4 *units*.)

This completes the list of constraints.

B. Costs

Each crew is paid time and one quarter for work beyond 40 hours. (We consider that half the crew is "exempt" and gets straight time, while the other half gets time and a half.) Thus a $(40 + 2k)$-hour work week is assigned a cost $40 + (5/2)k$, $k = 0, 1, 2, 3, 4$.

C. The Problem

Given the spacecraft configuration and the number of stations. If it is possible to track all spacecraft passes while satisfying all constraints, devise a minimum cost schedule of tracking, maintenance, and crew assignments that does so. If not all the passes can be tracked, find the maximum number of passes that can be tracked with the constraints still satisfied. Then find a minimum cost schedule that achieves this maximum.

III. Existence of Solutions

Let there be given n stations and $i + j$ spacecraft. From now on, a schedule of tracking, maintenance, and crew assignments that meets the constraints will be called simply a "schedule." We will soon see that schedules always exist. Any schedule tracks a whole number of passes; consider the nonempty set S of schedules that track the maximum possible number of passes. Since the cost of a $(40 + 2k)$-hour work week is $(5/2)(16 + k)$, the cost of any schedule is an integer multiple of 5/2. Therefore, there exist schedules in S that are cheapest.

It is *a priori* possible that the problem of finding the maximum possible amount of tracking is mixed inextricably with the maintenance and labor constraints, that a given tracking schedule cannot necessarily be completed to a schedule. Fortunately, this is not the case.

PROPOSITION 1. *Given a tracking schedule that satisfies Constraints 1 and 4. There exists a schedule of maintenance and crews that satisfies all the other constraints.*

Proof. If a given station is tracking fewer than 13 passes a week, then there are at least two 12-hour gaps in its tracking schedule. In these gaps, place a total of 16 hours of maintenance in blocks of at least 4 hours. Then schedule 4 crews, a, b, c, d, to this station as in Fig. 1. (We fill up the whole week even if the duty schedules do not demand it; since we are only proving existence we can be very wasteful—temporarily!) Call this a "row" of crews.

If a given station is tracking 13 passes a week, there is only one 12-hour gap in its schedule. Fill this gap with maintenance. Place a 6-hour block of maintenance anywhere else, to be performed simultaneously with tracking. This will yield 4 more units of maintenance. Now assign two separate rows of crews, each scheduled as in Fig. 1. Thus at all times there are two crews at the station. (The second crew does nothing, except during the 6-hour block of maintenance at efficiency 2/3; we said we would be wasteful.)

After carrying out this procedure for all stations, the reader can verify that all constraints are met.

It follows that to determine the maximum number of passes that can be tracked, we need consider only Constraints 1 and 4; this part of the problem can be solved first, without considering maintenance and crews.

IV. Computation of Cost Lower Bounds

Suppose that we find a lower bound for the costs of all schedules that maximize tracking. Suppose that we can construct a schedule that costs exactly this much. Then we have a minimum cost schedule. This we were able to do for all the lower 48 cases. If, for any reason, we had been unable to make a schedule whose cost equals the lower bound, but were able to make a higher-cost schedule, then at least we would have had both upper and lower bounds for the minimum cost.

We have no algorithm for finding minimum cost schedules in the general Case (i, j), n. However, we have prepared a structured flow chart (Figs. 2, 3, 4) that includes an algorithm for computing the maximum number of passes that can be tracked and a cost lower bound. This bound is valid for the general case and is sharp for the lower 48 cases.

The top of the flow chart, Boxes 1, 2, 3, 4, computes the maximum number p of passes that can be tracked. From then on, we consider only schedules that track this many passes. The total number of tracking hours is then $12p$.

Next comes the task of finding a lower bound for the number of crew hours that have to be paid for. Given a schedule that tracks p passes, let p_k be the number of passes tracked by Station k, $k = 1, 2, \cdots, n$. Then $p = \Sigma p_k$. Each station needs at least 16 units of maintenance. Since each crew hour results in 1 hour of tracking, 1 unit of maintenance, 2/3 units of maintenance, or nothing, the number of crew hours spent at Station k is at least $12p_k + 16$. Therefore, a lower bound for total crew hours is $\Sigma(12p_k + 16) = 12p + 16n$. Let us call this the *basic* hours lower bound.

Often, an hours lower bound greater than the basic one can be found. If at least $12p_k + 16 + c_k$ crew hours are worked at Station k, then the whole schedule has at least $12p + 16n + \Sigma c_k$ crew hours. In some cases, we can show that Σc_k is bounded below by some positive number.

After getting an hours lower bound, we compute the cost of the cheapest collection of work weeks such that the total hours worked is not less than the hours lower bound. The resulting cost must be a lower bound for the cost of any actual schedule.

The following paragraphs, keyed to the flow chart box numbers, explain the algorithm in detail.

Box 1. There are only n stations, so no more than n passes can be tracked at one time. If either i or j is greater than n, we can replace it by n and solve this new case. Then we will have done our best for the original case; we need only say which passes go untracked. So from now on, assume $j \leq i \leq n$.

Boxes 2, 3, 4. By Constraint 4, a total of no more than $13n$ passes a week can be tracked. The number of spacecraft passes is $7(i + j)$. Hence, the largest number p of passes that can be tracked cannot exceed the smaller of $13n$ and $7(i + j)$. Fortunately, this upper bound is attained.

PROPOSITION 2. *Assume $j \leq i \leq n$. There exists a schedule that tracks exactly minimum $(13n, 7(i + j))$ passes.*

Proof. By Proposition 1, we need only make a tracking schedule that meets Constraints 1 and 4.

Assume $7(i + j) \leq 13n$. For the first half of each day, we can relax a set of $n - i$ stations; for the second half, a set of $n - j$ stations. By the end of the week we have relaxed 14 sets of stations. Since the above inequality can be written $7(n - i) + 7(n - j) \geq n$, we can determine the sets so that their union is the set of all n stations. Then each station has been relaxed for at least one half-day, and all passes have been tracked.

Assume $7(i + j) > 13n$. Then $7(n - i) + 7(n - j) < n$. We can make the sets of relaxed stations disjoint. Then $7(n - i) + 7(n - j)$ stations have been relaxed exactly once, and tracking has been scheduled for all $7(i + j)$ passes. But there remain $n - 7(n - i) - 7(n - j) = 7(i + j) - 13n$ stations that need to be relaxed. Their relaxation periods can be stolen from the $7(i + j)$ passes that have just been scheduled. This leaves $7(i + j) - [7(i + j) - 13n] = 13n$ passes tracked.

If $7(i + j) \leq 13n$ then $p = 7(i + j)$. If $7(i + j) > 13n$, then $p = 13n$, and we will immediately establish an hours lower bound better than the basic one, which is $156n + 16n = 172n$. Each station has only one 12-hour period, or "gap," in which it is not tracking. By Constraint 5, there are no more than 12 crew hours spent on maintenance at efficiency 1, for such must take place when there is no tracking. To reach 16 units of maintenance, at least 6 crew hours must be spent at efficiency 2/3. Therefore, at least 18 crew hours per station are spent on maintenance. Since tracking takes up $12(13) = 156$ crew hours, each station accounts for at least 174 crew hours. Therefore, $174n$ is an hours lower bound.

Boxes 5, 6. At this point, all the $7(i + j)$ passes can be tracked, and the basic hours lower bound is $84(i + j) + 16n$. Even so, some stations may still have only one relaxation period. Assume $12n < 7(i + j) \leq 13n$. The number of relaxation periods is $14n - 7(i + j)$. If s is the number of stations with only one relaxation period, then the other $n - s$ stations have at least 2 relaxation periods. Therefore, $14n - 7(i + j) \geq s + 2(n - s)$, i.e., $s \geq 7(i + j) - 12n$. Let $s' = 7(i + j) - 12n$. There exist s' stations with one relaxation period. Each of these stations accounts for at least 174 crew hours, but contributes only $12(13) + 16 = 172$ hours to the basic hours lower bound. It follows that $2s'$ can be added to the basic hours lower bound. This gives a new hours lower bound of $84(i + j) + 16n + 14(i + j) - 24n = 98(i + j) - 8n$.

Boxes 7, 8. Here, $84(i + j) + 16n$ is an hours lower bound. By Constraint 3, so is $40n$. Hence, if $84(i + j) + 16n < 40n$, i.e., $7(i + j) < 2n$, we use $40n$ as our hours lower bound. Otherwise, we try to improve on the basic bound.

Boxes 9, 10, and Fig. 3. If $j = 0$ when we reach Box 9, then it may be possible to improve on the basic bound $84i + 16n$. There are $7i$ passes, and all are tracked during the first half of the day. Each 12-hour tracking interval is isolated from the others on that station's schedule. Since shifts are 8 or 10 hours, each interval must touch at least 2 shifts, and no shift touches more than one interval. It follows that each of the $7i$ tracking intervals accounts for at least 16 crew hours. Accordingly, $(7i)(16) = 112i$ is an hours lower bound. If $7i \leq 4n$, then $84i + 16n \geq 112i$; we keep the basic bound. If $7i > 4n$ then $112i$ is a better bound.

Boxes 11, 12, and Fig. 3. If $i = n$ at Box 11, then the tracking schedule may still be forced to have so many isolated intervals that the basic hours lower bound $84(i + j) + 16n = 100n + 84j$ can again be improved upon. The argument is more complicated; it is necessary to consider each station separately. All stations track during the first half of the day, and $n - j$ of them have a "gap" (are not tracking) during the second half of the day. The entire tracking schedule has $7(n - j)$ gaps, and if this number is large enough compared with n, some stations are forced to have 6 or 7 gaps: If $7(n - j) > 6n$, i.e., $n > 7j$, then at least one station has 7 gaps, otherwise the number of gaps would be at most $6n$. If $7(n - j) > 5n$, i.e., $2n > 7j$, then at least one station has at least 6 gaps. We will elaborate on this later.

Let us investigate the consequences of 7 gaps in the tracking schedule of a station. The schedule is the same as the right side of Fig. 5, except for a rotation. There are 7 isolated tracking intervals. As the argument for Box 10 shows, these intervals touch at least 14 crew shifts, which account for at least $8(14) = 112$ crew hours. This is 12 more than the $7(12) + 16$ hours contributed by this station to the basic hours lower bound.

If a station has 6 gaps in its schedule, then this schedule looks like the left side of Fig. 5. There are 5 isolated tracking intervals, which touch at least 10 shifts, which account for at least 80 crew hours. There are 3 other tracking intervals, which account for at least 36 more crew hours. Accordingly, this station accounts for at least 116 crew hours, which is 4 more than the $8(12) + 16$ hours contributed to the basic hours lower bound.

Consider now Case (n,j), n. There are $7(n-j)$ gaps; let the kth station have g_k gaps, where $1 \leq g_k \leq 7$. Without losing generality, we can assume $g_1 \geq g_2 \geq \cdots \geq g_n$. If $g_k = 7$, then set $c_k = 12$ (12 crew hours over the basic bound). If $g_k = 6$ set $c_k = 4$. If $g_k = 5$ set $c_k = 0$. There is a choice of the g_k that minimizes Σc_k subject to the constraint $\Sigma g_k = 7(n-j)$. This minimum we call "extra," and the new hours lower bound is $100n + 84j +$ extra.

PROPOSITION 3. *Let* $i = n$, $7(i+j) \leq 12n$. *Then*

$$\text{extra} = 0 \qquad \text{if } 7j \geq 2n$$

$$\text{extra} = 8n - 28j \qquad \text{if } n \leq 7j \leq 2n$$

$$\text{extra} = 12n - 56j \qquad \text{if } 7j < n.$$

We have relegated the proof to Appendix A.

The only case in the lower 48 such that $i = n$, $j > 0$, and extra > 0 is Case (4,1), 4. There are $7(4-1) = 21$ gaps, and the distribution of gaps that minimizes Σc_k is 6,5,5,5. Therefore, extra $= 4$.

Box 13. The basic hours lower bound is sharp for the lower 48 cases that reach this place in the flow chart.

Box 14. Let h be an hour's lower bound. To compute a cost lower bound, we must find a string of work weeks $40 + 2x_1, 40 + 2x_2, \cdots, 40 + 2x_m$ ($x_i = 0,1,2,3,4$; m not predetermined), such that the total crew time $\Sigma(40 + 2x_i) = 40m + 2\Sigma x_i$ is *at least* h, while the cost $\Sigma(40 + (5/2)x_i) = 40m + (5/2)\Sigma x_i$ is minimized. At this point we need only work with the two numbers m and $2\Sigma x_i$. It will suffice to give two examples from the lower 48 cases.

Case (3,1), 3. Here $h = 384$. Since $8(48) = 384$, at least 8 crews are needed. If 8 crews are used, the cost is $8(50) = 400$. If 9 crews are used, then there are $9(40) = 360$ regular hours and at least 24 overtime hours. The minimum cost of 9 crews is then $360 + (5/4)24 = 390$. If 10 or more crews are used, the cost is at least $10(40) = 400$. Therefore, a cost lower bound is 390.

Case (2,1), 4. Here $h = 316$. Since $6(48) < 316$, at least 7 crews are needed. If 7 crews are used, the cost is at least $7(40) + (5/4)36 = 325$. If 8 crews are used, the cost is at least $8(40) = 320$, which is therefore a cost lower bound. Notice that it pays to waste 4 crew hours.

Occasionally, the solution for m and Σx_i is not unique. See, for example, Case (1,1), 4.

Box 15. We have obtained the number of crews m and the overtime hours $2\Sigma x_i$ that achieve the cost lower bound. Before one attempts to construct a schedule that costs just this much, it may be helpful to list all the ways that these overtime hours can be distributed among the m work weeks (with the work weeks in non-increasing order, for example). For example, in Case (1,1), 1 we have $m = 4$, $x_1 + x_2 + x_3 + x_4 = 7$. The list of ways to write 7 as the sum of four non-increasing integers between 0 and 4 is $4+3+0+0$, $4+2+1+0$, $4+1+1+1$, $3+3+1+0$, $3+2+2+0$, $3+2+1+1$, $2+2+2+1$. These yield the following work week splits:

48, 46, 40, 40

48, 44, 42, 40

48, 42, 42, 42

46, 46, 42, 40

46, 44, 44, 40

46, 44, 42, 42

44, 44, 44, 42

V. Construction of Schedules (Figure 4, Box 16)

If this is the first time we have come to this box, then we have a list of work-week splits with cost equal to a cost lower bound. We can do no more than give some imprecise guidelines for constructing a weekly schedule that uses one of these splits.

First, we make a tracking schedule that satisfies Constraint 4 and tracks p passes. In doing this, we avoid iso-

lated tracking intervals as much as possible, for as we saw in the discussion of Boxes 10 and 12, each interval forces at least 4 hours of non-tracking crew hours, which are either spent on maintenance or wasted. If there are 4 isolated intervals at a station, then we can adjoin a 4-hour block of maintenance to each and cover the resulting 16 hours of work by two 8-hour shifts. If there are fewer than 4 isolated intervals at a station, then there is more freedom in assigning maintenance. If the algorithm has gone through Boxes 10 or 12, then we know how many isolated intervals we have to handle. Otherwise, we hope that we can get by with 4 or fewer per station. This is so for the lower 48 cases, but if we run into a case that requires more isolated intervals (and can prove that it does), then we can add something to the basic hours lower bound and go back to Box 14.

Next, we assign 16 hours of maintenance to each station while observing Constraints 5 and 6. The proof of Proposition 1 tells how to start. If a station is tracking fewer than 13 passes, so that maintenance can be disjoint from tracking, then, as a general rule, we try to assign maintenance so that the duty intervals of tracking plus contiguous maintenance have lengths which are multiples of 8 hours. Such an interval can be covered tightly by 8-hour shifts, which are easier to work with. If the length of a duty interval is an odd multiple of 4 hours and is at least 20 hours, then two 10-hour shifts plus some 8-hour shifts will cover it tightly.

Finally, we assign crew shifts. There is a list of work week splits (Box 15). Each work week can be split in turn into 8- and 10-hour shifts, perhaps in more than one way. We try to choose a work week split and shift splits so that there are just enough 10-hour shifts to suit the tracking and maintenance schedule. We give names a, b, c,$\cdots$ to the crews, and show the shift split for each. On the schedule, we show where the 8- and 10-hour shifts are to go. Then the shifts are labeled with crew names such that Constraint 2 (especially the 24-hour part) is satisfied. For all the lower 48 cases, this can be done by labeling from top down, then left to right. (We must make sure that the 10-hour shifts are labeled correctly.) It may then happen that the end of this week and the beginning of the next week violate the 24-hour constraint. If so, we try to remedy the situation by juggling the labels. For the lower 48 cases, this works.

At any point, it may be necessary or convenient to go back and choose a different shift split, work week split, maintenance schedule, or tracking schedule, and proceed again from there.

The scheduling process is really quite easy, for most of the thinking has been done by the time a good cost lower bound is derived. There seems to be considerable leeway in the construction of schedules; the first or second choice usually works. We were initially successful in all lower 48 cases (except for Case (4,1), 4; see the remark at the end of Section VI), and thus made it to Box 17 (cheapest schedule found).

VI. Improving the Bound (Figure 4)

Figure 4 is a guide to follow in case we cannot construct a schedule whose cost equals the cost lower bound we have on hand. The reason for this failure may be either that no such schedule exists, or that we have not been persistent or clever enough. By Proposition 1, it is possible to make *some* schedule that tracks the greatest possible number of passes. We do this as cheaply as we are able (Box 18). The cost of the schedule so made is an upper bound for the cost of a cheapest schedule.

If we cannot prove that our cost lower bound can be increased, then we leave the flow chart by way of Box 21 with upper and lower bounds for the cost of a cheapest schedule. If we *can* prove that there is a greater lower bound, we do so (Box 20). Then we try to make a schedule that achieves this new bound (Box 16). Thus we go around the loop (a finite number of times) until we achieve an exit through Box 17 or are forced out through Box 21.

Case (4,1), 4 drove us once around the loop; the cheapest schedule we could make exceeded our lower bound by 4 hours. This forced us to make the argument associated with Box 12; the lower bound increased by 4 hours; so we made it to Box 17. Of course, the improvement is now part of the algorithm.

The FLAG device is merely a way of avoiding a double exit from the loop; the entire flow chart follows the rules of structured algorithms, the proposed DSN standard for software.

VII. Proposed Changes in the Model

We have assumed that rises and sets of spacecraft are synchronized with each other modulo 12 hours. If we remove this constraint, the spacecraft passes could have lengths other than 12 hours, and rises would no longer

need to coincide with the starts of half-days. Perhaps some randomness could be built in. This modification would introduce more parameters into the problem.

Some of the labor constraints may have to be tightened. The International Brotherhood of Electrical Workers/ Philco-Ford Corporation Labor Agreement requires that each shift have a regular start time, that overtime be equalized among the crews, and that days off be consecutive. Exceptions to these rules can occur, but *each* such exception must be negotiated between the company and the union.

The cost function of the problem may need modification. For example, we have assumed that no overtime be paid for a work week of four 10-hour shifts. The Walsh-Healey Act requires that any business with a government contract pay overtime to non-exempt employees for hours worked in excess of 8 in a given work day. Philco-Ford Company policy requires that time and a half be paid to exempt employees for scheduled time in excess of 8 hours in a given work day. (A bill has been introduced in the California Legislature to repeal the State overtime requirement on 10-hour days, but the Federal would still control.)

a: 6(8). b, c, d: 5(8)

MON	TUE	WED	THU	FRI	SAT	SUN	MON
b a c	d a b	c d a	b c d	a b c	d a b	c a d	b a c

Fig. 1. A crew schedule that fills the week

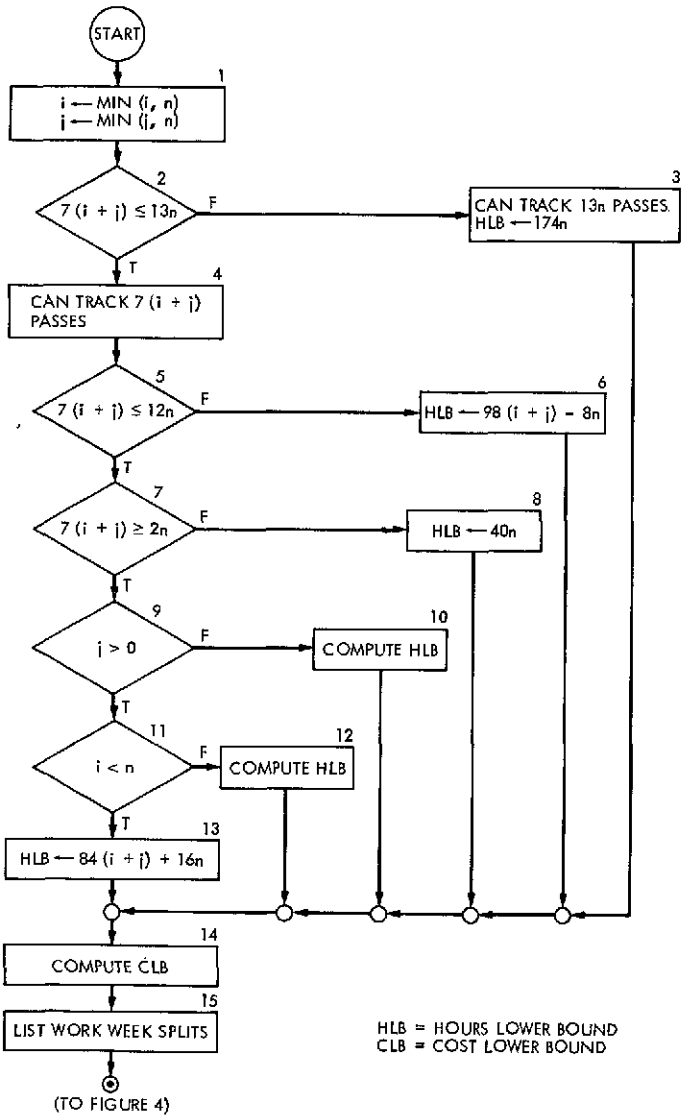

Fig. 2. Cost lower bound algorithm for Case (*i*, *j*) *n*

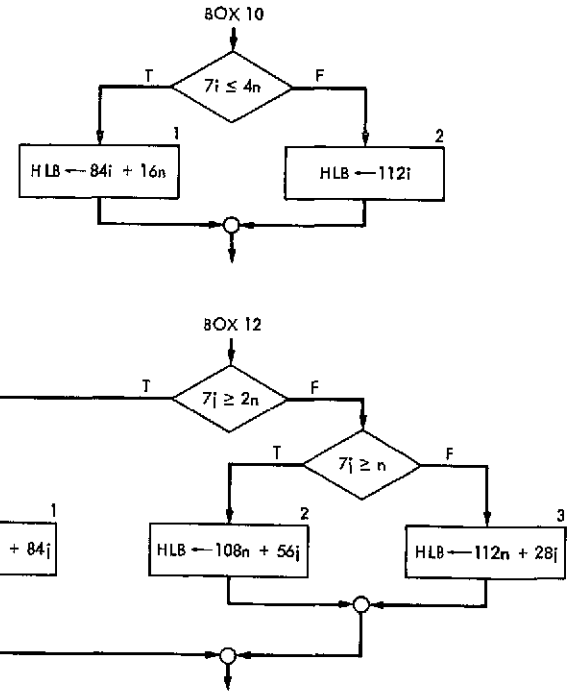

Fig. 3. Boxes 10 and 12 (Fig. 2)

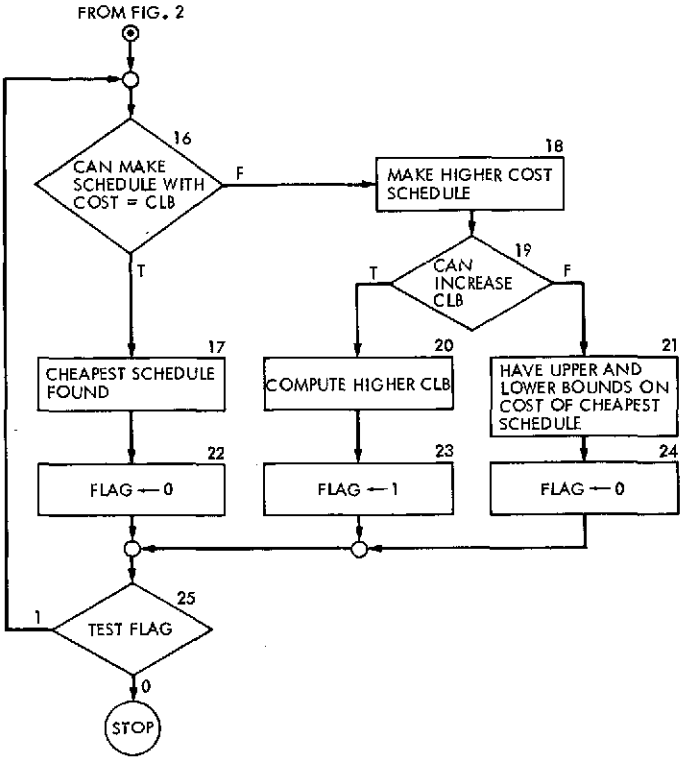

Fig. 4. Improving the bound from Fig. 2

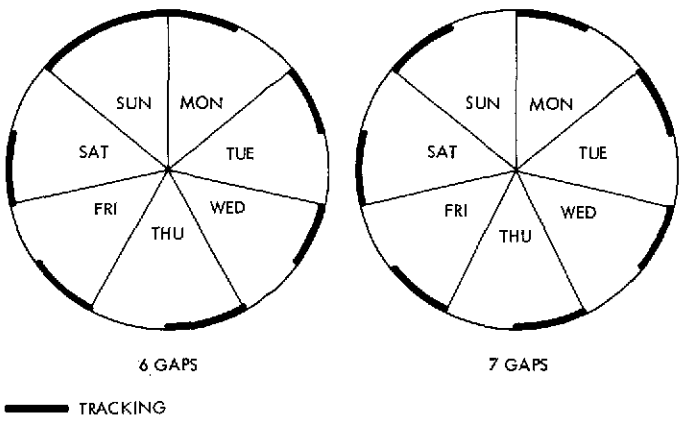

Fig. 5. Tracking schedules for Cases $i = n$

Appendix A

Proof of Proposition 3

Let n be a positive integer, j a nonnegative integer such that $7j \leq 6n$. (Actually, we know $7j \leq 5n$.) Define a function c by

$$\begin{aligned} c(g) &= 12, && \text{if } g = 7 \\ &= 4, && \text{if } g = 6 \\ &= 0, && \text{otherwise} \end{aligned}$$

Consider the problem

$$\text{Find } M = \text{minimum} \sum_{k=1}^{n} c(g_k)$$

subject to the constraints

(1) g_k an integer, $1 \leq g_k \leq 7 \qquad (k = 1, \cdots, n)$

(2) $\sum_{k=1}^{n} g_k = 7(n - j)$

The solution is

$$\begin{aligned} M &= 0 && \text{if } 7j \geq 2n \\ &= 8n - 28j && \text{if } n \leq 7j \leq 2n \\ &= 12n - 56j && \text{if } 7j < n \end{aligned}$$

Proof

Let $7j \geq 2n$. Then

$$n \leq 7(n - j) \leq 5n$$

Accordingly, $g_1, \cdots, g_n$ can be chosen between 1 and 5 to add up to $7(n - j)$.

Let $n \leq 7j < 2n$. Then $7(n - j) > 5n$; we need some 6's or 7's. Suppose that m of the g_k are 7. Then the remaining $n - m$ g_k add up to $7(n - j - m)$ and are between 1 and 6. Suppose

$$7(n - j - m) > 5(n - m)$$

Then at least $7(n - j - m) - 5(n - m) = 2n - 7j - 2m$ 6's are needed, for otherwise the sum of the $n - m$ terms is less than $7(n - j - m)$. In this case (with $c_k = c(g_k)$),

$$\begin{aligned} \Sigma c_k &\geq 12m + 4(2n - 7j - 2m) = 8n - 28j + 4m \\ &\geq 8n - 28j = 4(2n - 7j) \end{aligned}$$

Suppose on the other hand that

$$7(n - j - m) \leq 5(n - m)$$

Then $2m \geq 2n - 7j$, no 6's are needed, and

$$\Sigma c_k \geq 12m \geq 12n - 42j = 6(2n - 7j) > 4(2n - 7j)$$

since $2n - 7j > 0$. In either case, $\Sigma c_k \geq 8n - 28j$, and this bound can be achieved by using no 7's, $2n - 7j$ 6's, and the remaining $7j - n$ g_k equal to 5.

Let $7j < n$. Then at least $n - 7j$ 7's are needed. Suppose in fact that $n - 7j + r$ 7's are used.The remaining $7j - r$ g_k add to $7(n - j) - 7(n - 7j + r) = 42j - 7r$. Suppose $42j - 7r > 5(7j - r)$. Then at least $42j - 7r - 5(7j - r) = 7j - 2r$ of these g_k must be 6. In this case,

$$\begin{aligned} \Sigma c_k &\geq 12(n - 7j + r) + 4(7j - 2r) \\ &= 12n - 56j + 4r \geq 12n - 56j \end{aligned}$$

On the other hand, if $42j - 7r \leq 5(7j - r)$, then $2r \geq 7j$, no 6's are needed, and

$$\Sigma c_k \geq 12(n - 7j + r) \geq 12n - 84j + 42j = 12n - 42j$$

In either case, $\Sigma c_k \geq 12n - 56j$, and this bound is achieved by using $n - 7j$ 7's and $7j$ 6's.

Appendix B

Table of Minimum Costs for the Lower 48 Cases

Figure B-1 gives the minimum cost for each of the lower 48 cases. For each case we enter the minimum cost and the "slack," defined by slack = minimum cost $-$ $(12p + 16n)$, where p is the maximum number of passes that can be tracked, and $16n$ is the required maintenance. If it is not possible to track all spacecraft passes, then a "1" or a "3" is entered. A "1" means that either i or j is greater than n. (See Box 1 of Fig. 2.) A "3" means that the case runs into the constraint that no station can track 14 passes a week (Box 3 of the flow chart).

ENTRIES: MINIMUM COST/SLACK[a]

n \ (i, j)	(0, 0)	(1, 0)	(2, 0)	(1, 1)	(3, 0)	(2, 1)	(4, 0)	(3, 1)	(2, 2)	(5, 0)	(4, 1)	(3, 2)
1	40 / 24	120 / 20	120 / 1 20	177 1/2 / 3 5 1/2	120 / 1 20	177 1/2 / 3 1 5 1/2	120 / 1 20	177 1/2 / 3 1 5 1/2	177 1/2 / 3 1 5 1/2	120 / 1 20	177 1/2 / 3 1 5 1/2	177 1/2 / 3 1 5 1/2
2	80 / 48	120 / 4	230 / 30	200 / 0	230 / 1 30	285 / 1	230 / 1 30	285 / 1 1	355 / 3 11	230 / 1 30	285 / 1 1	355 / 3 1 11
3	120 / 72	135 / 3	230 / 14	220 / 4	340 / 40	305 / 5	340 / 1 40	390 / 6	390 / 6	340 / 1 40	390 / 1 6	475 / 7
4	160 / 96	160 / 12	240 / 8	240 / 8	340 / 24	320 / 4	450 / 50	400 / 0	400 / 0	450 / 1 50	490 / 6	485 / 1

[a]SLACK = COST - (TRACKING + MAINTENANCE)

Fig. B-1. Minimum cost of lower 48 Cases

Appendix C

Minimum Cost Schedules for the Lower 48 Cases

For each case, the stations are named A, B, C, D and the crews a, b, c,$\cdots$. The shift split of each crew is given. The days of the week run from Monday to Sunday, although this is arbitrary. Monday is repeated at the right end of the schedules. An interval of tracking is shown by a solid line; we do not bother to state which spacecraft is being tracked. Maintenance is shown by dashed lines. Below the tracking and maintenance schedules for a station we put the crew shifts. Each 10-hour shift is indicated by a superscript; otherwise it is 8 hours. Occasionally the minimum cost can be achieved with more than one value for crew hours. When this happens, we give an alternate crew schedule by using Greek letters $\alpha, \beta, \gamma, \cdots$. An example is Case (1,1), 4.

A flow chart box number, which refers to Fig. 2, shows which path the cost lower bound algorithm takes. If Box 10 or 12 is cited, then the next number in parentheses refers to the box numbers in Fig. 3.

The cases with $i > n$ or $j > n$ are omitted because they reduce to other cases. (See Box 1, Fig. 2.)

CASE (0, 0), 1. BOX 8. a: 5(8)

STATION \ DAY	MON	TUE	WED	THU	FRI	SAT	SUN	MON
A	a	a	a	a	a			a

CASE (0, 0), n. BOX 8

n COPIES OF THE ABOVE SCHEDULE

CASE (1, 0), 1. BOX 10(2). a, b, c: 5(8)

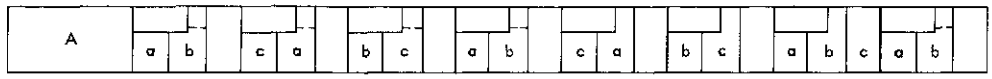

CASE (1, 0), 2. BOX 10(1). a, b, c: 5(8)

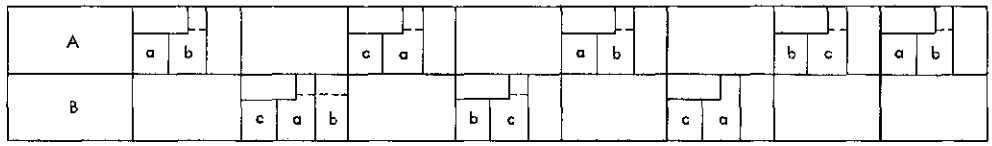

CASE (1, 0), 3. BOX 10(1). a: 5(8), b: 3(8) + 2(10), c: 6(8)

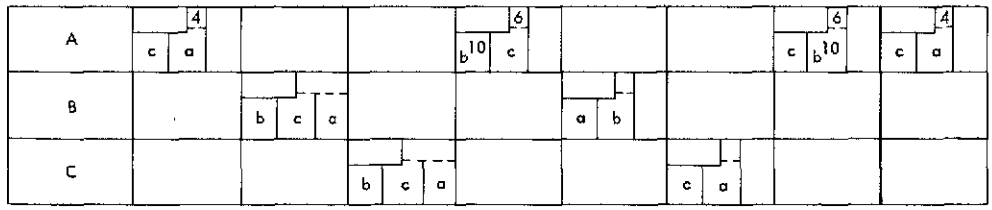

CASE (1, 0), 4. BOX 8. a, b, c, d: 5(8)

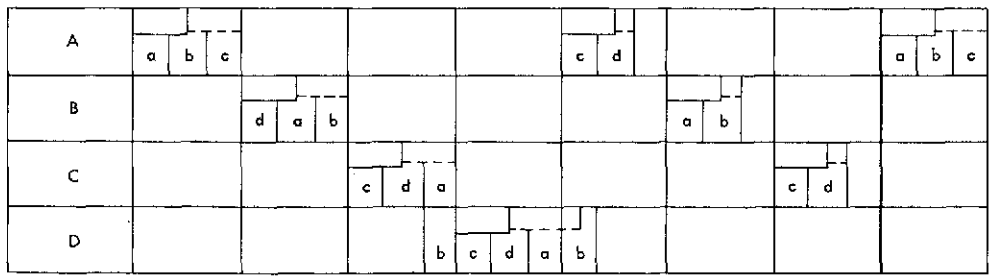

CASE (2, 0), 2. BOX 10(2). a, b, c: 6(8). d, e: 5(8)

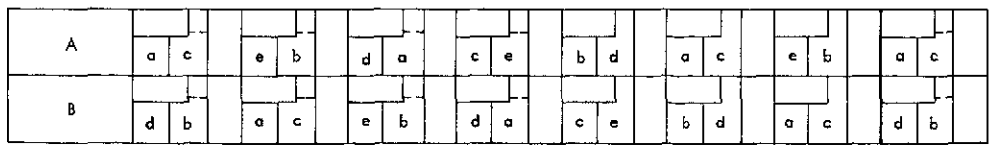

Fig. C-1. Minimum cost schedules for the lower 48 Cases

CASE (2, 0), 3. BOX 10(2). a, b, c: 6(8). d, e: 5(8)

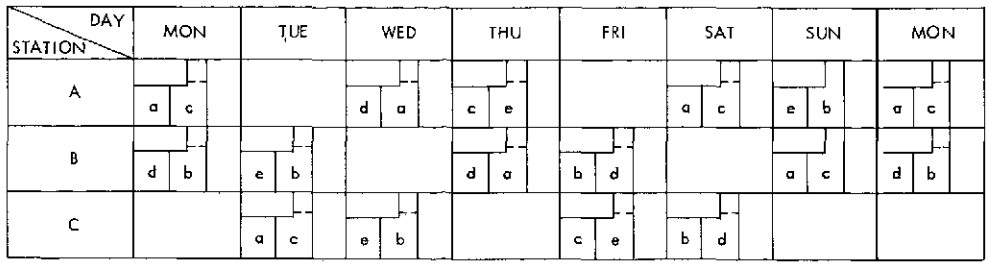

CASE (2, 0), 4. BOX 10(1). a, b, c, d: 6(8). e: 5(8)
α, β, γ, δ, ϵ, ζ: 5(8)

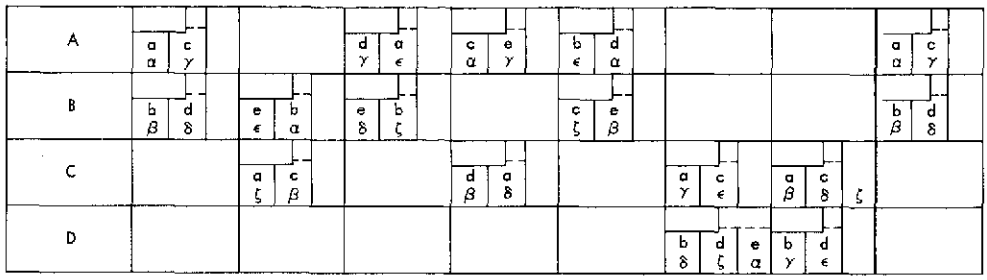

CASE (1, 1), 1. BOX 3. a: 6(8). b, c, d: 4(8) + 10

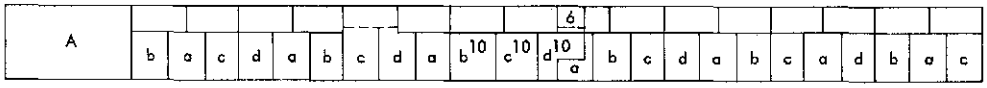

CASE (1, 1), 2. BOX 13. a, b, c, d, e: 5(8)

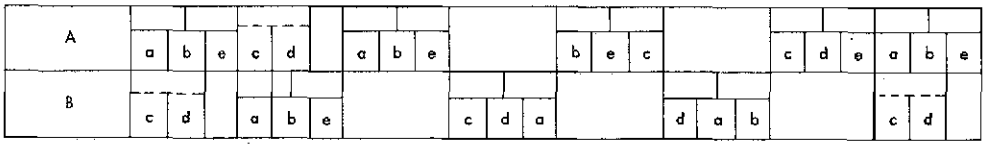

CASE (1, 1), 3. BOX 13. a, b: 6(8). c, d, e: 5(8)

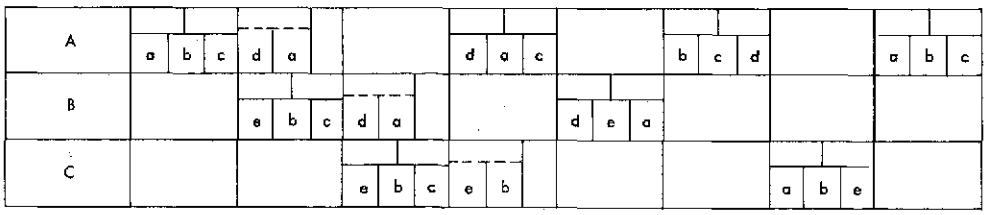

Fig. C-1 (contd)

CASE (1, 1), 4. BOX 13. a, b, c, d: 6(8). e: 5(8)
α, β, γ, ϵ, δ, ζ : 5(8)

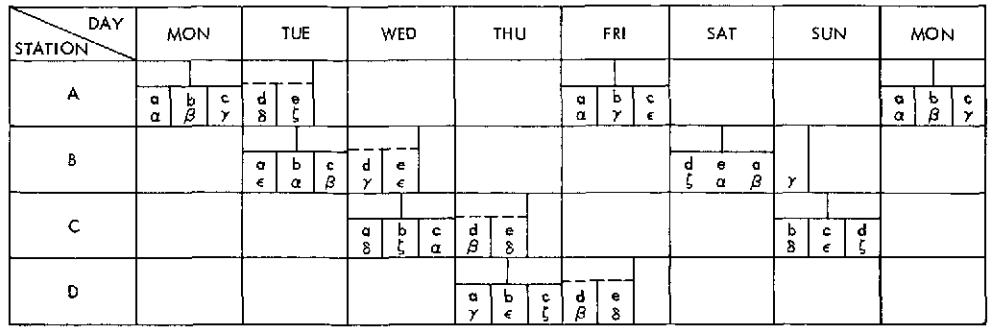

CASE (3, 0), 3. BOX 10(2). a, b: 6(8). c, d, e, f, g, h: 5(8)

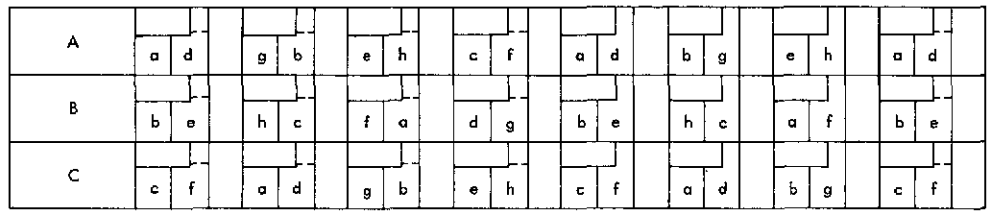

CASE (3, 0), 4. BOX 10(2). a, b: 6(8). c, d, e, f, g, h: 5(8)

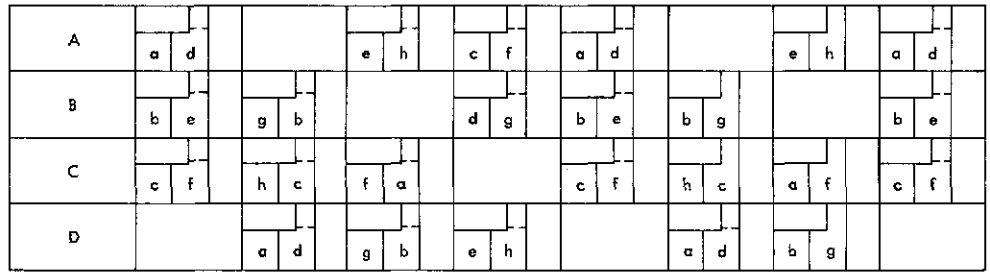

CASE (2, 1), 2. BOX 12(1). a, b: 4(8) + 10. c, d, e, f, g: 5(8)

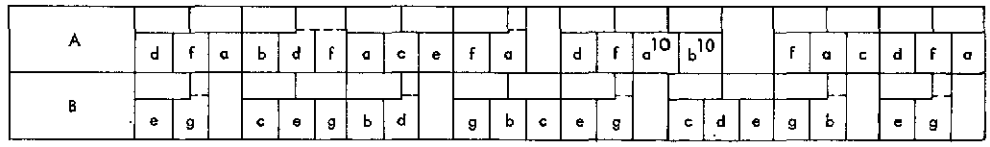

CASE (2, 1), 3. BOX 13. a, b: 6(8). c: 3(8) + 2(10). d, e, f, g: 5(8)

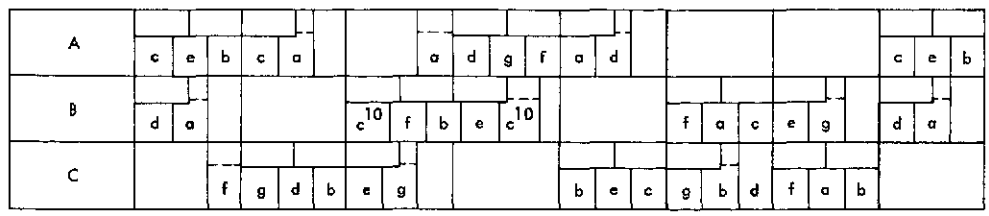

Fig. C-1 (contd)

CASE (2, 1), 4. BOX 13. a, b, c, d, e, f, g, h: 5(8)

DAY / STATION	MON	TUE	WED	THU	FRI	SAT	SUN	MON
A	a c e		e g a		a d f		d f	a c e
B	b d f		f h b		b e		e g h	b d f
C		g a c		c e g c		g a c		
D		h b d		d f h		h b		

CASE (4, 0), 4. BOX 10(2). a: 6(8). b, c, d, e, f, g, h, i, j, k: 5(8)

A	a	e	i	b	f	j	c	g	k	d	a	h	e	i	a	e
B	b	f	j	c	g	k	d	h	a	e	i	b	f	j	b	f
C	c	g	k	d	h	a	e	i	b	f	j	c	g	k	c	g
D	d	h	a	e	i	b	f	j	c	g	k	d	a	h	d	h

CASE (3, 1), 3. BOX 12(1). a, b, c: 6(8). d: 4(10). e, f, g, h, i: 5(8)

A	a	e	h	i	b		g	i		c	g	a	b	f		a	c		a	c	h	a	e	h
B	b	f		d^{10}	c	f	d^{10}			e	h		c	g	i	b	e		b	i		b	f	
C	g	c		a	e		h	a	b	f	i		e	h		d^{10}	f	g	d^{10}			g	c	

CASE (3, 1), 4. BOX 13. a, b, c, d, e, f, g, h, i, j: 5(8)

A	a	d				e	h		b	e		j	c	f			d	g		a	d	
B	b	e	g	h	a	d				c	f	h	a	d		g	j	c			b	e	g
C	c	f		i	b		f	i	a				b	e		h	a		e	h	j	c	f	
D				j	c		g	j		d	g	i				i	b		f	i				

CASE (2, 2), 2. BOX 3

TWO COPIES OF THE CASE (1, 1), 1 SCHEDULE

Fig. C-1 (contd)

CASE (2, 2), 3. BOX 13. a, b, c: 6(8). d, e, f, g, h, i: 5(8)

DAY / STATION	MON	TUE	WED	THU	FRI	SAT	SUN	MON
A	a c e	g a	f i c	e h b		a c e	b g i	a c e
B	b d f	h b d	g a	f i c	d f h		a c h	b d f
C		i c e	h b d	g a	e g i	b d f		

CASE (2, 2), 4. BOX 13

TWO COPIES OF THE CASE (1, 1), 2 SCHEDULE

CASE (4, 1), 4. BOX 12(2). d: 4(10) + 8. l: 4(10). a, b, c, e, f, g, h, i, j: 5(8)

A	a	e	h	i	l^{10}	d^{10}	i			b	f		k	c		g	k		e	i		a	e	h
B	b	f		j	b		f	j	l^{10}	c	g	j	l^{10}			h	a		f	j		b	f	
C	c	g		k	c		g	k		d	h		a	d^{10}	f	i	b	d^{10}	h			c	g	
D	d^{10}			a	e		h	a		e	i		b	e		j	c		g	k	l^{10}	d^{10}		

CASE (3, 2), 3. BOX 12(1). a, b, c: 6(8). d: 3(8) + 2(10). e, f, g, h, i, j, k: 5(8)

A	a	d	g	j	b	e	h	k	c	f	i	k	b	e		j	b	e	g	b	j	a	d	g
B	h	b	e	k	c	f	i	a	e	g	j	a	c	f	h	k	c		h	c	k	h	b	e
C	f	c	i	a	d^{10}	g	j	b	d^{10}	h			d	g	i	a	d	f	a	i		f	c	i

CASE (3, 2), 4. BOX 13. b: 2(10) + 3(8). a, c, d, e, f, g, h, i, j, k, l: 5(8)

A	a	d	g				g	j	a	d	g	j	a	d	g				e	h		a	d	g
B	b^{10}	f	i	f	b^{10}	f				e	h	k	b	e	h	i	l	c				b^{10}	f	i
C	c	e	h	j	a	d	h	k	b				c	f		j	a	d	f	i	k	c	e	h
D				k	c	e	i	l	c	f	i	l				k	b		g	j	l			

Fig. C-1 (contd)

A Preliminary Analysis of the Distribution of Energy Usage at Goldstone DSCC

J. Lu
Systems Analysis Section

A survey has been conducted of energy used for space cooling, space heating, electromechanical and other functions, lighting, and electronics. Results show a preliminary estimated distribution of 46%, 24%, 18%, 6%, 5%, respectively, for the aforementioned categories. The percentage figure for electromechanical and other functions was done by elimination. The total primary energy consumption for Fiscal Year 1973 was known prior to undertaking this task.

I. Introduction

This article presents the results of a Network Operations Performance Analysis Task on identifying an energy usage pattern at Goldstone DSCC. The goal of this study was to understand those patterns such that: (1) a rational short-term energy reduction policy could be formulated, and (2) a consequent dollar savings in Goldstone operations could be obtained. The study was also useful as a preliminary energy usage model for long-term reduction of Goldstone's dependence on external energy sources.

Toward these ends, energy use was allocated into the following categories: space cooling, space heating, lighting, electronics, and electromechanical functions and all other uses (Ref. 1). Energy values for each of these categories were then determined for each site and each building at Goldstone. An expanded description follows.

II. Definitions

The category of space cooling included all air refrigeration[1] loads associated with each building at each Deep Space Station (DSS). These loads did not differentiate between rated capacities for comfort cooling or electronic equipment cooling. In addition, no evaporative coolers were considered, and only small heat pumps used primarily for comfort conditioning were included (Ref. 2).

The category of space heating included all electrical resistance heating units used for warming air for personnel comfort. An account of heating using liquid propane gas as the fuel source was included (Ref. 3).

Electronic loads were delimited to include only the energy used for control room electronics. This work was

[1]Here taken to mean no adjustment of relative humidity.

done by DSN Engineering prior to the initiation of this task (Ref. 4).

Lighting included all sources of interior and exterior illumination at the Pioneer, Echo, Venus, and Mars DSSs. Neither the Spacecraft Test Facility nor the Microwave Test Facility was included (Ref. 5).

Energy used for electromechanical functions and all other uses included all energy consumers not specified within the preceding four categories. Hence, the energy value, GJ or gigajoules (1 GJ = 0.948 × 10^6 BTUs), associated with this category was calculated by subtracting the energy used for the preceding four categories from the primary energy total of 115,000 GJ used in 1973 (Ref. 6).

III. Data

The basic tenets of data collection were that the data would be collected on a non-interference basis, and that there would be no special data-gathering instrumentation installed for this survey. Non-interference implied that the process of collecting data would disrupt neither the reliability of tracking nor the regular maintenance routines performed by Support Services personnel. Special instrumentation would have been required for measurements of currents flowing in selected busbars. Furthermore, cables were oftentimes so densely packed that instrumentation would have been useless in any case. For these and other reasons, data were collected in the following forms.

Energy used for lighting was broken into energy used for exterior lighting and energy used for interior lighting. In both cases, the energy used was calculated by counting the lighting wattages associated with each building at each site. An estimated number of hours of usage was then specified with the help of De Wayne Feasel and William Carman in Support Services at Goldstone.

There were, however, uncertainties as to the area under which such lighting intensities could be assumed constant. For example, lighting a 40-m^2 room could have 1614 lm/m^2 (150 fc) over an immediate work area of 10 m^2. This assessment was not recorded as a part of the lighting intensity survey. Hence, accounting for such factors necessitated an appropriate sampling of representative rooms. Avoidance of this procedure led to usage of aggregated floor areas. This particular procedure yielded unreasonable results. Thus it became apparent that a sampling of rooms would be necessary. If such an account were to be made, it seemed just as simple to count the lighting wattage directly. This was the method that was chosen.

The data used for space cooling energy were also collected from records maintained by Support Services at Goldstone. These records do not distinguish between cooling requirements for comfort and cooling requirements for electronic equipment. These data were then combined with average monthly usage times which accounted for air refrigeration loads turned off during weekends and during nine paid holidays per year. During summer, the percentage of capacity loading on air refrigeration tonnage[2] was assessed at 80%. Winter, fall, and spring were assessed at percentage loadings of 33%, 55%, and 55%, respectively.

Energy used for space heaters was collected in the form of power ratings at each building and each DSS for electrical heaters and average yearly usage in gallons at each site for liquid propane gas. The total electrical power delivered to resistance heaters was assigned full operating capacity during the nine-month period, September through May, when average monthly outdoor temperatures were less than indoor temperatures (21°C (70°F) Ref. 7).

Energy used for control room electronic equipment was given in power loads specified by DSN Engineering. An assumption was made that such equipment would be on at all times. Although such an estimate was made, energy usage still did not amount to a significant portion of the total energy picture.

Once again, energy used for electromechanical and all other functions was not considered except as an all-inclusive category to account for equipment not covered by the other four categories.

Although the hypothetical energy allocation scheme was useful as a tool for approaching this survey, there were areas where practical reality differed markedly from the conception. For example, the small heat pumps included in the space cooling category rightfully belonged in the space heating category when the weather was cold. Equipment cooling could be included in the category of electromechanical functions, and the unaccounted portion of liquid propane gas usage belongs more to space heating

[2]A measure of refrigerative capacity. One ton of refrigeration = 12.7 MJ/h or 12,000 BTU/h.

than to electromechanical and all other functions. Pioneer, Echo, and Venus are equipped with an assortment of fifteen boilers, twenty-nine space heaters, four hot water heaters and four cooking ranges, all of which consume liquid propane gas. For these reasons, one must consider the obtained distribution to be a preliminary sketch only.

IV. Results

The energy distribution obtained using the preceding data is summarized in Fig. 1. Although this distribution is a preliminary survey, three definitive statements can be made regarding energy usage at Goldstone.

(1) Air refrigeration consumes a major portion of the energy used in any one year.

(2) Additional lighting conservation measures will not yield significant savings in energy.

(3) Control room electronics equipment consumes only a small portion of the total energy.

V. Conclusions and Recommendations

These results reflect the distribution of energy usage collected from the Support Services Group at Goldstone between October 1, 1973, and February 1, 1974. The lines which separate the categories of energy use are not firm, and will require more detailed analyses to specify exactly where divisions are to be assigned. In particular, a more detailed account will have to be made of the various types of air refrigeration equipment and electromechanical equipment.

In the future, both an organizational chart and a uniform reporting system should be established for energy systems development. Ideally, a single category could be associated with a chain of documents. For example, a category such as solar heating designed by a person within a group from DSN Engineering is coordinated by a person within a group from DSN Operations and is maintained by a person within a group at Goldstone. It will be much easier to trace future energy systems development with such a tool.

References

1. Bourke, R. D., and Lu, J. Y., "Goldstone Energy Use Patterns," IOM 393.3-798, Oct. 9, 1973 (JPL internal document).

2. Lu, J., "Air Conditioning Loads on Space Cooling," IOM 393.3-883, Mar. 20, 1974 (JPL internal document).

3. Lu, J., "Space Heating Energy Use at Goldstone (Rev. A)," IOM 393.3-907, May 13, 1974 (JPL internal document).

4. Kroll, G., Casperson, R. D., Merrick, W. D., "DSN Air Conditioning System Upgrade Master Plan CY-72 through CY-77, Report A/C-771," Aug. 1, 1971, first issue (JPL internal document).

5. Lu, J., "Energy Used for Lighting at Goldstone," IOM 393.3-868, Feb. 27, 1974 (JPL internal document).

6. Rapp, R. A., "Annual Utilities Report to Management," National Aeronautics and Space Administration, Washington, D.C., July 10, 1973.

7. Lu, J., "Weather at Goldstone," IOM 393.3-881. Mar. 20, 1974 (JPL internal document).

8. Mechtly, E. A., "The International System of Units," NASA SP-7012, National Aeronautics and Space Administration, Washington, D. C., 1973.

9. Reichhardt, Jr., H., "Power Conservation Effort, Goldstone Complex," Philco Intra Company Memorandum, Mar. 7, 1972 (JPL internal document).

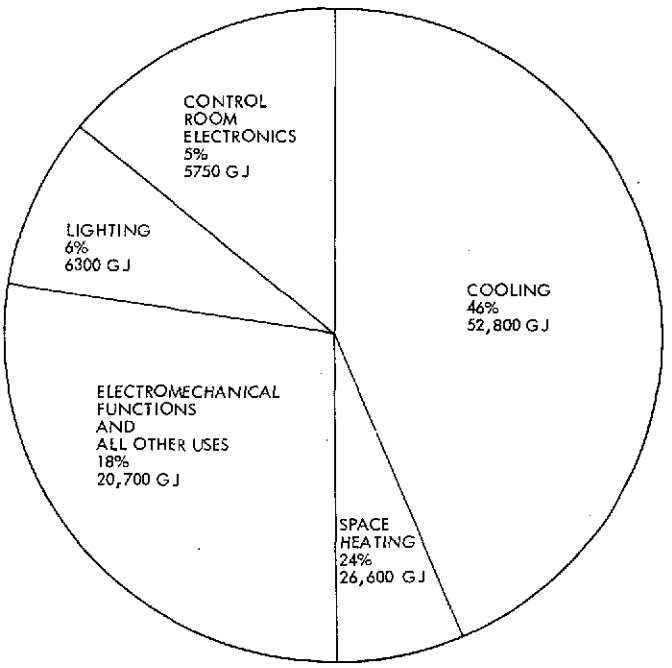

Fig. 1. Energy distribution by category for 1973

NASA — JPL — Coml., L.A., Calif.